

Transverse momentum, rapidity, and centrality dependence of inclusive charged-particle production in $\sqrt{s_{NN}} = 5.01$ TeV p+Pb collisions measured by the ATLAS experiment

Article (Published Version)

Allbrooke, B M M, Asquith, L, Cerri, A, Chavez Barajas, C A, De Santo, A, Salvatore, F, Santoyo Castillo, I, Suruliz, K, Sutton, M R, Vivarelli, I and The ATLAS collaboration, (2016) Transverse momentum, rapidity, and centrality dependence of inclusive charged-particle production in $\sqrt{s_{NN}} = 5.01$ TeV p+Pb collisions measured by the ATLAS experiment. Physics Letters B, 763. pp. 313-336. ISSN 0370-2693

This version is available from Sussex Research Online: <http://sro.sussex.ac.uk/id/eprint/65695/>

This document is made available in accordance with publisher policies and may differ from the published version or from the version of record. If you wish to cite this item you are advised to consult the publisher's version. Please see the URL above for details on accessing the published version.

Copyright and reuse:

Sussex Research Online is a digital repository of the research output of the University.

Copyright and all moral rights to the version of the paper presented here belong to the individual author(s) and/or other copyright owners. To the extent reasonable and practicable, the material made available in SRO has been checked for eligibility before being made available.

Copies of full text items generally can be reproduced, displayed or performed and given to third parties in any format or medium for personal research or study, educational, or not-for-profit purposes without prior permission or charge, provided that the authors, title and full bibliographic details are credited, a hyperlink and/or URL is given for the original metadata page and the content is not changed in any way.



Transverse momentum, rapidity, and centrality dependence of inclusive charged-particle production in $\sqrt{s_{NN}} = 5.02$ TeV $p + \text{Pb}$ collisions measured by the ATLAS experiment

The ATLAS Collaboration ^{*}

ARTICLE INFO

Article history:

Received 23 May 2016

Received in revised form 14 August 2016

Accepted 24 October 2016

Available online 29 October 2016

Editor: D.F. Geesaman

ABSTRACT

Measurements of the per-event charged-particle yield as a function of the charged-particle transverse momentum and rapidity are performed using $p + \text{Pb}$ collision data collected by the ATLAS experiment at the LHC at a centre-of-mass energy of $\sqrt{s_{NN}} = 5.02$ TeV. Charged particles are reconstructed over pseudorapidity $|\eta| < 2.3$ and transverse momentum between 0.1 GeV and 22 GeV in a dataset corresponding to an integrated luminosity of $1 \mu\text{b}^{-1}$. The results are presented in the form of charged-particle nuclear modification factors, where the $p + \text{Pb}$ charged-particle multiplicities are compared between central and peripheral $p + \text{Pb}$ collisions as well as to charged-particle cross sections measured in pp collisions. The $p + \text{Pb}$ collision centrality is characterized by the total transverse energy measured in $-4.9 < \eta < -3.1$, which is in the direction of the outgoing lead beam. Three different estimations of the number of nucleons participating in the $p + \text{Pb}$ collision are carried out using the Glauber model and two Glauber–Gribov colour-fluctuation extensions to the Glauber model. The values of the nuclear modification factors are found to vary significantly as a function of rapidity and transverse momentum. A broad peak is observed for all centralities and rapidities in the nuclear modification factors for charged-particle transverse momentum values around 3 GeV. The magnitude of the peak increases for more central collisions as well as rapidity ranges closer to the direction of the outgoing lead nucleus.

© 2016 The Author(s). Published by Elsevier B.V. This is an open access article under the CC BY license (<http://creativecommons.org/licenses/by/4.0/>). Funded by SCOAP³.

1. Introduction

Proton–nucleus collisions at ultrarelativistic energies provide an opportunity to understand the role of the nuclear environment in modifying hard scattering rates. Several physics effects are expected to induce deviations from a simple proportionality between the scattering rate and the number of binary nucleon–nucleon collisions [1]. First, nuclear shadowing effects have long been observed in deep-inelastic scattering on nuclei, as well as in proton–nucleus collisions, indicating that nucleons embedded in a nucleus have a modified structure. This modification tends to suppress hadron production at low to moderate momentum, and is addressed by a variety of theoretical approaches [2,3]. Some of these approaches describe hadron production cross sections in terms of a universal set of nuclear parton distribution functions (nPDF), which are parameterized as modifications to the free nucleon PDFs [4–12]. Second, energy loss in “cold nuclear matter” is expected to modify hadron production rates at high transverse momentum (p_T) [13–16]. Third, a relative enhancement of hadron pro-

duction rates at moderate momenta is observed in proton–nucleus collisions [17], which can be attributed to initial-state scattering of the incoming nucleon [18,19] or radial flow effects [20]. Finally, the appearance of “ridge-like” structures in high-multiplicity pp and $p + \text{Pb}$ events [21–25] suggests that small collision systems have the same hydrodynamic origin as $\text{Pb} + \text{Pb}$ events [26], or that there are already strong correlations in the initial state from gluon saturation [27]. All these effects can be explored experimentally by the measurement of charged-hadron production as a function of transverse momentum.

For proton–lead ($p + \text{Pb}$) collisions, assuming that the initial parton densities are the incoherent superposition of the nucleonic parton densities, the per-event particle production yield can be estimated by the product $\sigma_{NN} \times \langle T_{\text{Pb}} \rangle$. Here σ_{NN} is the cross section for the analogous nucleon–nucleon collision process and $\langle T_{\text{Pb}} \rangle$ is the average value of the nuclear thickness function over a distribution of the impact parameters of protons incident on the nuclear target. It can be thought of as a per-collision luminosity. The nuclear modification factor, $R_{p\text{Pb}}$, is defined as the ratio of the measured charged-particle production yield in $p + \text{Pb}$ collisions, normalized by $\langle T_{\text{Pb}} \rangle$, to the cross section of the charged-particle production yield in pp collisions:

^{*} E-mail address: atlas.publications@cern.ch.

$$R_{pPb}(p_T, y^*) = \frac{1}{\langle T_{Pb} \rangle} \frac{1/N_{evt} d^2 N_{pPb}/dy^* dp_T}{d^2 \sigma_{pp}/dy^* dp_T}, \quad (1)$$

where N_{evt} is the number of $p + Pb$ events, $d^2 N_{pPb}/dy^* dp_T$ is the differential yield of charged particles in $p + Pb$ collisions and $d^2 \sigma_{pp}/dy^* dp_T$ is the differential charged-particle production cross section in pp collisions. Both numerator and denominator are presented in terms of y^* , the rapidity in the nucleon–nucleon centre-of-mass frame. In the absence of initial-state and nuclear effects, the ratio R_{pPb} is expected to be unity at high p_T [28]. Another measure of nuclear modification is the quantity R_{CP} , which is defined to be:

$$R_{CP}(p_T, \eta) = \frac{\langle T_{Pb,P} \rangle (1/N_{evt,C}) d^2 N_{pPb,C}/d\eta dp_T}{\langle T_{Pb,C} \rangle (1/N_{evt,P}) d^2 N_{pPb,P}/d\eta dp_T}, \quad (2)$$

and can be constructed without the need for a pp reference spectrum. The indices “P” and “C” label peripheral (large impact parameter) and central (small impact parameter) centrality intervals, respectively. The R_{CP} is presented as a function of pseudorapidity (η) rather than y^* since both numerator and denominator are from the same colliding systems. Measurements of R_{pPb} and R_{CP} provide useful input for constraining models of shadowing, energy loss and radial flow effects. They should also provide useful input for the determination of nuclear parton distribution functions, in particular as a function of proton impact parameter [6]. The absolute values of the nuclear modification depend on the $\langle T_{Pb} \rangle$ values and should be interpreted with respect to the assumptions underlying the particular model used to calculate the normalization.

A recent ATLAS publication [29] has reported measurements of the mean charged-particle multiplicity as a function of pseudorapidity and collision centrality and explored the relationship between the centrality dependence of the particle production and models of the initial nuclear geometry. The results presented here utilize the same centrality definition and geometric models, but build upon that work by exploring the p_T , η and y^* dependence of per-event charged-particle yields in $p + Pb$ collisions at a centre-of-mass energy $\sqrt{s_{NN}} = 5.02$ TeV and comparing that dependence to the expectations from pp collisions through the quantities R_{pPb} and R_{CP} .

These measurements are an extension of a similar programme carried out at the Relativistic Heavy Ion Collider, where all experiments reported the absence of charged-particle suppression at $2 < p_T < 10$ GeV in $d + Au$ collisions [30–35], in contrast to the strong suppression found in $Au + Au$ collisions [31,33]. Measurements of nuclear modification factors as a function of transverse momentum in a narrow pseudorapidity window relative to the centre-of-mass frame $|\eta_{CM}| < 0.3$ have been reported by ALICE integrated over centrality [36,37] and differentially for several centrality classes [38,39]. Similarly, CMS results have been reported integrated over centrality and in a broader pseudorapidity window, $|\eta_{CM}| < 1$ [40].

2. The ATLAS detector

The ATLAS detector [41] at the Large Hadron Collider (LHC) covers almost the entire solid angle¹ around the collision point. It

consists of an inner tracking detector surrounded by a thin superconducting solenoid, electromagnetic and hadronic calorimeters, and a muon spectrometer incorporating three large superconducting toroidal magnets.

The inner detector (ID) system is immersed in a 2 T axial magnetic field and provides charged-particle tracking in the pseudorapidity range $|\eta| < 2.5$. The ID tracker is composed of three detector subsystems. Closest to the interaction point is a high-granularity silicon pixel detector covering $|\eta| < 2.7$, which typically provides three measurements per track. Next is a silicon microstrip tracker (SCT), which typically yields four pairs of hits per track, each providing a two-dimensional measurement point. The silicon detectors are complemented by the straw-tube transition radiation tracker, which enables radially extended track reconstruction up to $|\eta| = 2.0$.

The calorimeter system covers the pseudorapidity range $|\eta| < 4.9$. Within the region $|\eta| < 3.2$, electromagnetic calorimetry is provided by high-granularity lead/liquid-argon (LAr) electromagnetic calorimeters, with an additional thin LAr presampler covering $|\eta| < 1.8$, to measure the contribution of showers initiated in the material upstream of the calorimeters. Hadronic calorimetry is provided by a steel/scintillator-tile calorimeter, segmented into three barrel structures within $|\eta| < 1.7$, and two copper/LAr hadronic endcap calorimeters covering $1.5 < |\eta| < 3.2$. The calorimeter coverage is completed with forward copper/LAr and tungsten/LAr calorimeter modules optimized for electromagnetic and hadronic measurements, respectively, covering $3.1 < |\eta| < 4.9$. The minimum-bias trigger scintillators (MBTS) detect charged particles over $2.1 < |\eta| < 3.9$ using two hodoscopes, each of which is subdivided into 16 counters positioned at $z = \pm 3.6$ m.

A three-level trigger system is used to select events [42]. The Level-1 trigger is implemented in hardware and uses a subset of detector information to reduce the event rate to 100 kHz. This is followed by two software-based trigger levels which together reduce the event rate to about 1000 Hz, which is recorded for data analysis.

3. Datasets and event selection

3.1. Event selection in $p + Pb$ collisions

The $p + Pb$ collisions were recorded by the ATLAS detector in September 2012 using a trigger that selected events with at least one hit in each side of the MBTS, with the resulting dataset corresponding to an integrated luminosity of $1 \mu\text{b}^{-1}$. During that run the LHC was configured with a clockwise 4 TeV proton beam and an anti-clockwise 1.57 TeV per-nucleon ^{208}Pb beam that together produced collisions with a nucleon–nucleon centre-of-mass energy of $\sqrt{s} = 5.02$ TeV and a longitudinal rapidity boost of $y_{lab} = 0.465$ units with respect to the ATLAS laboratory frame. Following a common convention used for $p + A$ measurements, the rapidity is taken to be positive in the direction of the proton beam, i.e. opposite to the usual ATLAS convention for pp collisions. With this convention, the ATLAS laboratory frame rapidity, y , and the $p + Pb$ centre-of-mass system rapidity, y^* , are related by $y^* = y - 0.465$.

Charged-particle tracks and collision vertices are reconstructed from clusters in the pixel detector and the SCT using an algorithm optimized for minimum-bias pp measurements [43]. The $p + Pb$ events are required to have a collision vertex satisfying $|z_{vtx}| < 150$ mm, at least one hit in each side of the MBTS, and a difference between the time measurements in the two MBTS hodoscopes of less than 10 ns. Events containing multiple $p + Pb$ collisions (pile-up) are suppressed by rejecting events that contain a second reconstructed vertex with a scalar transverse momentum

¹ ATLAS uses a right-handed coordinate system with its origin at the nominal interaction point (IP) in the centre of the detector and the z -axis along the beam pipe. The x -axis points from the IP to the centre of the LHC ring, and the y -axis points upwards. Cylindrical coordinates (r, ϕ) are used in the transverse plane, ϕ being the azimuthal angle around the z -axis. The pseudorapidity is defined in terms of the polar angle θ as $\eta = -\ln \tan(\theta/2)$. Angular distance is measured in units of $\Delta R \equiv \sqrt{(\Delta\eta)^2 + (\Delta\phi)^2}$.

sum of associated tracks of $\Sigma p_T^2 > 5$ GeV. The residual contamination from pile-up events has been estimated to be 10^{-4} [24].

To remove contributions from electromagnetic and diffractive processes, a rapidity gap criterion is applied to the $p + \text{Pb}$ data using the procedure outlined in Ref. [29]. The procedure utilizes energy deposits in the calorimeter identified using so-called topological clusters [44]. The detector is divided into slices of $\Delta\eta = 0.2$, and “edge” gaps are calculated as the distance from the edge of the calorimeter ($\eta = -4.9$) to the nearest slice that contains a cluster with a minimum transverse energy of 200 MeV. Events with a large edge gap ($\Delta\eta_{\text{gap}}^{\text{Pb}} > 2$) in the negative η (Pb) direction are excluded from the analysis. The gap requirement removes 1% of the events passing the vertex and MBTS timing cuts, which yields a total of 2.1×10^6 events used for further analysis.

3.2. Event selection in pp collisions

The pp spectrum used as a reference for the $p + \text{Pb}$ measurement is based on an interpolation of two data samples taken at $\sqrt{s} = 2.76$ TeV and 7 TeV. Proton–proton collisions at $\sqrt{s} = 2.76$ TeV with total integrated luminosity 200 nb^{-1} were obtained by the ATLAS experiment in March 2011. Proton–proton collisions at $\sqrt{s} = 7$ TeV with total integrated luminosity 130 pb^{-1} were obtained in April 2010. In both cases, the trigger selected events with at least one hit in the MBTS detector. The average number of collisions per bunch crossing during these data-taking periods is 0.4 and 0.01 for the $\sqrt{s} = 2.76$ TeV and $\sqrt{s} = 7$ TeV datasets, respectively. Events are required to satisfy the same z_{vtx} and MBTS requirements as for $p + \text{Pb}$ analysis.

3.3. Monte Carlo event simulation

The response of the ATLAS detector and the performance of reconstruction algorithms are evaluated using one million simulated minimum-bias $p + \text{Pb}$ events at $\sqrt{s} = 5.02$ TeV, produced by version 1.38b of the HIJING event generator [45]. Diffractive processes are disabled. To match the LHC $p + \text{Pb}$ beam conditions, the four-momentum of each generated particle is longitudinally boosted by a rapidity of -0.465 . The generator-level events are then passed through a GEANT4 simulation of the ATLAS detector [46,47]. The simulated events are digitized using data conditions appropriate to the $p + \text{Pb}$ run and are reconstructed using the same algorithms that are applied to the experimental data.

For the pp analysis, 20 million events were produced using the PYTHIA6 [48] event generator with the AUET2B parameter set [49] at both $\sqrt{s} = 2.76$ TeV and 7 TeV (with versions 6.423 and 6.421 respectively). Additional samples produced using PYTHIA8 [50] with the 4C parameter set [51], and Herwig++ with the UEE5 parameter set [52], are used for studying systematic uncertainties (see Sections 6 and 7).

4. Centrality selection

The centrality determination for $p + \text{Pb}$ collisions in ATLAS uses the total transverse energy, ΣE_T^{Pb} , measured in the negative pseudorapidity sections of the forward calorimeter in the range $-4.9 < \eta < -3.1$ (in the direction of the Pb beam) [29]. The transverse energies in the forward calorimeter are evaluated at an energy scale calibrated for electromagnetic showers and are not corrected for hadronic response [44]. Centrality intervals are defined in terms of percentiles of the ΣE_T^{Pb} distribution after accounting for an estimated inefficiency of approximately $(2 \pm 2)\%$ for inelastic $p + \text{Pb}$ events to satisfy the applied event selection criteria. This inefficiency affects mainly the most peripheral events. The following centrality intervals are used in this analysis: 0–1%, 1–5%, 5–10%,

Table 1

Mean values of T_{Pb} in b^{-1} for all centrality intervals, along with asymmetric systematic uncertainties shown as absolute as well as relative uncertainties. The columns correspond to the Glauber model (left), Glauber–Gribov model with $\omega_\sigma = 0.11$ (middle), and Glauber–Gribov model with $\omega_\sigma = 0.2$ (right).

Centrality	Glauber	Glauber–Gribov	
		$\omega_\sigma = 0.11$	$\omega_\sigma = 0.2$
60–90%	42.3 $^{+2.8}_{-4.3}$ $\left(\begin{smallmatrix} +7\% \\ -10\% \end{smallmatrix}\right)$	36.6 $^{+2.7}_{-2.2}$ $\left(\begin{smallmatrix} +7\% \\ -6\% \end{smallmatrix}\right)$	34.4 $^{+3.7}_{-2.1}$ $\left(\begin{smallmatrix} +11\% \\ -6\% \end{smallmatrix}\right)$
40–60%	92 $^{+4}_{-7}$ $\left(\begin{smallmatrix} +5\% \\ -7\% \end{smallmatrix}\right)$	80.2 $^{+4.6}_{-3.3}$ $\left(\begin{smallmatrix} +6\% \\ -4\% \end{smallmatrix}\right)$	75.9 $^{+6.5}_{-3.3}$ $\left(\begin{smallmatrix} +9\% \\ -4\% \end{smallmatrix}\right)$
30–40%	125.6 $^{+3.3}_{-4.5}$ $\left(\begin{smallmatrix} +3\% \\ -4\% \end{smallmatrix}\right)$	116.7 $^{+3.8}_{-3.2}$ $\left(\begin{smallmatrix} +3.2\% \\ -2.7\% \end{smallmatrix}\right)$	113.1 $^{+6.6}_{-3.3}$ $\left(\begin{smallmatrix} +6\% \\ -3\% \end{smallmatrix}\right)$
20–30%	147.9 $^{+3.6}_{-2.6}$ $\left(\begin{smallmatrix} +2.4\% \\ -1.8\% \end{smallmatrix}\right)$	145.5 $^{+3.6}_{-3.0}$ $\left(\begin{smallmatrix} +2.5\% \\ -2.1\% \end{smallmatrix}\right)$	144.6 $^{+5.6}_{-3.1}$ $\left(\begin{smallmatrix} +4\% \\ -2\% \end{smallmatrix}\right)$
10–20%	172 $^{+7}_{-3}$ $\left(\begin{smallmatrix} +4\% \\ -2\% \end{smallmatrix}\right)$	181.9 $^{+4.4}_{-3.1}$ $\left(\begin{smallmatrix} +2.4\% \\ -1.7\% \end{smallmatrix}\right)$	186.8 $^{+5}_{-2.9}$ $\left(\begin{smallmatrix} +3\% \\ -2\% \end{smallmatrix}\right)$
5–10%	194 $^{+15}_{-4}$ $\left(\begin{smallmatrix} +8\% \\ -2\% \end{smallmatrix}\right)$	221 $^{+6}_{-5}$ $\left(\begin{smallmatrix} +3\% \\ -2\% \end{smallmatrix}\right)$	235 $^{+7}_{-7}$ $\left(\begin{smallmatrix} +3\% \\ -3\% \end{smallmatrix}\right)$
1–5%	215 $^{+22}_{-5}$ $\left(\begin{smallmatrix} +10\% \\ -2\% \end{smallmatrix}\right)$	264 $^{+9}_{-10}$ $\left(\begin{smallmatrix} +3\% \\ -4\% \end{smallmatrix}\right)$	292 $^{+8}_{-23}$ $\left(\begin{smallmatrix} +3\% \\ -8\% \end{smallmatrix}\right)$
0–1%	245 $^{+40}_{-7}$ $\left(\begin{smallmatrix} +15\% \\ -3\% \end{smallmatrix}\right)$	330 $^{+15}_{-23}$ $\left(\begin{smallmatrix} +5\% \\ -7\% \end{smallmatrix}\right)$	377 $^{+12}_{-60}$ $\left(\begin{smallmatrix} +3\% \\ -16\% \end{smallmatrix}\right)$
0–90%	106.3 $^{+4.4}_{-2.7}$ $\left(\begin{smallmatrix} +4\% \\ -2\% \end{smallmatrix}\right)$	107.3 $^{+3.9}_{-2.6}$ $\left(\begin{smallmatrix} +4\% \\ -2\% \end{smallmatrix}\right)$	109 $^{+4}_{-2}$ $\left(\begin{smallmatrix} +4\% \\ -2\% \end{smallmatrix}\right)$

10–20%, 20–30%, 30–40%, 40–60%, 60–90% (with the 0–1% interval defined by the highest ΣE_T^{Pb} values). Since the composition of the events and the uncertainty on the inelastic $p + \text{Pb}$ events selection efficiency in the most peripheral 90–100% interval is not well constrained, these events are excluded from the analysis, and events from the 60–90% centrality interval are used as the reference for R_{CP} .

Following the procedure adopted in Ref. [29], three different estimations of the average number of nucleons participating in the $p + \text{Pb}$ collisions (N_{part}) are carried out in each centrality interval. The first estimation uses the standard Glauber model [53], which is characterized by a fixed total nucleon–nucleon cross section. The other two estimations use the Glauber–Gribov colour-fluctuation (GGCF) model [54,55], which includes event-by-event fluctuations in the nucleon–nucleon cross section σ_{NN} ($N + N \rightarrow X$). In the GGCF model, the magnitude of the fluctuations is characterized by the parameter ω_σ , with $\omega_\sigma = 0$ corresponding to the standard Glauber model. Two values, $\omega_\sigma = 0.11$ and $\omega_\sigma = 0.2$, based on the calculations in Refs. [54,55], are used in this measurement.

In both geometric models the value of $\langle T_{\text{Pb}} \rangle$ is directly related to $\langle N_{\text{part}} \rangle$ via the relation $\langle N_{\text{part}} \rangle - 1 = \langle T_{\text{Pb}} \rangle \sigma_{\text{NN}}$, with σ_{NN} taken to be $70 \pm 5 \text{ mb}$ [38]. The obtained $\langle T_{\text{Pb}} \rangle$ values for the Glauber and Glauber–Gribov models in different centrality intervals are listed in Table 1. For central collisions, the $\langle T_{\text{Pb}} \rangle$ uncertainties are dominated by the uncertainty in the Glauber/Glauber–Gribov modelling. For more peripheral collisions, the uncertainty in the efficiency for selecting inelastic events also makes a significant contribution.

Ratios of the $\langle T_{\text{Pb}} \rangle$ values, which are relevant to R_{CP} , in a given centrality interval to the respective value in the 60–90% interval are presented in Table 2.

5. Reconstruction of charged-particle spectra

5.1. Track selection

The analysis of the charged-particle spectra presented in this paper refers to primary charged particles directly produced in the $p + \text{Pb}$ or pp interactions and having a mean lifetime greater than $0.3 \times 10^{-10} \text{ s}$, or long-lived charged particles created by subsequent decays of particles with a shorter lifetime [43]. All other particles are considered secondary. Tracks produced by primary and secondary particles are referred to from now on as primary and secondary tracks, respectively.

Table 2

Ratios of the mean values of T_{Pb} for all centrality bins with respect to the 60–90% centrality interval, along with the corresponding total systematic uncertainty. The columns correspond to the Glauber model (left), Glauber–Gribov model with $\omega_\sigma = 0.11$ (middle), and Glauber–Gribov model with $\omega_\sigma = 0.2$ (right).

Centrality	Glauber	Glauber–Gribov	
		$\omega_\sigma = 0.11$	$\omega_\sigma = 0.2$
40–60%/60–90%	2.16 ^{+0.09} _{-0.06} (+4% -3%)	2.19 ^{+0.04} _{-0.06} (+2.6% -2.7%)	2.21 ^{+0.05} _{-0.06} (+2.4% -2.8%)
30–40%/60–90%	2.97 ^{+0.22} _{-0.13} (+7% -4%)	3.19 ^{+0.13} _{-0.13} (+4% -4%)	3.29 ^{+0.12} _{-0.16} (+4% -5%)
20–30%/60–90%	3.49 ^{+0.34} _{-0.17} (+10% -5%)	3.98 ^{+0.18} _{-0.21} (+5% -5%)	4.21 ^{+0.19} _{-0.28} (+4% -7%)
10–20%/60–90%	4.06 ^{+0.5} _{-0.21} (+13% -5%)	4.98 ^{+0.25} _{-0.31} (+5% -6%)	5.43 ^{+0.28} _{-0.5} (+5% -9%)
5–10%/60–90%	4.58 ^{+0.8} _{-0.24} (+16% -5%)	6.05 ^{+0.33} _{-0.5} (+5% -7%)	6.8 ^{+0.4} _{-0.8} (+6% -12%)
1–5%/60–90%	5.08 ^{+0.9} _{-0.27} (+18% -5%)	7.2 ^{+0.4} _{-0.6} (+6% -9%)	8.5 ^{+0.5} _{-1.4} (+6% -16%)
0–1%/60–90%	5.8 ^{+1.3} _{-0.33} (+23% -6%)	9 ^{+0.5} _{-1.1} (+6% -12%)	11 ^{+0.6} _{-2.6} (+5% -23%)

Tracks are required to be in the kinematic range of transverse momentum $p_T > 0.1$ GeV and absolute pseudorapidity $|\eta| < 2.3$. Additional requirements on the number of hits in the ID subsystems are imposed in order to reduce the contribution from ‘fake’ tracks that do not correspond to the passage of charged particles through the detector. All tracks are required to have at least one hit in the pixel detector and a hit in the first pixel layer if one is expected by the track trajectory. Tracks with $p_T < 0.2$ GeV are required to have at least two hits in the SCT, tracks with $0.2 < p_T < 0.3$ GeV are required to have at least four hits in the SCT, and all other tracks are required to have at least six hits in the SCT. To ensure that the tracks originate from the event vertex, the transverse (d_0) and longitudinal ($z_0 \sin \theta$) impact parameters of the reconstructed track trajectory with respect to the reconstructed primary vertex are required to be less than 1.5 mm. Finally, tracks are required to satisfy the significance conditions $|d_0/\sigma_{d_0}| < 3.0$ and $|z_0 \sin \theta/\sigma_{z_0 \sin \theta}| < 3.0$, where the quantities σ_{d_0} and $\sigma_{z_0 \sin \theta}$ are the uncertainties in the determination of d_0 and $z_0 \sin \theta$ obtained from the covariance matrix provided by the ATLAS track model [43].

In pp collisions, tracks originating from all reconstructed vertices are used in the analysis. The track-to-vertex matching uses the track z_0 parameter and the z coordinate of the vertex. These parameters of the tracks in pp collisions are often less precisely defined than in $p + \text{Pb}$ due to the fact that the vertices are typically reconstructed with fewer tracks. Thus in the pp data analysis the track selection cuts related to the vertex are relaxed such that the $z_0 \sin \theta$ impact parameter condition is required to be less than 2.5 mm and the transverse and longitudinal impact parameter significances are required to be less than 4.0.

For the calculation of R_{pPb} , the momentum three-vector is used to calculate the rapidity of the particle, assuming it has the mass of the pion (m_π). A correction for this assumption is discussed in Section 5.2.

5.2. Reconstruction of the invariant particle distributions

The per-event $p + \text{Pb}$ charged-particle multiplicity distributions are measured differentially as a function of p_T and either η or y^* , and are referred to as the differential invariant yields. They are defined as:

$$\frac{1}{N_{\text{evt}}} \frac{1}{2\pi p_T} \frac{d^2 N_{\text{ch}}}{dp_T d\eta} = \frac{1}{N_{\text{evt}}} \frac{1}{2\pi p_T} \frac{N_{\text{ch}}(p_T, \eta)}{\Delta p_T \Delta \eta} \frac{\mathcal{P}(p_T, \eta)}{\mathcal{C}_{\text{trk}}(p_T, \eta)} \quad \text{and} \quad (3)$$

$$\frac{1}{N_{\text{evt}}} \frac{1}{2\pi p_T} \frac{d^2 N_{\text{ch}}}{dp_T dy^*} = \frac{1}{N_{\text{evt}}} \frac{1}{2\pi p_T} \frac{N_{\text{ch}}(p_T, y^*)}{\Delta p_T \Delta y^*} \frac{\mathcal{P}(p_T, \eta) \mathcal{A}(p_T, y^*)}{\mathcal{C}_{\text{trk}}(p_T, \eta)}, \quad (4)$$

where Δp_T , $\Delta \eta$ and Δy^* are the widths of the transverse momentum, pseudorapidity and rapidity intervals being studied, and N_{evt} is the number of events in the analyzed centrality interval. The correction factors \mathcal{C}_{trk} , \mathcal{P} , and \mathcal{A} are used to correct for track efficiency and transverse momentum resolution, contributions from fake tracks and secondaries, and to transform the distributions from y_π to hadron rapidity, respectively.

The correction factor used to correct for the track reconstruction inefficiency is estimated from simulation and is defined as:

$$\mathcal{C}_{\text{trk}}(p_T, \eta) = \frac{N_{\text{Primary}}^{\text{Rec}}(p_T, \eta)}{N_{\text{Primary}}^{\text{Gen}}(p_T^{\text{Gen}}, \eta^{\text{Gen}})}, \quad (5)$$

where $N_{\text{Primary}}^{\text{Gen}}$ is the number of primary charged particles and $N_{\text{Primary}}^{\text{Rec}}$ is the number of reconstructed tracks that are matched to those charged particles. A track is matched to a generated particle if that particle contributes more than 50% to the weighted number of hits on the track. The hits are weighted such that all subdetectors have the same weight in the sum. The algorithm to match reconstructed tracks to generated particles is discussed in Ref. [56]. These correction factors are calculated using Monte Carlo events generated with the HIJING event generator. The correction factors are calculated after reweighting the particle-level spectra to achieve better agreement in the transverse momentum distribution between data and simulation. The track reconstruction correction factor values are smaller at low p_T , starting at around 20% in the lowest measured interval of $0.1 < p_T < 0.2$ GeV, and then increase rapidly to reach a plateau value at approximately 1 GeV. The plateau of the correction factor values is generally higher in the centre of the detector, reaching 80% for highest p_T and $\eta = 0$, but only 60% at $|\eta| = 2.3$. This correction has a very weak centrality dependence; the maximum variation from peripheral to central collisions does not exceed 2% over the range of measured centralities at any p_T or η value.

The correction factors to remove the contributions from fake and residual secondary tracks are estimated from simulation and are given by:

$$\mathcal{P}(p_T, \eta) = \frac{N_{\text{Primary}}^{\text{Rec}}(p_T, \eta)}{N_{\text{Rec}}(p_T, \eta)}, \quad (6)$$

where N_{Rec} is the total number of reconstructed particles. This correction has a strong dependence on both η and p_T at the lowest transverse momentum. The value of \mathcal{P} is 0.98 for tracks with $p_T > 1$ GeV in all η and centrality intervals, dropping to 0.8 for tracks at $|\eta| \sim 2.3$ in the 0–1% centrality interval.

The assumption that the particle mass is equal to the pion mass is used to calculate y^* from the track’s momentum three-vector. For tracks that are not pions, the y^* is computed incorrectly and the particle contributes to the yield in the wrong y^* bin. A correction for this effect is derived from the simulation as the ratio in p_T and y^* space of the generated charged particles with their correct mass to the corresponding distribution of generated charged particles assumed to be pions:

$$\mathcal{A}(p_T, y^*) = \frac{N_{\text{Primary}}^{\text{Gen}}(m, p_T, y^*)}{N_{\text{Primary}}^{\text{Gen}}(m_\pi, p_T, y^*)}. \quad (7)$$

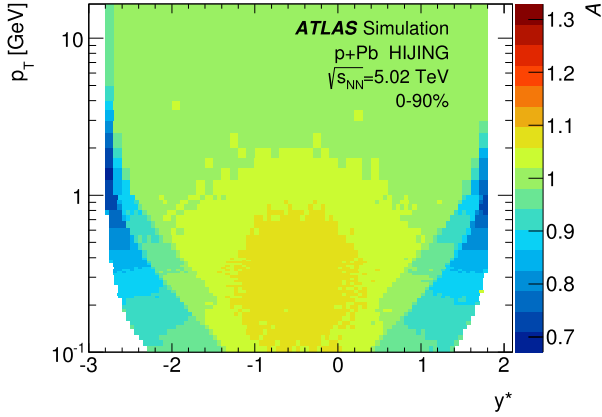


Fig. 1. $\mathcal{A}(p_T, y^*)$ as a function of p_T and y^* for the $p + \text{Pb}$ MC sample.

Table 3

Fiducial cuts for the combination of $p + \text{Pb}$ and pp acceptance effects.

p_T range [GeV]	$p + \text{Pb}$ y^* range	pp y^* range	Combined y^* range
$0.1 < p_T < 0.4$	$-2.3 < y^* < 1.3$	$-1.8 < y^* < 1.8$	$-1.8 < y^* < 1.3$
$0.4 < p_T < 1$	$-2.5 < y^* < 1.5$	$-2.0 < y^* < 2.0$	$-2.0 < y^* < 1.5$
$1 < p_T < 2$	$-2.7 < y^* < 1.7$	$-2.2 < y^* < 2.2$	$-2.2 < y^* < 1.7$
$2 < p_T < 3$	$-2.75 < y^* < 1.75$	$-2.25 < y^* < 2.25$	$-2.25 < y^* < 1.75$
$p_T > 3$	$-2.8 < y^* < 1.8$	$-2.3 < y^* < 2.3$	$-2.3 < y^* < 1.8$

The correction function is shown in Fig. 1 as a two-dimensional distribution for p_T and y^* in the $p + \text{Pb}$ system. The correction is approximately 1.1 at $y^* = 0$ and decreases to unity with increasing p_T , as the influence of the mass of the particle on the rapidity becomes negligible. At the edges of acceptance ($y^* \approx \pm 2.3$), the value of \mathcal{A} is approximately 0.8 for particles with $p_T \approx 0.7$ GeV. Fiducial regions with $\mathcal{A} \leq 0.9$ are removed from the analysis of $R_{p\text{Pb}}$, using the selection criteria documented in Table 3. This ensures minimal model dependence in the correction factor.

6. Reference spectra from pp collisions

The differential charged-particle cross sections for pp collisions are defined in an analogous way to those used for $p + \text{Pb}$ differential invariant yield by:

$$\frac{1}{2\pi p_T} \frac{d^2\sigma_{pp}}{dp_T dy^*} = \frac{1}{2\pi p_T L} \frac{N_{\text{ch}}(p_T, y^*)}{\Delta p_T \Delta y^*} \frac{\mathcal{P}(p_T, \eta) \mathcal{A}(p_T, y^*)}{C_{\text{trk}}(p_T, \eta)}, \quad (8)$$

where L is the integrated luminosity of the dataset under consideration. The values of C_{trk} , \mathcal{P} , and \mathcal{A} are calculated using MC events produced by the PYTHIA6 event generator. The trigger and vertex reconstruction efficiency in pp data analysis is estimated in Ref. [43] to be close to unity and is therefore not corrected for in the analysis (the systematic uncertainty due to this choice is discussed in Section 7).

Once the differential cross sections at 2.76 and 7 TeV are measured, the charged-particle cross section at $\sqrt{s} = 5.02$ TeV is estimated by interpolation. Two interpolation functions are investigated for every p_T bin in each rapidity interval. The first function is proportional to \sqrt{s} , and the second is proportional to $\ln(\sqrt{s})$. The $\ln(\sqrt{s})$ -based interpolation is taken as the default in the analysis and the \sqrt{s} -based interpolation is used to assess the systematic uncertainty due to the choice of interpolation function. Possible distortions introduced by the interpolation algorithm are evaluated using MC simulations based on PYTHIA8. The ratio of the simulated differential cross section at $\sqrt{s} = 5.02$ TeV to the cross section interpolated with $\ln(\sqrt{s})$ -based or \sqrt{s} -based function, obtained from simulated samples at $\sqrt{s} = 7$ TeV and $\sqrt{s} = 2.76$ TeV, is taken as a multiplicative correction factor to be applied to the data. The correction factors obtained using PYTHIA8 and Herwig++ are presented in Fig. 2(a) for the region $-1.8 < y^* < 1.3$. The correction obtained from PYTHIA8 is the default applied to the data and the correction obtained using Herwig++ is used to assess the systematic uncertainty as discussed in Section 7, and calculated separately for either the $\ln(\sqrt{s})$ -based or \sqrt{s} -based interpolation functions.

Fig. 2(b) summarizes the relative shapes of the differential cross sections measured at $\sqrt{s} = 2.76$, 7 and 5.02 TeV, with the last ob-

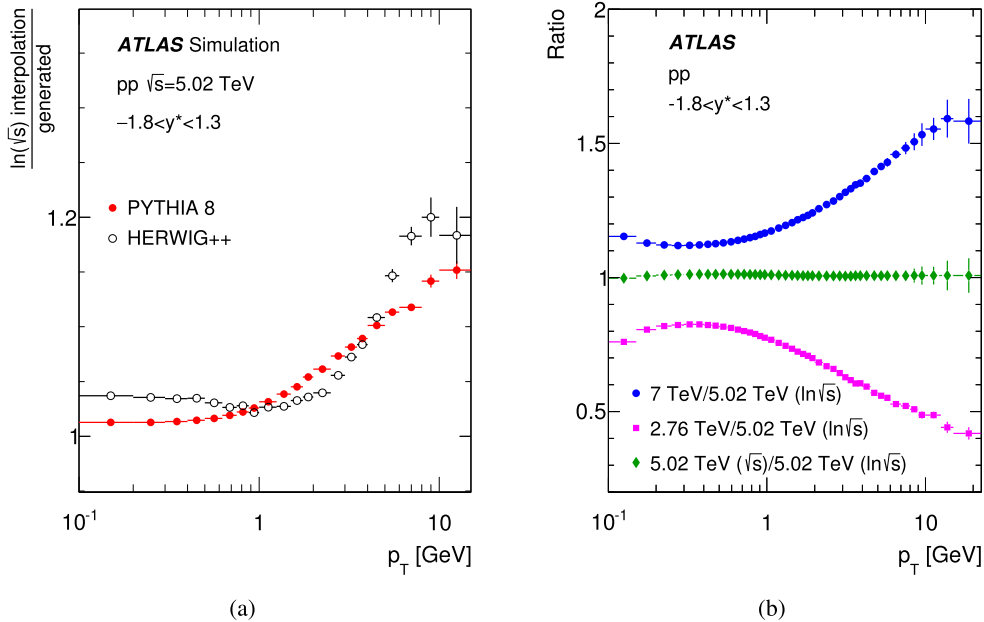


Fig. 2. (a) The correction factors that are applied to the data. They are obtained as a ratio of the simulated differential cross section at $\sqrt{s} = 5.02$ TeV to the interpolated cross section, obtained from simulated samples at $\sqrt{s} = 7$ TeV and $\sqrt{s} = 2.76$ TeV with PYTHIA8 and Herwig++. (b) The ratios of the input invariant cross sections at $\sqrt{s} = 7$ TeV (blue circles) and at $\sqrt{s} = 2.76$ TeV (magenta squares) to the interpolated cross section at $\sqrt{s}_{\text{NN}} = 5.02$ TeV. The error bars represent the statistical uncertainties of the input spectra. The comparison between interpolation using \sqrt{s} and $\ln(\sqrt{s})$ is shown with green diamond markers. All the ratios are extracted within the maximal acceptance of the ID detector ($-1.8 < y^* < 1.3$). (For interpretation of the references to colour in this figure legend, the reader is referred to the web version of this article.)

Table 4

Systematic uncertainties on charged-particle yields for $p + \text{Pb}$ and pp at 2.76 TeV. The uncertainty in the luminosity does not contribute to the $p + \text{Pb}$ results, since they are expressed as per-event invariant yields. The uncertainty in the trigger and event selection is included in the uncertainty in the efficiency for selecting inelastic events, and thus is already contained in the centrality selection's uncertainties.

Uncertainty	$p + \text{Pb}$	pp	Variation
Track selection	2%	1%	decreases with p_T , increases with $ \eta $
Particle composition	1–5%	1–2%	changes with p_T and y^*
Material budget		0.5–4%	decreases with p_T , increases with $ \eta $
p_T reweighting	0.1–0.5%	0.1–2.5%	decreases with p_T , increases with η
Centrality selection	0.1–8%	–	increases with p_T and asymmetric in η , increases with centrality interval width
Trigger efficiency	0.01%	0.5%	
Luminosity	–	2.7% (1.8%)	$\sqrt{s} = 2.76 \text{ TeV}$ (7 TeV)
pp reference interpolation	–	0.1–5%	increases with p_T and constant in η
Vertex reconstruction	0.1%	1%	

tained by interpolation. It shows that the effect of the interpolation on the input cross section at $\sqrt{s} = 2.76 \text{ TeV}$ ($\sqrt{s} = 7 \text{ TeV}$) compared to the interpolated cross section at $\sqrt{s} = 5.02 \text{ TeV}$, using $\ln(\sqrt{s})$, is 0.8 (1.1) at low p_T values and is 0.4 (1.6) at the highest transverse momentum. The ratio of \sqrt{s} -based interpolation to the default $\ln(\sqrt{s})$ -based interpolation shown in the Fig. 2(b) is one of the systematic uncertainties in the cross section interpolation, which are discussed in Section 7.

7. Systematic uncertainties

The systematic uncertainties in the measurement of invariant charged-particle yields arise from inaccuracies of the detector description in the simulation, sensitivity to selection criteria used in the analysis and differences between the composition of particle

species in the simulation and in the data samples. To evaluate each source of uncertainty, each parameter used in the analysis, such as the values of the quantities used in the track selection criteria or simulated particle composition, is altered within appropriate limits, as described below. All sources of systematic uncertainty are evaluated independently in terms of η and y^* .

The uncertainty due to the track selection is sensitive to possible differences in performance of the track reconstruction algorithms in data and in MC simulation. To estimate this uncertainty, the basic requirements on the number of detector hits and the track impact parameters were relaxed and tightened in both data and MC simulation. For the relaxed criteria the d_0 and $z_0 \sin \theta$ impact parameters for $p + \text{Pb}$ (pp) samples are required to be less than 2 mm (3 mm) and significance conditions are not required. To tighten the selection, tracks are required to have at least seven SCT hits, traverse an active module in each layer of the pixel detector, and the impact parameter requirement is changed to be less than 1 mm and 2 mm for $p + \text{Pb}$ and pp samples respectively. These variations produce up to a 2% shift in the fully corrected charged-particle yield. The uncertainty in the charged-particle yield due to simulation of inactive material is estimated using dedicated $p + \text{Pb}$ simulated samples in which the inactive material is increased in the central and forward regions of the inner detector [57]. The net effect on the per-event charged-particle yields is found to vary from 0.5% at low pseudorapidity to 4% at high pseudorapidity, but is independent of centrality. The systematic uncertainty estimated in this way from $p + \text{Pb}$ simulated samples is applied to both $p + \text{Pb}$ and pp data, taking into account the rapidity boost.

The correction for track reconstruction inefficiency, secondaries and fake tracks is calculated from simulated samples after reweighting the track p_T and η distributions to match those observed in data. The systematic uncertainty in this procedure is derived by taking the difference between the results obtained with reweighting and without reweighting of the simulation.

Our imperfect knowledge of the particle composition in $p + \text{Pb}$ collisions is a source of systematic uncertainty, which influences $\mathcal{A}(p_T, y^*)$ for $\eta \rightarrow y^*$ transformation. To assess the sensitivity of the analysis to the particle composition in the Hijing samples

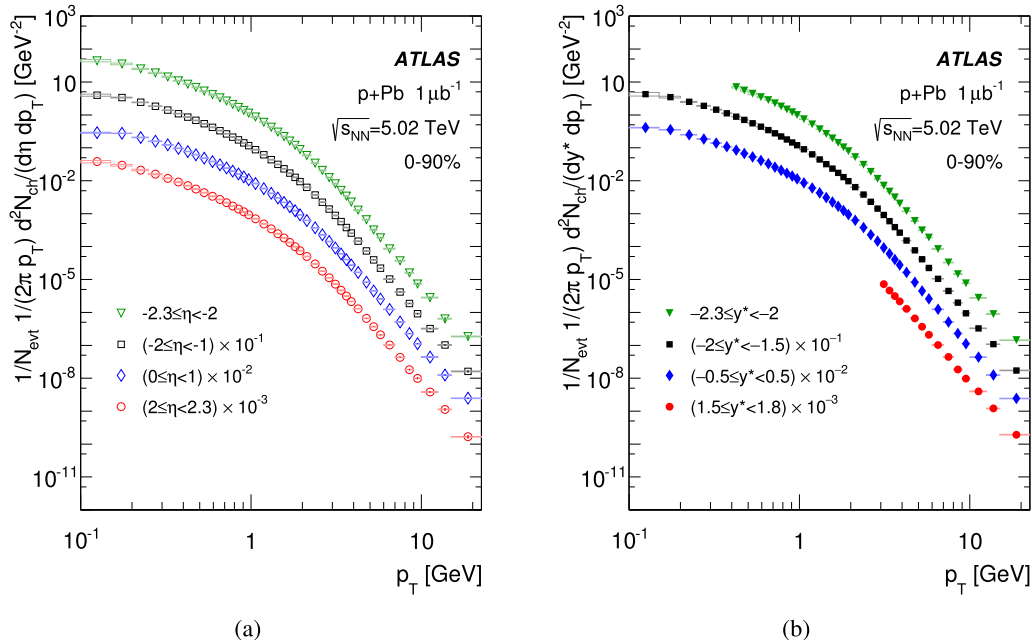


Fig. 3. Invariant differential p_T spectra of charged particles which are produced in $p + \text{Pb}$ collisions at $\sqrt{s} = 5.02 \text{ TeV}$ shown in (a) four η intervals and (b) four y^* intervals, for the 0–90% centrality interval. The individual spectra are scaled by constant factors (indicated in the legend) for visibility. The statistical uncertainties are indicated with vertical lines and the systematic uncertainties are indicated with boxes, but are generally much smaller than the size of the symbols.

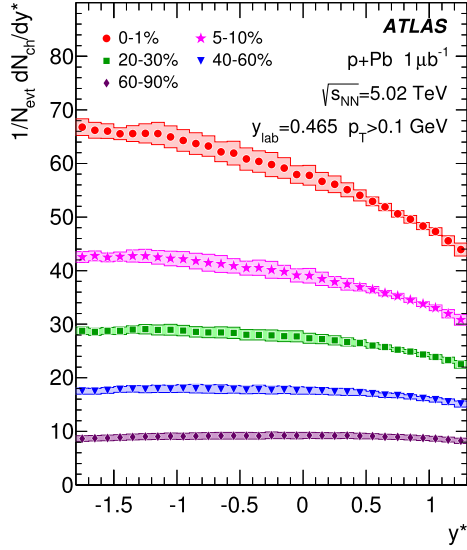


Fig. 4. The invariant differential y^* spectra of charged particles produced in $p + \text{Pb}$ collisions at $\sqrt{s} = 5.02$ TeV are shown in five centrality intervals for $p_T > 0.1$ GeV. The statistical uncertainties are indicated with vertical lines and the systematic uncertainties are indicated with boxes.

used to correct the data, the relative contributions of the pions, kaons and protons in HIJING were reweighted to match the fractions obtained from the identified particle multiplicity measured by the ALICE experiment [58]. The weights of the charged-particle yields vary from 0.5 to 1.5 at low p_T and high p_T respectively, increase with centrality, and do not depend on η . The change in the charged-particle yields is found to be between 4% and 0.1% at low p_T and high p_T respectively, but the variation does not depend on η . Variation of the particle composition results in a maximum 5% difference in the fully corrected charged-particle yields at moderate and high y^* and low p_T . The difference decreases with p_T and depends on y^* , reaching minimum values close to $y^* = -2$ and 1. For the pp analysis, the $p + \text{Pb}$ multiplicity measurement by the ALICE experiment for the peripheral centrality interval was adopted to estimate the weights. The change in the charged-particle yields is found to be between 2% and 0.1% at

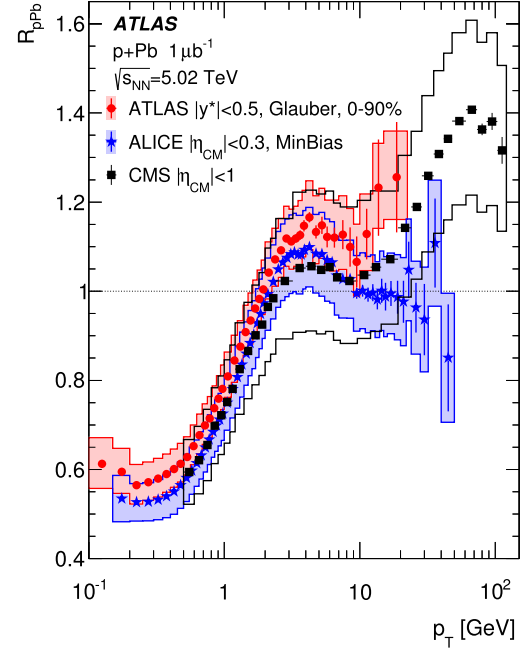


Fig. 6. R_{pPb} values as a function of p_T in the 0–90% centrality interval averaged over $|y^*| < 0.5$, are compared to the minimum-bias (0–100%) results from a different pseudorapidity range in the centre-of-mass system: ALICE for $|\eta_{CM}| < 0.3$ [36] and CMS for $|\eta_{CM}| < 1$ [40]. The $\langle T_{pPb} \rangle$ value for the ATLAS centrality correction is calculated with the Glauber model. The total systematic uncertainties, which include the uncertainty in $\langle T_{pPb} \rangle$, are indicated by lines of the same colour. Strict quantitative agreement is not expected as each measurement uses different rapidity intervals for the centrality determination and apply different event selection criteria to reject diffractive collisions.

low p_T and high p_T respectively, and the variation does not depend on η and y^* .

The uncertainties associated with the centrality selection contain the effects of the trigger and event selection criteria. Using the procedure outlined in Ref. [29], the centrality intervals are re-defined after assuming a total event selection efficiency, differing by $\pm 2\%$ from the nominal one, and the change in the multiplicity spectrum reconstructed in each centrality interval is taken as

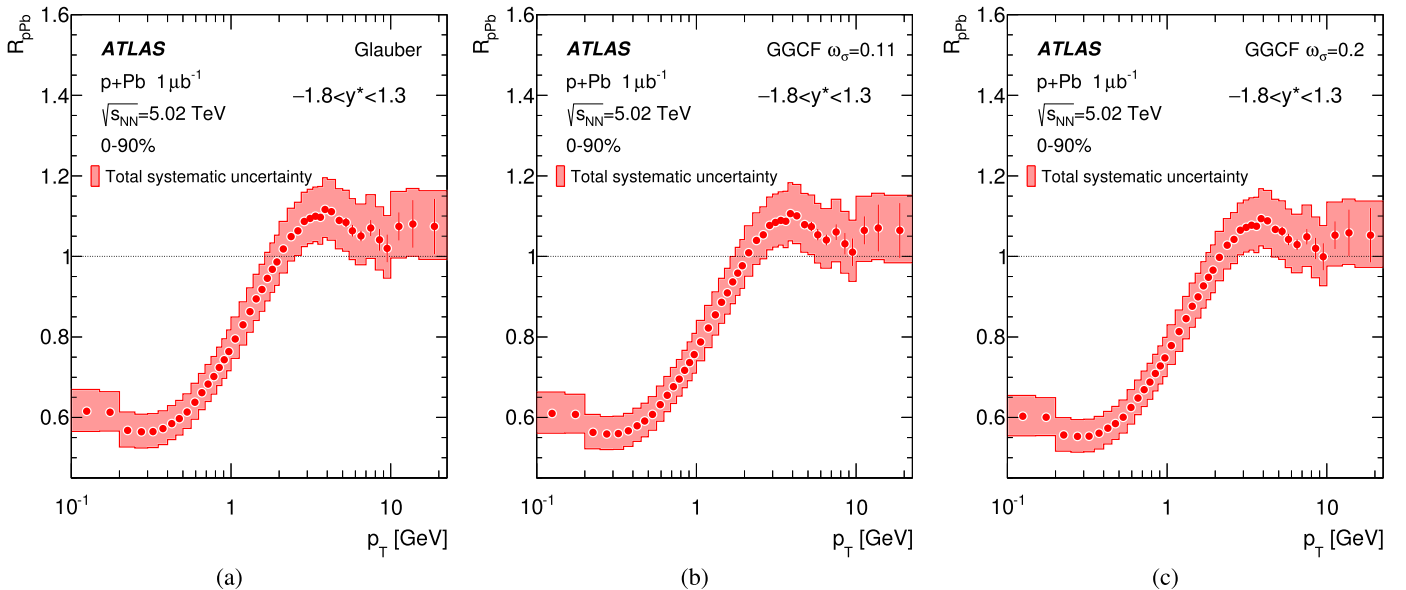


Fig. 5. R_{pPb} as a function of p_T integrated over rapidity range $-1.8 < y^* < 1.3$ for the 0–90% centrality interval for the three geometric models: (a) Glauber, (b) Glauber–Gribov with $\omega_\sigma = 0.11$ and (c) Glauber–Gribov with $\omega_\sigma = 0.2$.

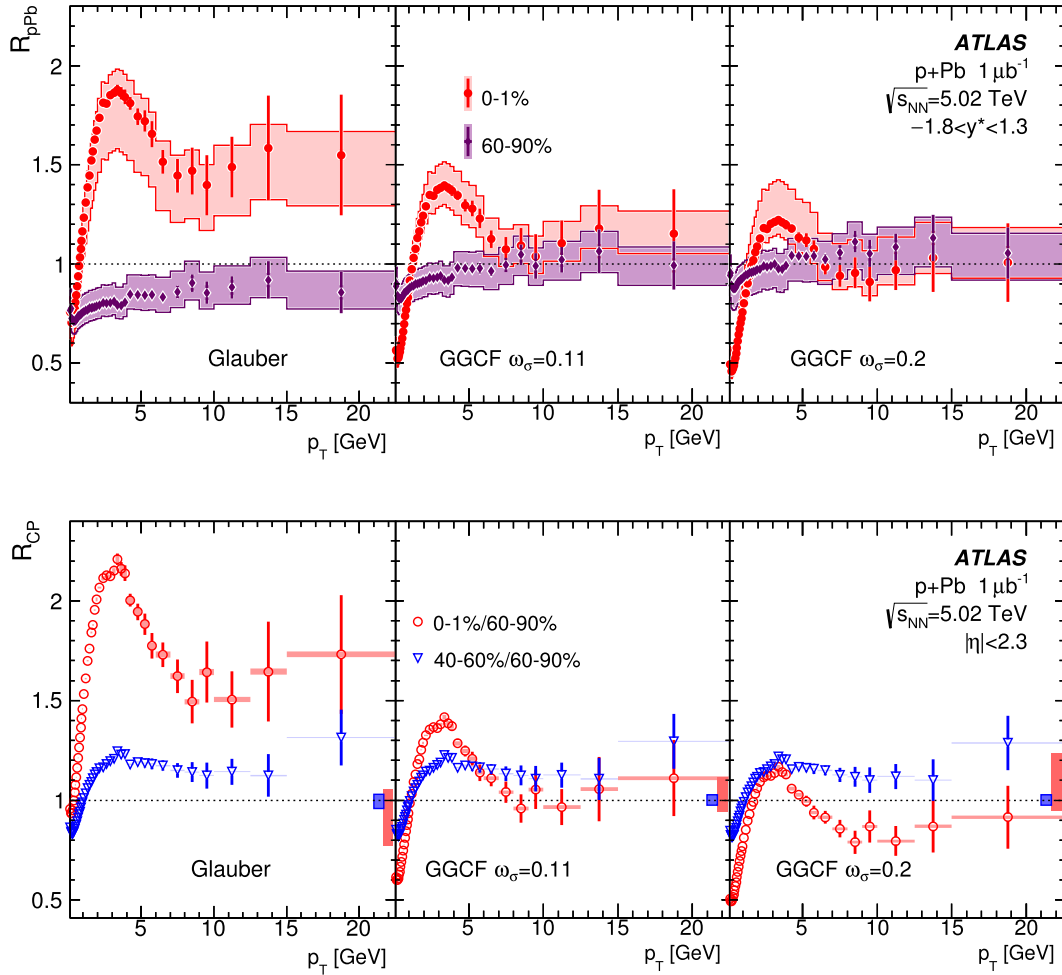


Fig. 7. (Top row) R_{pPb} as a function of p_T extracted from the invariant yields integrated over $-1.8 < y^* < 1.3$ for the 0–1% and 60–90% centrality intervals, and for different geometrical models used to calculate $\langle T_{pb} \rangle$: Glauber, Glauber–Gribov $\omega_\sigma = 0.11$ and Glauber–Gribov $\omega_\sigma = 0.2$; (bottom row) R_{CP} for 0–1% and 40–60% central collisions with respect to the 60–90% centrality interval, also for the geometrical models, which are used to calculate $\langle T_{pb} \rangle$. Statistical errors are indicated with vertical lines and the systematic uncertainties in the invariant yields are indicated by a shaded area. The total systematic uncertainties, which include the uncertainty in $\langle T_{pb} \rangle$ are indicated by lines of the same colour. The systematic uncertainties in the ratios of $\langle T_{pb} \rangle$ are indicated by boxes of the same colour.

a systematic uncertainty associated with the centrality determination.

In the pp data analysis, the systematic uncertainty assigned to the trigger efficiency is 1% for events containing two tracks and decreases rapidly with higher track multiplicities. A transverse momentum and rapidity independent uncertainty of 0.5% is assigned to the differential cross sections. In the same way as for the trigger efficiency, the uncertainty in the vertex reconstruction efficiency in the pp data analysis is taken to be 1% [43].

The systematic uncertainty in the interpolated pp cross section is needed for the correction applied to the interpolated data derived from simulated samples. The systematic uncertainty is taken to be the difference between the corrections obtained from PYTHIA8 and Herwig++, which are shown in Fig. 2(a). An additional systematic uncertainty is estimated by considering the relative difference between spectra obtained using the two different interpolation functions (\sqrt{s} or $\ln(\sqrt{s})$) as shown in Fig. 2(b).

The uncertainties in the calculated luminosity values for the corresponding pp data samples at $\sqrt{s} = 7$ TeV and $\sqrt{s} = 2.76$ TeV are 1.8% [59] and 2.7% [60], respectively. They are taken to be fully uncorrelated, thus the total uncertainty in the interpolated spectra at $\sqrt{s} = 5.02$ TeV is obtained by adding in quadrature the luminosity uncertainties of the inputs.

A summary of the systematic uncertainties in the charged-particle invariant yields in $p + Pb$ and pp data analysis is shown in Table 4. For R_{pPb} and R_{CP} , some of the errors are correlated between numerator and denominator. Track selection, particle composition, reweighting, trigger efficiency and vertex reconstruction uncertainties largely cancel for R_{CP} , since the corrections do not vary with centrality interval and the yields are compared in the same p_T and η bins. However, for R_{pPb} , there is little cancellation between $p + Pb$ and pp , since the results are presented as a function of y^* and the two systems are in two different centre-of-mass frames. The systematic uncertainties in $\langle T_{pb} \rangle$ and their ratios which are presented in Tables 1 and 2 are added in quadrature to the experimental uncertainties of R_{pPb} and R_{CP} respectively.

8. Results

The differential invariant yields of charged particles produced in $p + Pb$ collisions at $\sqrt{s} = 5.02$ TeV are presented as a function of charged-particle transverse momentum in Fig. 3 for several intervals of η and y^* .

Fig. 4 shows the invariant charged-particle yield as a function of y^* for $p_T > 0.1$ GeV in several centrality intervals. In collisions that are more central, the charged-particle yields become progressively more asymmetric, as shown in the ATLAS multiplicity

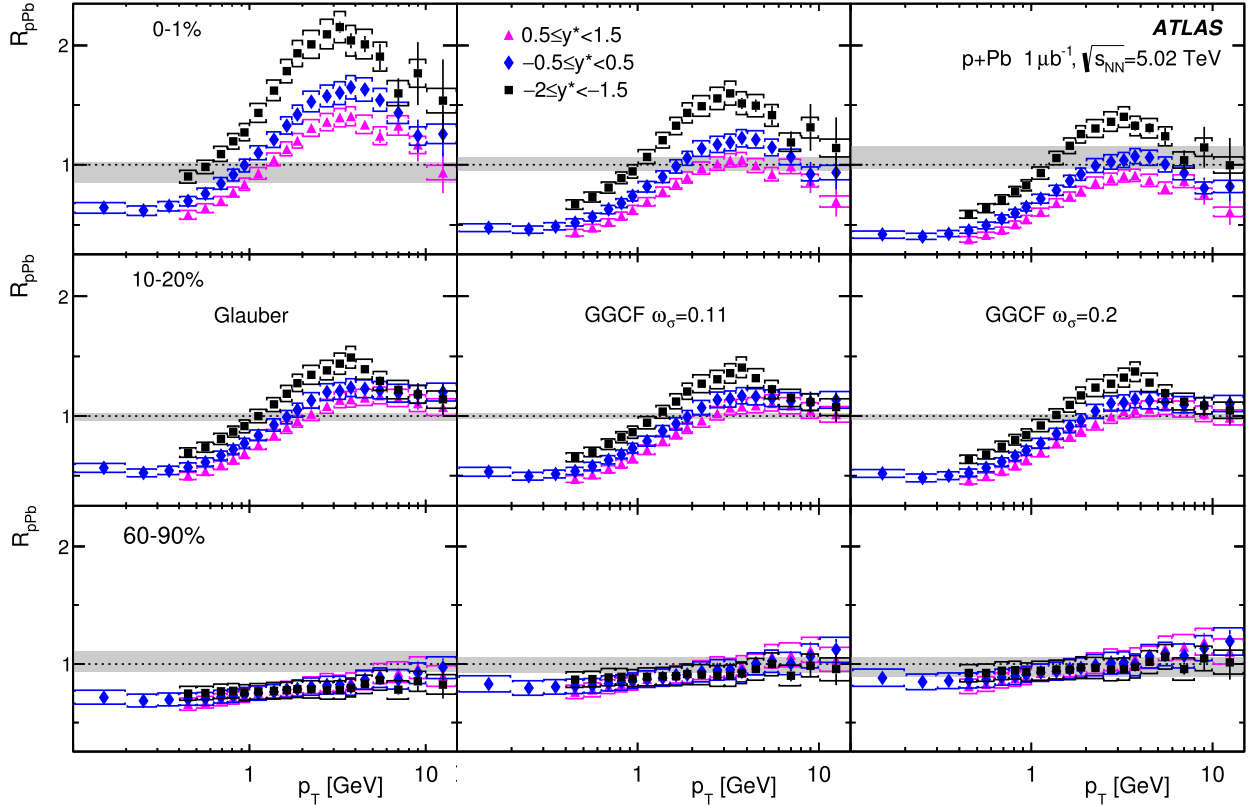


Fig. 8. The R_{pPb} values for the 0–1% (top panels), 10–20% (middle panels) and 60–90% (lower panels) centrality intervals. The data points are shown for three different rapidity intervals indicated in the legends. The columns correspond to the Glauber model (left), Glauber–Gribov model with $\omega_\sigma = 0.11$ (middle), and Glauber–Gribov model with $\omega_\sigma = 0.2$ (right). The grey band in each panel reflects the systematic uncertainty associated with the centrality interval and with the model assumption. Statistical uncertainties are shown with vertical bars and systematic uncertainties with brackets.

measurement [29], with more particles produced in the Pb-going direction than in the proton-going direction.

The transverse momentum dependence of R_{pPb} for the rapidity range $-1.8 < y^* < 1.3$ and for the 0–90% centrality interval is shown in Fig. 5 for the Glauber and Glauber–Gribov calculations of $\langle T_{Pb} \rangle$. The 0–90% $\langle T_{Pb} \rangle$ values which are given in Table 1 are similar for all three estimations, therefore the curves in all three panels show little difference. For $p_T > 8$ GeV, R_{pPb} is consistent with unity for all three models in the range of statistical and systematic uncertainties. The R_{pPb} values obtained using the Glauber model for the $\langle T_{Pb} \rangle$ calculation are compared to the ALICE [36] and CMS [40] measurements in Fig. 6. The results show the same basic features for the nuclear modification factors, although strict quantitative agreement is not expected as each measurement uses different rapidity intervals for the centrality determination and apply different event selection criteria to reject diffractive collisions.

The R_{pPb} and R_{CP} values are shown in Fig. 7 as a function of the charged-particle p_T in different centrality intervals and for different geometrical models used to calculate the value of $\langle T_{Pb} \rangle$. The data are integrated over $-1.8 < y^* < 1.3$ for R_{pPb} and $|\eta| < 2.3$ for R_{CP} . The data from the 0–1% centrality interval show similar features in all panels. Both R_{pPb} and R_{CP} increase with transverse momentum, reaching a maximum value at approximately $p_T \sim 3$ GeV and then decrease until reaching $p_T \sim 8$ GeV. Above this value, the ratios are approximately constant within the experimental uncertainties. The R_{pPb} and R_{CP} distributions in the region of the peak, $1 < p_T < 8$ GeV, have larger values for central events than for peripheral events. The magnitude of the peak depends quantitatively on the choice of geometrical model: the results obtained using the Glauber model have larger peak values than either of the Glauber–Gribov models. The magnitude of the peak relative

to the constant (plateau) region ($p_T \gtrsim 8$ GeV) is compatible for R_{CP} and R_{pPb} given the systematic uncertainties. The peripheral events show a smaller rise at low p_T . There is also only a slight indication of a peak at $p_T \sim 3$ GeV in R_{CP} and no pronounced indication of a peak in the R_{pPb} . The magnitude of R_{pPb} and R_{CP} in the constant region ($p_T \gtrsim 8$ GeV) is significantly above unity in the most central collisions for the Glauber model. In contrast, plateau regions are consistent with unity for Glauber–Gribov with $\omega_\sigma = 0.11$ and for Glauber–Gribov with $\omega_\sigma = 0.2$. For the peripheral centrality interval, the plateau region is consistent with unity for R_{pPb} and deviates from unity for R_{CP} . In peripheral collisions, R_{pPb} and R_{CP} depend only weakly on the choice of Glauber or Glauber–Gribov model in all panels.

Figs. 8 and 9 show R_{pPb} as a function of p_T and y^* respectively. The three panels in each column correspond to the most central (upper panels), mid-central (middle panels) and most peripheral (lower panels) centrality intervals. The three columns show the results from different geometrical models: Glauber (left), Glauber–Gribov with $\omega_\sigma = 0.11$ (middle), and Glauber–Gribov with $\omega_\sigma = 0.2$ (right). The grey box on each axis reflects the fractional systematic uncertainty corresponding to the centrality interval and geometric model, which applies to all data points in the panel. The systematic uncertainties in the invariant yields are indicated with boxes, and the vertical bars reflect the statistical uncertainty at each point. Fig. 8 shows R_{pPb} as a function of p_T . In the peripheral collisions, R_{pPb} is close to unity and shows almost no y^* dependence. The R_{pPb} values in the 10–20% and 0–1% centrality classes exhibit a stronger y^* dependence. To illustrate the y^* dependence, Fig. 9 shows the value of R_{pPb} measured for $2 < p_T < 3$ GeV (peaking region) compared to the value measured for $p_T > 8$ GeV (the plateau region) as a function of y^* , for different centrality intervals

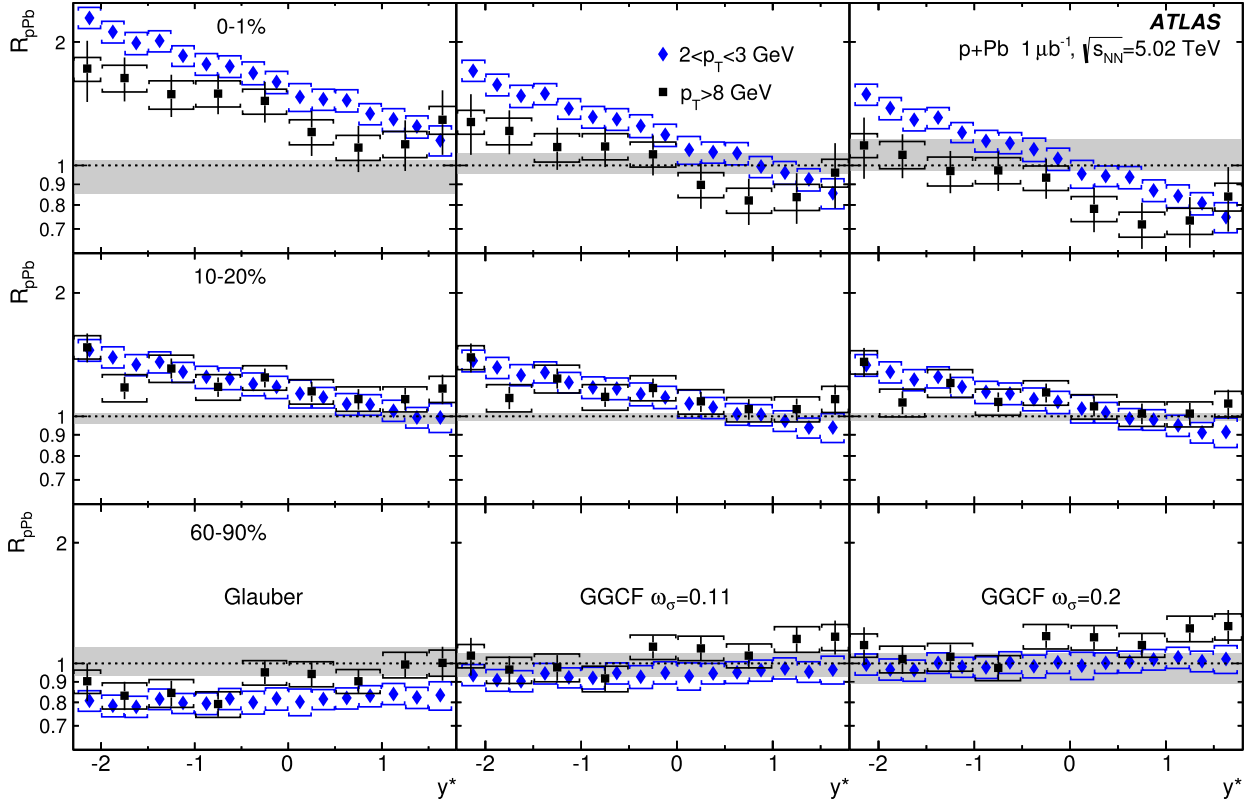


Fig. 9. The R_{pPb} values for the 0–1% (top panels), 10–20% (middle panels) and 60–90% (lower panels) centrality intervals. The data points are shown for two different transverse momentum intervals indicated in the legends. The columns correspond to the Glauber model (left), Glauber–Gribov model with $\omega_\sigma = 0.11$ (middle), and Glauber–Gribov model with $\omega_\sigma = 0.2$ (right). The grey box in each panel reflects the systematic uncertainty associated with the centrality interval and with the model assumption. Statistical uncertainties are shown with vertical bars and systematic uncertainties with brackets.

and geometrical models. In both regions, R_{pPb} increases with y^* towards the Pb-going direction and with increasingly central collisions. The variation of R_{pPb} with centrality is much larger for the peaking region than for the plateau region. The R_{pPb} values in the two centrality intervals have similar variations as a function of y^* .

9. Conclusions

This paper presents measurements of the per-event charged-particle multiplicity in $1 \mu\text{b}^{-1}$ of $p + \text{Pb}$ collisions at $\sqrt{s_{NN}} = 5.02 \text{ TeV}$ with the ATLAS detector at the LHC. The differential particle yields in $p + \text{Pb}$ collisions are compared with those in pp collisions using the nuclear modification factor, R_{pPb} . The pp reference cross sections at $\sqrt{s_{NN}} = 5.02 \text{ TeV}$ are constructed by interpolation of measurements performed at $\sqrt{s} = 2.76 \text{ TeV}$ and 7 TeV . The measurements of R_{pPb} are presented in the centre-of-mass frame in the rapidity range $-2.3 < y^* < 1.8$ and transverse momentum $0.1 < p_T < 22 \text{ GeV}$. The measurements of R_{CP} are presented in the laboratory frame over the pseudorapidity range $-2.3 < \eta < 2.3$ and the same transverse momentum region. The results for R_{pPb} and R_{CP} are presented as a function of transverse momentum and centrality in different y^* and η intervals and also as a function of rapidity for different p_T intervals. The results are using two choices of geometric model (Glauber and Glauber–Gribov colour-fluctuation model with $\omega_\sigma = 0.11$ and $\omega_\sigma = 0.2$) for the calculation of the nuclear thickness function $\langle T_{Pb} \rangle$ in the selected centrality intervals.

The measured nuclear modification factors are observed to increase with transverse momentum from 0.1 GeV to a peak value at $p_T \sim 3 \text{ GeV}$, at which point they decrease slowly up to $p_T \sim 8 \text{ GeV}$.

Above $p_T \sim 8 \text{ GeV}$ the nuclear modification factors are constant within the experimental uncertainties.

The magnitude of the peak strongly depends both on rapidity and centrality. It increases from the proton beam direction to the Pb beam direction and from peripheral to central collisions. The constant region above $p_T \sim 8 \text{ GeV}$ is less sensitive to the different centrality and (pseudo)rapidity intervals. Measurements of the absolute magnitudes of R_{pPb} integrated over centrality and averaged over rapidity are similar for different geometric models, although their centrality dependence is strongly influenced by the choice of geometric model. Such behaviour is directly related to the multiplicity dependence of the particle production. In particular, there is an enhancement of protons with respect to pions at intermediate p_T , as observed by experiments at the LHC as well as at lower energies.

The momentum and rapidity dependence of the nuclear modification factor measured in $p + \text{Pb}$ collisions assist in determining the correct theoretical description of the cold nuclear matter effects. The results will also be important for constraining the choice of Glauber or Glauber–Gribov model parameters suitable to use in determining the average values for the number of participating nucleons and the nuclear thickness function in $p + \text{Pb}$ collisions.

Acknowledgements

We thank CERN for the very successful operation of the LHC, as well as the support staff from our institutions without whom ATLAS could not be operated efficiently.

We acknowledge the support of ANPCyT, Argentina; YerPhI, Armenia; ARC, Australia; BMWFW and FWF, Austria; ANAS, Azerbaijan; SSTC, Belarus; CNPq and FAPESP, Brazil; NSERC, NRC and

CFI, Canada; CERN; CONICYT, Chile; CAS, MOST and NSFC, China; COLCIENCIAS, Colombia; MSMT CR, MPO CR and VSC CR, Czech Republic; DNRF and DNSRC, Denmark; IN2P3-CNRS, CEA-DSM/IRFU, France; GNSF, Georgia; BMBF, HGF, and MPG, Germany; GSRT, Greece; RGC, Hong Kong SAR, China; ISF, I-CORE and Benoziyo Center, Israel; INFN, Italy; MEXT and JSPS, Japan; CNRS, Morocco; FOM and NWO, Netherlands; RCN, Norway; MNISW and NCN, Poland; FCT, Portugal; MNE/IFA, Romania; MES of Russia and NRC KI, Russian Federation; JINR; MESTD, Serbia; MSSR, Slovakia; ARRS and MIZŠ, Slovenia; DST/NRF, South Africa; MINECO, Spain; SRC and Knut and Alice Wallenberg Foundation, Sweden; SERI, SNSF and Cantons of Bern and Geneva, Switzerland; MOST, Taiwan; TAEK, Turkey; STFC, United Kingdom; DOE and NSF, United States of America. In addition, individual groups and members have received support from BCKDF, the Canada Council, CANARIE, CRC, Compute Canada, FQRNT, and the Ontario Innovation Trust, Canada; EPLANET, ERC, FP7, Horizon 2020 and Marie Skłodowska-Curie Actions, European Union; Investissements d'Avenir Labex and Idex, ANR, Région Auvergne and Fondation Partager le Savoir, France; DFG and AvH Foundation, Germany; Herakleitos, Thales and Aristeia programmes co-financed by EU-ESF and the Greek NSRF; BSF, GIF and Minerva, Israel; BRF, Norway; Generalitat de Catalunya, Generalitat Valenciana, Spain; the Royal Society and Leverhulme Trust, United Kingdom.

The crucial computing support from all WLCG partners is acknowledged gratefully, in particular from CERN, the ATLAS Tier-1 facilities at TRIUMF (Canada), NDGF (Denmark, Norway, Sweden), CC-IN2P3 (France), KIT/GridKA (Germany), INFN-CNAF (Italy), NL-T1 (Netherlands), PIC (Spain), ASGC (Taiwan), RAL (UK) and BNL (USA), the Tier-2 facilities worldwide and large non-WLCG resource providers. Major contributors of computing resources are listed in Ref. [61].

References

- [1] J. Albacete, et al., Predictions for $p + \text{Pb}$ collisions at $\sqrt{s_{NN}} = 5$ TeV, *Int. J. Mod. Phys. E* 22 (2013) 1330007, arXiv:1301.3395 [hep-ph].
- [2] B.Z. Kopeliovich, A. Schafer, A.V. Tarasov, Nonperturbative effects in gluon radiation and photoproduction of quark pairs, *Phys. Rev. D* 62 (2000) 054022, arXiv:hep-ph/9908245.
- [3] J.-w. Qiu, I. Vitev, Coherent QCD multiple scattering in proton-nucleus collisions, *Phys. Lett. B* 632 (2006) 507–511, arXiv:hep-ph/0405068.
- [4] K. Eskola, H. Paukkunen, C. Salgado, EPS09: a new generation of NLO and LO nuclear parton distribution functions, *J. High Energy Phys.* 0904 (2009) 065, arXiv:0902.4154 [hep-ph].
- [5] K. Eskola, V. Kolhinen, P. Ruuskanen, Scale evolution of nuclear parton distributions, *Nucl. Phys. B* 535 (1998) 351–371, arXiv:hep-ph/9802350.
- [6] I. Helenius, et al., Impact-parameter dependent nuclear parton distribution functions: EPS09s and EKS98s and their applications in nuclear hard processes, *J. High Energy Phys.* 1207 (2012) 073, arXiv:1205.5359 [hep-ph].
- [7] M. Hirai, S. Kumano, T.-H. Nagai, Determination of nuclear parton distribution functions and their uncertainties in next-to-leading order, *Phys. Rev. C* 76 (2007) 065207, arXiv:0709.3038 [hep-ph].
- [8] D. de Florian, et al., Global analysis of nuclear parton distributions, *Phys. Rev. D* 85 (2012) 074028, arXiv:1112.6324 [hep-ph].
- [9] L.D. McLerran, R. Venugopalan, Computing quark and gluon distribution functions for very large nuclei, *Phys. Rev. D* 49 (1994) 2233–2241, arXiv:hep-ph/9309289.
- [10] D. Kharzeev, Y.V. Kovchegov, K. Tuchin, Cronin effect and high $p(T)$ suppression in pA collisions, *Phys. Rev. D* 68 (2003) 094013, arXiv:hep-ph/0307037.
- [11] J.L. Albacete, C. Marquet, Single inclusive hadron production at RHIC and the LHC from the color glass condensate, *Phys. Lett. B* 687 (2010) 174–179, arXiv:1001.1378 [hep-ph].
- [12] P. Tribedy, R. Venugopalan, QCD saturation at the LHC: comparisons of models to pp and A + A data and predictions for $p + \text{Pb}$ collisions, *Phys. Lett. B* 710 (2012) 125–133, arXiv:1112.2445 [hep-ph].
- [13] Z.-B. Kang, I. Vitev, H. Xing, Nuclear modification of high transverse momentum particle production in $p + \text{A}$ collisions at RHIC and LHC, *Phys. Lett. B* 718 (2012) 482–487, arXiv:1209.6030 [hep-ph].
- [14] J. Jalilian-Marian, A.H. Rezaeian, Hadron production in pA collisions at the LHC from the color glass condensate, *Phys. Rev. D* 85 (2012) 014017, arXiv:1110.2810 [hep-ph].
- [15] J.L. Albacete, et al., CGC predictions for $p + \text{Pb}$ collisions at the LHC, *Nucl. Phys. A* 897 (2013) 1–27, arXiv:1209.2001 [hep-ph].
- [16] A.H. Rezaeian, CGC predictions for $p + \text{A}$ collisions at the LHC and signature of QCD saturation, *Phys. Lett. B* 718 (2013) 1058–1069, arXiv:1210.2385 [hep-ph].
- [17] J.W. Cronin, et al., Production of hadrons at large transverse momentum at 200, 300, and 400 GeV, *Phys. Rev. D* 11 (1975) 3105–3123.
- [18] B. Kopeliovich, et al., Cronin effect in hadron production off nuclei, *Phys. Rev. Lett.* 88 (2002) 232303, arXiv:hep-ph/0201010.
- [19] I. Vitev, Initial state parton broadening and energy loss probed in $d + \text{Au}$ at RHIC, *Phys. Lett. B* 562 (2003) 36–44, arXiv:nucl-th/0302002.
- [20] K. Werner, et al., Analysing radial flow features in $p + \text{Pb}$ and pp collisions at several TeV by studying identified particle production in EPOS3, *Phys. Rev. C* 89 (2014) 064903, arXiv:1312.1233 [nucl-th].
- [21] CMS Collaboration, Observation of long-range near-side angular correlations in proton–proton collisions at the LHC, *J. High Energy Phys.* 09 (2010) 091, arXiv:1009.4122 [hep-ex].
- [22] CMS Collaboration, Observation of long-range near-side angular correlations in proton–lead collisions at the LHC, *Phys. Lett. B* 718 (2013) 795–814, arXiv:1210.5482 [nucl-ex].
- [23] ALICE Collaboration, B. Abelev, et al., Long-range angular correlations on the near and away side in $p\text{-Pb}$ collisions at $\sqrt{s_{NN}} = 5.02$ TeV, *Phys. Lett. B* 719 (2013) 29–41, arXiv:1212.2001 [nucl-ex].
- [24] ATLAS Collaboration, Measurement with the ATLAS detector of multi-particle azimuthal correlations in $p + \text{Pb}$ collisions at $\sqrt{s_{NN}} = 5.02$ TeV, *Phys. Lett. B* 725 (2013) 60–78, arXiv:1303.2084 [hep-ex].
- [25] CMS Collaboration, Multiplicity and transverse momentum dependence of two- and four-particle correlations in pPb and PbPb collisions, *Phys. Lett. B* 724 (2013) 213–240, arXiv:1305.0609 [nucl-ex].
- [26] P. Božek, W. Broniowski, Collective dynamics in high-energy proton–nucleus collisions, *Phys. Rev. C* 88 (2013) 014903, arXiv:1304.3044 [nucl-th].
- [27] K. Dusling, R. Venugopalan, Comparison of the color glass condensate to di-hadron correlations in proton–proton and proton–nucleus collisions, *Phys. Rev. D* 87 (2013) 094034, arXiv:1302.7018 [hep-ph].
- [28] G. Barnaföldi, et al., Predictions for $p + \text{Pb}$ at 4.4A TeV to test initial state nuclear shadowing at energies available at the CERN Large Hadron Collider, *Phys. Rev. C* 85 (2012) 024903, arXiv:1111.3646 [nucl-th].
- [29] ATLAS Collaboration, Measurement of the centrality dependence of the charged-particle pseudorapidity distribution in proton–lead collisions at $\sqrt{s_{NN}} = 5.02$ TeV with the ATLAS detector, *Eur. Phys. J. C* 76 (2016) 199, arXiv:1508.00848 [hep-ex].
- [30] BRAHMS Collaboration, I. Arsene, et al., Transverse momentum spectra in Au + Au and d + Au collisions at $\sqrt{s} = 200$ GeV and the pseudorapidity dependence of high p_T suppression, *Phys. Rev. Lett.* 91 (2003) 072305, arXiv:nucl-ex/0307003.
- [31] PHENIX Collaboration, S.S. Adler, et al., Absence of suppression in particle production at large transverse momentum in $\sqrt{s_{NN}} = 200$ GeV $d + \text{Au}$ collisions, *Phys. Rev. Lett.* 91 (2003) 072303, arXiv:nucl-ex/0306021.
- [32] PHOBOS Collaboration, B.B. Back, et al., Centrality dependence of charged hadron transverse momentum spectra in $d + \text{Au}$ collisions at $\sqrt{s_{NN}} = 200$ GeV, *Phys. Rev. Lett.* 91 (2003) 072302, arXiv:nucl-ex/0306025.
- [33] STAR Collaboration, J. Adams, et al., Evidence from $d + \text{Au}$ measurements for final state suppression of high p_T hadrons in Au + Au collisions at RHIC, *Phys. Rev. Lett.* 91 (2003) 072304, arXiv:nucl-ex/0306024.
- [34] PHENIX Collaboration, A. Adare, et al., Spectra and ratios of identified particles in Au + Au and $d + \text{Au}$ collisions at $\sqrt{s_{NN}} = 200$ GeV, *Phys. Rev. C* 88 (2) (2013) 024906.
- [35] STAR Collaboration, J. Adams, et al., Identified hadron spectra at large transverse momentum in $p + p$ and $d + \text{Au}$ collisions at $\sqrt{s_{NN}} = 200$ GeV, *Phys. Lett. B* 637 (2006) 161–169.
- [36] ALICE Collaboration, B. Abelev, et al., Transverse momentum distribution and nuclear modification factor of charged particles in $p + \text{Pb}$ collisions at $\sqrt{s_{NN}} = 5.02$ TeV, *Phys. Rev. Lett.* 110 (2013) 082302, arXiv:1210.4520 [nucl-ex].
- [37] ALICE Collaboration, B. Abelev, et al., Transverse momentum dependence of inclusive primary charged-particle production in $p + \text{Pb}$ collisions at $\sqrt{s_{NN}} = 5.02$ TeV, *Eur. Phys. J. C* 74 (2014) 3054, arXiv:1405.2737 [nucl-ex].
- [38] ALICE Collaboration, J. Adam, et al., Centrality dependence of particle production in $p + \text{Pb}$ collisions at $\sqrt{s_{NN}} = 5.02$ TeV, *Phys. Rev. C* 91 (2015) 064905, arXiv:1412.6828 [nucl-ex].
- [39] ALICE Collaboration, J. Adam, et al., Multiplicity dependence of charged pion, kaon, and (anti)proton production at large transverse momentum in $p\text{-Pb}$ collisions at $\sqrt{s_{NN}} = 5.02$ TeV, *Phys. Lett. B* 760 (2016) 720–735.
- [40] CMS Collaboration, Nuclear effects on the transverse momentum spectra of charged particles in $p + \text{Pb}$ collisions at $\sqrt{s_{NN}} = 5.02$ TeV, *Eur. Phys. J. C* 75 (2015) 237, arXiv:1502.05387 [nucl-ex].
- [41] ATLAS Collaboration, The ATLAS experiment at the CERN Large Hadron Collider, *J. Instrum.* 3 (2008) S08003.
- [42] ATLAS Collaboration, Performance of the ATLAS trigger system in 2010, *Eur. Phys. J. C* 72 (2012) 1849, arXiv:1110.1530 [hep-ex].

- [43] ATLAS Collaboration, Charged-particle multiplicities in pp interactions measured with the ATLAS detector at the LHC, *New J. Phys.* **13** (2011) 053033, arXiv:1012.5104 [hep-ex].
- [44] ATLAS Collaboration, Measurement of inclusive jet and dijet cross sections in proton–proton collisions at 7 TeV centre-of-mass energy with the ATLAS detector, *Eur. Phys. J. C* **71** (2011) 1512, arXiv:1009.5908 [hep-ex].
- [45] X.-N. Wang, M. Gyulassy, HIJING: a Monte Carlo model for multiple jet production in p p, p A and A A collisions, *Phys. Rev. D* **44** (1991) 3501–3516.
- [46] S. Agostinelli, et al., GEANT4: a simulation toolkit, *Nucl. Instrum. Methods A* **506** (2003) 250–303.
- [47] ATLAS Collaboration, The ATLAS simulation infrastructure, *Eur. Phys. J. C* **70** (2010) 823–874.
- [48] T. Sjöstrand, S. Mrenna, P.Z. Skands, PYTHIA 6.4 physics and manual, *J. High Energy Phys.* **0605** (2006) 026, arXiv:hep-ph/0603175.
- [49] ATLAS Collaboration, ATLAS tunes of PYTHIA 6 and Pythia 8 for MC11, ATL-PHYS-PUB-2011-009, <http://cds.cern.ch/record/1363300>, 2011.
- [50] T. Sjöstrand, S. Mrenna, P.Z. Skands, A brief introduction to PYTHIA 8.1, *Comput. Phys. Commun.* **178** (2008) 852–867, arXiv:0710.3820 [hep-ph].
- [51] J.M. Katzy, QCD Monte-Carlo model tunes for the LHC, *Prog. Part. Nucl. Phys.* **73** (2013) 141–187.
- [52] M. Bahr, et al., Herwig++ physics and manual, *Eur. Phys. J. C* **58** (2008) 639–707, arXiv:0803.0883 [hep-ph].
- [53] M.L. Miller, et al., Glauber modeling in high energy nuclear collisions, *Annu. Rev. Nucl. Part. Sci.* **57** (2007) 205–243.
- [54] V. Guzey, M. Strikman, Proton–nucleus scattering and cross section fluctuations at RHIC and LHC, *Phys. Lett. B* **633** (2006) 245–252, arXiv:hep-ph/0505088.
- [55] M. Alvioli, M. Strikman, Color fluctuation effects in proton–nucleus collisions, *Phys. Lett. B* **722** (2013) 347–354, arXiv:1301.0728 [hep-ph].
- [56] ATLAS Collaboration, Single track performance of the inner detector new track reconstruction (NEWT), ATL-INDET-PUB-2008-002, <http://cds.cern.ch/record/1092934>, 2008.
- [57] ATLAS Collaboration, A study of the material in the ATLAS inner detector using secondary hadronic interactions, *J. Instrum.* **7** (2012) P01013, arXiv:1110.6191 [hep-ex].
- [58] ALICE Collaboration, B. Abelev, et al., Multiplicity dependence of pion, kaon, proton and lambda production in p + Pb collisions at $\sqrt{s_{NN}} = 5.02$ TeV, *Phys. Lett. B* **728** (2014) 25–38, arXiv:1307.6796 [nucl-ex].
- [59] ATLAS Collaboration, Improved luminosity determination in pp collisions at $\sqrt{s} = 7$ TeV using the ATLAS detector at the LHC, *Eur. Phys. J. C* **73** (2013) 2518, arXiv:1302.4393 [hep-ex].
- [60] ATLAS Collaboration, Measurement of the inclusive jet cross section in pp collisions at $\sqrt{s} = 2.76$ TeV and comparison to the inclusive jet cross section at $\sqrt{s} = 7$ TeV using the ATLAS detector, *Eur. Phys. J. C* **73** (2013) 2509, arXiv:1304.4739 [hep-ex].
- [61] ATLAS Collaboration, ATLAS computing acknowledgements 2016–2017, ATL-GEN-PUB-2016-002, <http://cds.cern.ch/record/2202407>, 2016.

ATLAS Collaboration

G. Aad⁸⁷, B. Abbott¹¹⁴, J. Abdallah⁶⁵, O. Abidinov¹², B. Abeloos¹¹⁸, R. Aben¹⁰⁸, O.S. AbouZeid¹³⁸, N.L. Abraham¹⁵⁰, H. Abramowicz¹⁵⁴, H. Abreu¹⁵³, R. Abreu¹¹⁷, Y. Abulaiti^{147a,147b}, B.S. Acharya^{164a,164b,a}, L. Adamczyk^{40a}, D.L. Adams²⁷, J. Adelman¹⁰⁹, S. Adomeit¹⁰¹, T. Adye¹³², A.A. Affolder⁷⁶, T. Agatonovic-Jovin¹⁴, J. Agricola⁵⁶, J.A. Aguilar-Saavedra^{127a,127f}, S.P. Ahlen²⁴, F. Ahmadov^{67,b}, G. Aielli^{134a,134b}, H. Akerstedt^{147a,147b}, T.P.A. Åkesson⁸³, A.V. Akimov⁹⁷, G.L. Alberghi^{22a,22b}, J. Albert¹⁶⁹, S. Albrand⁵⁷, M.J. Alconada Verzini⁷³, M. Aleksa³², I.N. Aleksandrov⁶⁷, C. Alexa^{28b}, G. Alexander¹⁵⁴, T. Alexopoulos¹⁰, M. Alhroob¹¹⁴, M. Aliev^{75a,75b}, G. Alimonti^{93a}, J. Alison³³, S.P. Alkire³⁷, B.M.M. Allbrooke¹⁵⁰, B.W. Allen¹¹⁷, P.P. Allport¹⁹, A. Aloisio^{105a,105b}, A. Alonso³⁸, F. Alonso⁷³, C. Alpigiani¹³⁹, M. Alstady⁸⁷, B. Alvarez Gonzalez³², D. Álvarez Piqueras¹⁶⁷, M.G. Alviggi^{105a,105b}, B.T. Amadio¹⁶, K. Amako⁶⁸, Y. Amaral Coutinho^{26a}, C. Amelung²⁵, D. Amidei⁹¹, S.P. Amor Dos Santos^{127a,127c}, A. Amorim^{127a,127b}, S. Amoroso³², G. Amundsen²⁵, C. Anastopoulos¹⁴⁰, L.S. Ancu⁵¹, N. Andari¹⁰⁹, T. Andeen¹¹, C.F. Anders^{60b}, G. Anders³², J.K. Anders⁷⁶, K.J. Anderson³³, A. Andreazza^{93a,93b}, V. Andrei^{60a}, S. Angelidakis⁹, I. Angelozzi¹⁰⁸, P. Anger⁴⁶, A. Angerami³⁷, F. Anghinolfi³², A.V. Anisenkov^{110,c}, N. Anjos¹³, A. Annovi^{125a,125b}, M. Antonelli⁴⁹, A. Antonov⁹⁹, F. Anulli^{133a}, M. Aoki⁶⁸, L. Aperio Bella¹⁹, G. Arabidze⁹², Y. Arai⁶⁸, J.P. Araque^{127a}, A.T.H. Arce⁴⁷, F.A. Arduh⁷³, J.-F. Arguin⁹⁶, S. Argyropoulos⁶⁵, M. Arik^{20a}, A.J. Armbruster¹⁴⁴, L.J. Armitage⁷⁸, O. Arnaez³², H. Arnold⁵⁰, M. Arratia³⁰, O. Arslan²³, A. Artamonov⁹⁸, G. Artoni¹²¹, S. Artz⁸⁵, S. Asai¹⁵⁶, N. Asbah⁴⁴, A. Ashkenazi¹⁵⁴, B. Åsman^{147a,147b}, L. Asquith¹⁵⁰, K. Assamagan²⁷, R. Astalos^{145a}, M. Atkinson¹⁶⁶, N.B. Atlay¹⁴², K. Augsten¹²⁹, G. Avolio³², B. Axen¹⁶, M.K. Ayoub¹¹⁸, G. Azuelos^{96,d}, M.A. Baak³², A.E. Baas^{60a}, M.J. Baca¹⁹, H. Bachacou¹³⁷, K. Bachas^{75a,75b}, M. Backes³², M. Backhaus³², P. Bagiacchi^{133a,133b}, P. Bagnaia^{133a,133b}, Y. Bai^{35a}, J.T. Baines¹³², O.K. Baker¹⁷⁶, E.M. Baldin^{110,c}, P. Balek¹³⁰, T. Balestri¹⁴⁹, F. Balli¹³⁷, W.K. Balunas¹²³, E. Banas⁴¹, Sw. Banerjee^{173,e}, A.A.E. Bannoura¹⁷⁵, L. Barak³², E.L. Barberio⁹⁰, D. Barberis^{52a,52b}, M. Barbero⁸⁷, T. Barillari¹⁰², T. Barklow¹⁴⁴, N. Barlow³⁰, S.L. Barnes⁸⁶, B.M. Barnett¹³², R.M. Barnett¹⁶, Z. Barnovska⁵, A. Baronecelli^{135a}, G. Barone²⁵, A.J. Barr¹²¹, L. Barranco Navarro¹⁶⁷, F. Barreiro⁸⁴, J. Barreiro Guimarães da Costa^{35a}, R. Bartoldus¹⁴⁴, A.E. Barton⁷⁴, P. Bartos^{145a}, A. Basalaev¹²⁴, A. Bassalat¹¹⁸, R.L. Bates⁵⁵, S.J. Batista¹⁵⁹, J.R. Batley³⁰, M. Battaglia¹³⁸, M. Bause^{133a,133b}, F. Bauer¹³⁷, H.S. Bawa^{144,f}, J.B. Beacham¹¹², M.D. Beattie⁷⁴, T. Beau⁸², P.H. Beauchemin¹⁶², P. Bechtel²³, H.P. Beck^{18,g}, K. Becker¹²¹, M. Becker⁸⁵, M. Beckingham¹⁷⁰, C. Becot¹¹¹, A.J. Beddall^{20e}, A. Beddall^{20b}, V.A. Bednyakov⁶⁷, M. Bedognetti¹⁰⁸, C.P. Bee¹⁴⁹, L.J. Beemster¹⁰⁸, T.A. Beermann³², M. Begel²⁷, J.K. Behr⁴⁴, C. Belanger-Champagne⁸⁹, A.S. Bell⁸⁰, G. Bella¹⁵⁴, L. Bellagamba^{22a}, A. Bellerive³¹, M. Bellomo⁸⁸, K. Belotskiy⁹⁹, O. Beltramello³², N.L. Belyaev⁹⁹, O. Benary¹⁵⁴, D. Benchekroun^{136a}, M. Bender¹⁰¹, K. Bendtz^{147a,147b}, N. Benekos¹⁰, Y. Benhammou¹⁵⁴, E. Benhar Noccioli¹⁷⁶, J. Benitez⁶⁵, D.P. Benjamin⁴⁷, J.R. Bensinger²⁵, S. Bentvelsen¹⁰⁸, L. Beresford¹²¹, M. Beretta⁴⁹, D. Berge¹⁰⁸, E. Bergeaas Kuutmann¹⁶⁵, N. Berger⁵,

J. Beringer¹⁶, S. Berlendis⁵⁷, N.R. Bernard⁸⁸, C. Bernius¹¹¹, F.U. Bernlochner²³, T. Berry⁷⁹, P. Berta¹³⁰, C. Bertella⁸⁵, G. Bertoli^{147a,147b}, F. Bertolucci^{125a,125b}, I.A. Bertram⁷⁴, C. Bertsche⁴⁴, D. Bertsche¹¹⁴, G.J. Besjes³⁸, O. Bessidskaia Bylund^{147a,147b}, M. Bessner⁴⁴, N. Besson¹³⁷, C. Betancourt⁵⁰, S. Bethke¹⁰², A.J. Bevan⁷⁸, W. Bhimji¹⁶, R.M. Bianchi¹²⁶, L. Bianchini²⁵, M. Bianco³², O. Biebel¹⁰¹, D. Biedermann¹⁷, R. Bielski⁸⁶, N.V. Biesuz^{125a,125b}, M. Biglietti^{135a}, J. Bilbao De Mendizabal⁵¹, H. Bilokon⁴⁹, M. Bindi⁵⁶, S. Binet¹¹⁸, A. Bingul^{20b}, C. Bini^{133a,133b}, S. Biondi^{22a,22b}, D.M. Bjergaard⁴⁷, C.W. Black¹⁵¹, J.E. Black¹⁴⁴, K.M. Black²⁴, D. Blackburn¹³⁹, R.E. Blair⁶, J.-B. Blanchard¹³⁷, J.E. Blanco⁷⁹, T. Blazek^{145a}, I. Bloch⁴⁴, C. Blocker²⁵, W. Blum^{85,*}, U. Blumenschein⁵⁶, S. Blunier^{34a}, G.J. Bobbink¹⁰⁸, V.S. Bobrovnikov^{110,c}, S.S. Bocchetta⁸³, A. Bocci⁴⁷, C. Bock¹⁰¹, M. Boehler⁵⁰, D. Boerner¹⁷⁵, J.A. Bogaerts³², D. Bogavac¹⁴, A.G. Bogdanchikov¹¹⁰, C. Bohm^{147a}, V. Boisvert⁷⁹, P. Bokan¹⁴, T. Bold^{40a}, A.S. Boldyrev^{164a,164c}, M. Bomben⁸², M. Bona⁷⁸, M. Boonekamp¹³⁷, A. Borisov¹³¹, G. Borissov⁷⁴, J. Bortfeldt¹⁰¹, D. Bortoletto¹²¹, V. Bortolotto^{62a,62b,62c}, K. Bos¹⁰⁸, D. Boscherini^{22a}, M. Bosman¹³, J.D. Bossio Sola²⁹, J. Boudreau¹²⁶, J. Bouffard², E.V. Bouhova-Thacker⁷⁴, D. Boumediene³⁶, C. Bourdarios¹¹⁸, S.K. Boutle⁵⁵, A. Boveia³², J. Boyd³², I.R. Boyko⁶⁷, J. Bracinik¹⁹, A. Brandt⁸, G. Brandt⁵⁶, O. Brandt^{60a}, U. Bratzler¹⁵⁷, B. Brau⁸⁸, J.E. Brau¹¹⁷, H.M. Braun^{175,*}, W.D. Breaden Madden⁵⁵, K. Brendlinger¹²³, A.J. Brennan⁹⁰, L. Brenner¹⁰⁸, R. Brenner¹⁶⁵, S. Bressler¹⁷², T.M. Bristow⁴⁸, D. Britton⁵⁵, D. Britzger⁴⁴, F.M. Brochu³⁰, I. Brock²³, R. Brock⁹², G. Brooijmans³⁷, T. Brooks⁷⁹, W.K. Brooks^{34b}, J. Brosamer¹⁶, E. Brost¹¹⁷, J.H. Broughton¹⁹, P.A. Bruckman de Renstrom⁴¹, D. Bruncko^{145b}, R. Bruneliere⁵⁰, A. Bruni^{22a}, G. Bruni^{22a}, B.H. Brunt³⁰, M. Bruschi^{22a}, N. Bruscino²³, P. Bryant³³, L. Bryngemark⁸³, T. Buanes¹⁵, Q. Buat¹⁴³, P. Buchholz¹⁴², A.G. Buckley⁵⁵, I.A. Budagov⁶⁷, F. Buehrer⁵⁰, M.K. Bugge¹²⁰, O. Bulekov⁹⁹, D. Bullock⁸, H. Burckhart³², S. Burdin⁷⁶, C.D. Burgard⁵⁰, B. Burghgrave¹⁰⁹, K. Burka⁴¹, S. Burke¹³², I. Burmeister⁴⁵, E. Busato³⁶, D. Büscher⁵⁰, V. Büscher⁸⁵, P. Bussey⁵⁵, J.M. Butler²⁴, C.M. Buttar⁵⁵, J.M. Butterworth⁸⁰, P. Butti¹⁰⁸, W. Buttinger²⁷, A. Buzatu⁵⁵, A.R. Buzykaev^{110,c}, S. Cabrera Urbán¹⁶⁷, D. Caforio¹²⁹, V.M. Cairo^{39a,39b}, O. Cakir^{4a}, N. Calace⁵¹, P. Calafiura¹⁶, A. Calandri⁸⁷, G. Calderini⁸², P. Calfayan¹⁰¹, L.P. Caloba^{26a}, D. Calvet³⁶, S. Calvet³⁶, T.P. Calvet⁸⁷, R. Camacho Toro³³, S. Camarda³², P. Camarri^{134a,134b}, D. Cameron¹²⁰, R. Caminal Armadans¹⁶⁶, C. Camincher⁵⁷, S. Campana³², M. Campanelli⁸⁰, A. Camplani^{93a,93b}, A. Campoverde¹⁴⁹, V. Canale^{105a,105b}, A. Canepa^{160a}, M. Cano Bret^{35e}, J. Cantero¹¹⁵, R. Cantrill^{127a}, T. Cao⁴², M.D.M. Capeans Garrido³², I. Caprini^{28b}, M. Caprini^{28b}, M. Capua^{39a,39b}, R. Caputo⁸⁵, R.M. Carbone³⁷, R. Cardarelli^{134a}, F. Cardillo⁵⁰, I. Carli¹³⁰, T. Carli³², G. Carlino^{105a}, L. Carminati^{93a,93b}, S. Caron¹⁰⁷, E. Carquin^{34b}, G.D. Carrillo-Montoya³², J.R. Carter³⁰, J. Carvalho^{127a,127c}, D. Casadei¹⁹, M.P. Casado^{13,h}, M. Casolino¹³, D.W. Casper¹⁶³, E. Castaneda-Miranda^{146a}, R. Castelijns¹⁰⁸, A. Castelli¹⁰⁸, V. Castillo Gimenez¹⁶⁷, N.F. Castro^{127a,i}, A. Catinaccio³², J.R. Catmore¹²⁰, A. Cattai³², J. Caudron⁸⁵, V. Cavaliere¹⁶⁶, E. Cavallaro¹³, D. Cavalli^{93a}, M. Cavalli-Sforza¹³, V. Cavasinni^{125a,125b}, F. Ceradini^{135a,135b}, L. Cerda Alberich¹⁶⁷, B.C. Cerio⁴⁷, A.S. Cerqueira^{26b}, A. Cerri¹⁵⁰, L. Cerrito⁷⁸, F. Cerutti¹⁶, M. Cerv³², A. Cervelli¹⁸, S.A. Cetin^{20d}, A. Chafaq^{136a}, D. Chakraborty¹⁰⁹, S.K. Chan⁵⁹, Y.L. Chan^{62a}, P. Chang¹⁶⁶, J.D. Chapman³⁰, D.G. Charlton¹⁹, A. Chatterjee⁵¹, C.C. Chau¹⁵⁹, C.A. Chavez Barajas¹⁵⁰, S. Che¹¹², S. Cheatham⁷⁴, A. Chegwidan⁹², S. Chekanov⁶, S.V. Chekulaev^{160a}, G.A. Chelkov^{67,j}, M.A. Chelstowska⁹¹, C. Chen⁶⁶, H. Chen²⁷, K. Chen¹⁴⁹, S. Chen^{35c}, S. Chen¹⁵⁶, X. Chen^{35f}, Y. Chen⁶⁹, H.C. Cheng⁹¹, H.J. Cheng^{35a}, Y. Cheng³³, A. Cheplakov⁶⁷, E. Cheremushkina¹³¹, R. Cherkaoui El Moursli^{136e}, V. Chernyatin^{27,*}, E. Cheu⁷, L. Chevalier¹³⁷, V. Chiarella⁴⁹, G. Chiarelli^{125a,125b}, G. Chiodini^{75a}, A.S. Chisholm¹⁹, A. Chitan^{28b}, M.V. Chizhov⁶⁷, K. Choi⁶³, A.R. Chomont³⁶, S. Chouridou⁹, B.K.B. Chow¹⁰¹, V. Christodoulou⁸⁰, D. Chromek-Burckhart³², J. Chudoba¹²⁸, A.J. Chuinard⁸⁹, J.J. Chwastowski⁴¹, L. Chytka¹¹⁶, G. Ciapetti^{133a,133b}, A.K. Ciftci^{4a}, D. Cinca⁵⁵, V. Cindro⁷⁷, I.A. Cioara²³, A. Ciocio¹⁶, F. Ciotto^{105a,105b}, Z.H. Citron¹⁷², M. Citterio^{93a}, M. Ciubancan^{28b}, A. Clark⁵¹, B.L. Clark⁵⁹, M.R. Clark³⁷, P.J. Clark⁴⁸, R.N. Clarke¹⁶, C. Clement^{147a,147b}, Y. Coadou⁸⁷, M. Cobal^{164a,164c}, A. Coccaro⁵¹, J. Cochran⁶⁶, L. Coffey²⁵, L. Colasurdo¹⁰⁷, B. Cole³⁷, A.P. Colijn¹⁰⁸, J. Collot⁵⁷, T. Colombo³², G. Compostella¹⁰², P. Conde Muiño^{127a,127b}, E. Coniavitis⁵⁰, S.H. Connell^{146b}, I.A. Connelly⁷⁹, V. Consorti⁵⁰, S. Constantinescu^{28b}, G. Conti³², F. Conventi^{105a,k}, M. Cooke¹⁶, B.D. Cooper⁸⁰, A.M. Cooper-Sarkar¹²¹, K.J.R. Cormier¹⁵⁹, T. Cornelissen¹⁷⁵, M. Corradi^{133a,133b}, F. Corriveau^{89,l}, A. Corso-Radu¹⁶³, A. Cortes-Gonzalez¹³, G. Cortiana¹⁰², G. Costa^{93a}, M.J. Costa¹⁶⁷, D. Costanzo¹⁴⁰, G. Cottin³⁰, G. Cowan⁷⁹, B.E. Cox⁸⁶, K. Cranmer¹¹¹, S.J. Crawley⁵⁵, G. Cree³¹, S. Crépé-Renaudin⁵⁷,

F. Crescioli⁸², W.A. Cribbs^{147a,147b}, M. Crispin Ortuzar¹²¹, M. Cristinziani²³, V. Croft¹⁰⁷, G. Crosetti^{39a,39b}, T. Cuhadar Donszelmann¹⁴⁰, J. Cummings¹⁷⁶, M. Curatolo⁴⁹, J. Cúth⁸⁵, C. Cuthbert¹⁵¹, H. Czirr¹⁴², P. Czodrowski³, G. D'amen^{22a,22b}, S. D'Auria⁵⁵, M. D'Onofrio⁷⁶, M.J. Da Cunha Sargedas De Sousa^{127a,127b}, C. Da Via⁸⁶, W. Dabrowski^{40a}, T. Dado^{145a}, T. Dai⁹¹, O. Dale¹⁵, F. Dallaire⁹⁶, C. Dallapiccola⁸⁸, M. Dam³⁸, J.R. Dandoy³³, N.P. Dang⁵⁰, A.C. Daniells¹⁹, N.S. Dann⁸⁶, M. Danninger¹⁶⁸, M. Dano Hoffmann¹³⁷, V. Dao⁵⁰, G. Darbo^{52a}, S. Darmora⁸, J. Dassoulas³, A. Dattagupta⁶³, W. Davey²³, C. David¹⁶⁹, T. Davidek¹³⁰, M. Davies¹⁵⁴, P. Davison⁸⁰, E. Dawe⁹⁰, I. Dawson¹⁴⁰, R.K. Daya-Ishmukhametova⁸⁸, K. De⁸, R. de Asmundis^{105a}, A. De Benedetti¹¹⁴, S. De Castro^{22a,22b}, S. De Cecco⁸², N. De Groot¹⁰⁷, P. de Jong¹⁰⁸, H. De la Torre⁸⁴, F. De Lorenzi⁶⁶, A. De Maria⁵⁶, D. De Pedis^{133a}, A. De Salvo^{133a}, U. De Sanctis¹⁵⁰, A. De Santo¹⁵⁰, J.B. De Vivie De Regie¹¹⁸, W.J. Dearnaley⁷⁴, R. Debbe²⁷, C. Debenedetti¹³⁸, D.V. Dedovich⁶⁷, N. Dehghanian³, I. Deigaard¹⁰⁸, M. Del Gaudio^{39a,39b}, J. Del Peso⁸⁴, T. Del Prete^{125a,125b}, D. Delgove¹¹⁸, F. Deliot¹³⁷, C.M. Delitzsch⁵¹, M. Deliyergiyev⁷⁷, A. Dell'Acqua³², L. Dell'Asta²⁴, M. Dell'Orso^{125a,125b}, M. Della Pietra^{105a,k}, D. della Volpe⁵¹, M. Delmastro⁵, P.A. Delsart⁵⁷, C. Deluca¹⁰⁸, D.A. DeMarco¹⁵⁹, S. Demers¹⁷⁶, M. Demichev⁶⁷, A. Demilly⁸², S.P. Denisov¹³¹, D. Denysiuk¹³⁷, D. Derendarz⁴¹, J.E. Derkaoui^{136d}, F. Derue⁸², P. Dervan⁷⁶, K. Desch²³, C. Deterre⁴⁴, K. Dette⁴⁵, P.O. Deviveiros³², A. Dewhurst¹³², S. Dhaliwal²⁵, A. Di Ciaccio^{134a,134b}, L. Di Ciaccio⁵, W.K. Di Clemente¹²³, C. Di Donato^{133a,133b}, A. Di Girolamo³², B. Di Girolamo³², B. Di Micco^{135a,135b}, R. Di Nardo³², A. Di Simone⁵⁰, R. Di Sipio¹⁵⁹, D. Di Valentino³¹, C. Diaconu⁸⁷, M. Diamond¹⁵⁹, F.A. Dias⁴⁸, M.A. Diaz^{34a}, E.B. Diehl⁹¹, J. Dietrich¹⁷, S. Diglio⁸⁷, A. Dimitrievska¹⁴, J. Dingfelder²³, P. Dita^{28b}, S. Dita^{28b}, F. Dittus³², F. Djama⁸⁷, T. Djobava^{53b}, J.I. Djuvsland^{60a}, M.A.B. do Vale^{26c}, D. Dobos³², M. Dobre^{28b}, C. Doglioni⁸³, T. Dohmae¹⁵⁶, J. Dolejsi¹³⁰, Z. Dolezal¹³⁰, B.A. Dolgoshein^{99,*}, M. Donadelli^{26d}, S. Donati^{125a,125b}, P. Dondero^{122a,122b}, J. Donini³⁶, J. Dopke¹³², A. Doria^{105a}, M.T. Dova⁷³, A.T. Doyle⁵⁵, E. Drechsler⁵⁶, M. Dris¹⁰, Y. Du^{35d}, J. Duarte-Camperros¹⁵⁴, E. Duchovni¹⁷², G. Duckeck¹⁰¹, O.A. Ducu^{96,m}, D. Duda¹⁰⁸, A. Dudarev³², E.M. Duffield¹⁶, L. Dufnot¹¹⁸, L. Duguid⁷⁹, M. Dührssen³², M. Dumancic¹⁷², M. Dunford^{60a}, H. Duran Yildiz^{4a}, M. Düren⁵⁴, A. Durglishvili^{53b}, D. Duschinger⁴⁶, B. Dutta⁴⁴, M. Dyndal⁴⁴, C. Eckardt⁴⁴, K.M. Ecker¹⁰², R.C. Edgar⁹¹, N.C. Edwards⁴⁸, T. Eifert³², G. Eigen¹⁵, K. Einsweiler¹⁶, T. Ekelof¹⁶⁵, M. El Kacimi^{136c}, V. Ellajosyula⁸⁷, M. Ellert¹⁶⁵, S. Elles⁵, F. Ellinghaus¹⁷⁵, A.A. Elliot¹⁶⁹, N. Ellis³², J. Elmsheuser²⁷, M. Elsing³², D. Emelianov¹³², Y. Enari¹⁵⁶, O.C. Endner⁸⁵, M. Endo¹¹⁹, J.S. Ennis¹⁷⁰, J. Erdmann⁴⁵, A. Ereditato¹⁸, G. Ernis¹⁷⁵, J. Ernst², M. Ernst²⁷, S. Errede¹⁶⁶, E. Ertel⁸⁵, M. Escalier¹¹⁸, H. Esch⁴⁵, C. Escobar¹²⁶, B. Esposito⁴⁹, A.I. Etiennevre¹³⁷, E. Etzion¹⁵⁴, H. Evans⁶³, A. Ezhilov¹²⁴, F. Fabbri^{22a,22b}, L. Fabbri^{22a,22b}, G. Facini³³, R.M. Fakhruddinov¹³¹, S. Falciano^{133a}, R.J. Falla⁸⁰, J. Faltova¹³⁰, Y. Fang^{35a}, M. Fanti^{93a,93b}, A. Farbin⁸, A. Farilla^{135a}, C. Farina¹²⁶, T. Farooque¹³, S. Farrell¹⁶, S.M. Farrington¹⁷⁰, P. Farthouat³², F. Fassi^{136e}, P. Fassnacht³², D. Fassouliotis⁹, M. Fauci Giannelli⁷⁹, A. Favareto^{52a,52b}, W.J. Fawcett¹²¹, L. Fayard¹¹⁸, O.L. Fedin^{124,n}, W. Fedorko¹⁶⁸, S. Feigl¹²⁰, L. Feligioni⁸⁷, C. Feng^{35d}, E.J. Feng³², H. Feng⁹¹, A.B. Fenyuk¹³¹, L. Feremenga⁸, P. Fernandez Martinez¹⁶⁷, S. Fernandez Perez¹³, J. Ferrando⁵⁵, A. Ferrari¹⁶⁵, P. Ferrari¹⁰⁸, R. Ferrari^{122a}, D.E. Ferreira de Lima^{60b}, A. Ferrer¹⁶⁷, D. Ferrere⁵¹, C. Ferretti⁹¹, A. Ferretto Parodi^{52a,52b}, F. Fiedler⁸⁵, A. Filipčič⁷⁷, M. Filipuzzi⁴⁴, F. Filthaut¹⁰⁷, M. Fincke-Keeler¹⁶⁹, K.D. Finelli¹⁵¹, M.C.N. Fiolhais^{127a,127c}, L. Fiorini¹⁶⁷, A. Firan⁴², A. Fischer², C. Fischer¹³, J. Fischer¹⁷⁵, W.C. Fisher⁹², N. Flaschel⁴⁴, I. Fleck¹⁴², P. Fleischmann⁹¹, G.T. Fletcher¹⁴⁰, R.R.M. Fletcher¹²³, T. Flick¹⁷⁵, A. Floderus⁸³, L.R. Flores Castillo^{62a}, M.J. Flowerdew¹⁰², G.T. Forcolin⁸⁶, A. Formica¹³⁷, A. Forti⁸⁶, A.G. Foster¹⁹, D. Fournier¹¹⁸, H. Fox⁷⁴, S. Fracchia¹³, P. Francavilla⁸², M. Franchini^{22a,22b}, D. Francis³², L. Franconi¹²⁰, M. Franklin⁵⁹, M. Frate¹⁶³, M. Fraternali^{122a,122b}, D. Freeborn⁸⁰, S.M. Fressard-Batraneanu³², F. Friedrich⁴⁶, D. Froidevaux³², J.A. Frost¹²¹, C. Fukunaga¹⁵⁷, E. Fullana Torregrosa⁸⁵, T. Fusayasu¹⁰³, J. Fuster¹⁶⁷, C. Gabaldon⁵⁷, O. Gabizon¹⁷⁵, A. Gabrielli^{22a,22b}, A. Gabrielli¹⁶, G.P. Gach^{40a}, S. Gadatsch³², S. Gadomski⁵¹, G. Gagliardi^{52a,52b}, L.G. Gagnon⁹⁶, P. Gagnon⁶³, C. Galea¹⁰⁷, B. Galhardo^{127a,127c}, E.J. Gallas¹²¹, B.J. Gallop¹³², P. Gallus¹²⁹, G. Galster³⁸, K.K. Gan¹¹², J. Gao^{35b,87}, Y. Gao⁴⁸, Y.S. Gao^{144,f}, F.M. Garay Walls⁴⁸, C. García¹⁶⁷, J.E. García Navarro¹⁶⁷, M. Garcia-Sciveres¹⁶, R.W. Gardner³³, N. Garelli¹⁴⁴, V. Garonne¹²⁰, A. Gascon Bravo⁴⁴, C. Gatti⁴⁹, A. Gaudiello^{52a,52b}, G. Gaudio^{122a}, B. Gaur¹⁴², L. Gauthier⁹⁶, I.L. Gavrilenko⁹⁷, C. Gay¹⁶⁸, G. Gaycken²³, E.N. Gazis¹⁰, Z. Gecse¹⁶⁸, C.N.P. Gee¹³², Ch. Geich-Gimbel²³, M.P. Geisler^{60a}, C. Gemme^{52a},

M.H. Genest⁵⁷, C. Geng^{35b,o}, S. Gentile^{133a,133b}, S. George⁷⁹, D. Gerbaudo¹³, A. Gershon¹⁵⁴, S. Ghasemi¹⁴², H. Ghazlane^{136b}, M. Ghneimat²³, B. Giacobbe^{22a}, S. Giagu^{133a,133b}, P. Giannetti^{125a,125b}, B. Gibbard²⁷, S.M. Gibson⁷⁹, M. Gignac¹⁶⁸, M. Gilchriese¹⁶, T.P.S. Gillam³⁰, D. Gillberg³¹, G. Gilles¹⁷⁵, D.M. Gingrich^{3,d}, N. Giokaris⁹, M.P. Giordani^{164a,164c}, F.M. Giorgi^{22a}, F.M. Giorgi¹⁷, P.F. Giraud¹³⁷, P. Giromini⁵⁹, D. Giugni^{93a}, F. Giuli¹²¹, C. Giuliani¹⁰², M. Giulini^{60b}, B.K. Gjelsten¹²⁰, S. Gkaitatzis¹⁵⁵, I. Gkialas¹⁵⁵, E.L. Gkoukousis¹¹⁸, L.K. Gladilin¹⁰⁰, C. Glasman⁸⁴, J. Glatzer³², P.C.F. Glaysheer⁴⁸, A. Glazov⁴⁴, M. Goblirsch-Kolb¹⁰², J. Godlewski⁴¹, S. Goldfarb⁹¹, T. Golling⁵¹, D. Golubkov¹³¹, A. Gomes^{127a,127b,127d}, R. Gonçalves^{127a}, J. Goncalves Pinto Firmino Da Costa¹³⁷, L. Gonella¹⁹, A. Gongadze⁶⁷, S. González de la Hoz¹⁶⁷, G. Gonzalez Parra¹³, S. Gonzalez-Sevilla⁵¹, L. Goossens³², P.A. Gorbounov⁹⁸, H.A. Gordon²⁷, I. Gorelov¹⁰⁶, B. Gorini³², E. Gorini^{75a,75b}, A. Gorišek⁷⁷, E. Gornicki⁴¹, A.T. Goshaw⁴⁷, C. Gössling⁴⁵, M.I. Gostkin⁶⁷, C.R. Goudet¹¹⁸, D. Goujdami^{136c}, A.G. Goussiou¹³⁹, N. Govender^{146b,p}, E. Gozani¹⁵³, L. Graber⁵⁶, I. Grabowska-Bold^{40a}, P.O.J. Gradin⁵⁷, P. Grafström^{22a,22b}, J. Gramling⁵¹, E. Gramstad¹²⁰, S. Grancagnolo¹⁷, V. Gratchev¹²⁴, P.M. Gravila^{28e}, H.M. Gray³², E. Graziani^{135a}, Z.D. Greenwood^{81,q}, C. Greife²³, K. Gregersen⁸⁰, I.M. Gregor⁴⁴, P. Grenier¹⁴⁴, K. Grevtsov⁵, J. Griffiths⁸, A.A. Grillo¹³⁸, K. Grimm⁷⁴, S. Grinstein^{13,r}, Ph. Gris³⁶, J.-F. Grivaz¹¹⁸, S. Groh⁸⁵, J.P. Grohs⁴⁶, E. Gross¹⁷², J. Grosse-Knetter⁵⁶, G.C. Grossi⁸¹, Z.J. Grout¹⁵⁰, L. Guan⁹¹, W. Guan¹⁷³, J. Guenther¹²⁹, F. Guescini⁵¹, D. Guest¹⁶³, O. Gueta¹⁵⁴, E. Guido^{52a,52b}, T. Guillemain⁵, S. Guindon², U. Gul⁵⁵, C. Gumpert³², J. Guo^{35e}, Y. Guo^{35b,o}, S. Gupta¹²¹, G. Gustavino^{133a,133b}, P. Gutierrez¹¹⁴, N.G. Gutierrez Ortiz⁸⁰, C. Gutsche⁴⁶, C. Guyot¹³⁷, C. Gwenlan¹²¹, C.B. Gwilliam⁷⁶, A. Haas¹¹¹, C. Haber¹⁶, H.K. Hadavand⁸, N. Haddad^{136e}, A. Hadeef⁸⁷, P. Haefner²³, S. Hageböck²³, Z. Hajduk⁴¹, H. Hakobyan^{177,*}, M. Haleem⁴⁴, J. Haley¹¹⁵, G. Halladjian⁹², G.D. Hallowell⁸⁷, K. Hamacher¹⁷⁵, P. Hamal¹¹⁶, K. Hamano¹⁶⁹, A. Hamilton^{146a}, G.N. Hamity¹⁴⁰, P.G. Hamnett⁴⁴, L. Han^{35b}, K. Hanagaki^{68,s}, K. Hanawa¹⁵⁶, M. Hance¹³⁸, B. Haney¹²³, P. Hanke^{60a}, R. Hanna¹³⁷, J.B. Hansen³⁸, J.D. Hansen³⁸, M.C. Hansen²³, P.H. Hansen³⁸, K. Hara¹⁶¹, A.S. Hard¹⁷³, T. Harenberg¹⁷⁵, F. Hariri¹¹⁸, S. Harkusha⁹⁴, R.D. Harrington⁴⁸, P.F. Harrison¹⁷⁰, F. Hartjes¹⁰⁸, N.M. Hartmann¹⁰¹, M. Hasegawa⁶⁹, Y. Hasegawa¹⁴¹, A. Hasib¹¹⁴, S. Hassani¹³⁷, S. Haug¹⁸, R. Hauser⁹², L. Hauswald⁴⁶, M. Havranek¹²⁸, C.M. Hawkes¹⁹, R.J. Hawkings³², D. Hayden⁹², C.P. Hays¹²¹, J.M. Hays⁷⁸, H.S. Hayward⁷⁶, S.J. Haywood¹³², S.J. Head¹⁹, T. Heck⁸⁵, V. Hedberg⁸³, L. Heelan⁸, S. Heim¹²³, T. Heim¹⁶, B. Heinemann¹⁶, J.J. Heinrich¹⁰¹, L. Heinrich¹¹¹, C. Heinz⁵⁴, J. Hejbal¹²⁸, L. Helary²⁴, S. Hellman^{147a,147b}, C. Hensens³², J. Henderson¹²¹, R.C.W. Henderson⁷⁴, Y. Heng¹⁷³, S. Henkelmann¹⁶⁸, A.M. Henriques Correia³², S. Henrot-Versille¹¹⁸, G.H. Herbert¹⁷, Y. Hernández Jiménez¹⁶⁷, G. Herten⁵⁰, R. Hertenberger¹⁰¹, L. Hervas³², G.G. Hesketh⁸⁰, N.P. Hessey¹⁰⁸, J.W. Hetherly⁴², R. Hickling⁷⁸, E. Higón-Rodríguez¹⁶⁷, E. Hill¹⁶⁹, J.C. Hill³⁰, K.H. Hiller⁴⁴, S.J. Hillier¹⁹, I. Hinchliffe¹⁶, E. Hines¹²³, R.R. Hinman¹⁶, M. Hirose¹⁵⁸, D. Hirschbuehl¹⁷⁵, J. Hobbs¹⁴⁹, N. Hod^{160a}, M.C. Hodgkinson¹⁴⁰, P. Hodgson¹⁴⁰, A. Hoecker³², M.R. Hoefkamp¹⁰⁶, F. Hoenig¹⁰¹, D. Hohn²³, T.R. Holmes¹⁶, M. Homann⁴⁵, T.M. Hong¹²⁶, B.H. Hooberman¹⁶⁶, W.H. Hopkins¹¹⁷, Y. Horii¹⁰⁴, A.J. Horton¹⁴³, J.-Y. Hostachy⁵⁷, S. Hou¹⁵², A. Hoummada^{136a}, J. Howarth⁴⁴, M. Hrabovsky¹¹⁶, I. Hristova¹⁷, J. Hrivnac¹¹⁸, T. Hryn'ova⁵, A. Hrynevich⁹⁵, C. Hsu^{146c}, P.J. Hsu^{152,t}, S.-C. Hsu¹³⁹, D. Hu³⁷, Q. Hu^{35b}, Y. Huang⁴⁴, Z. Hubacek¹²⁹, F. Hubaut⁸⁷, F. Huegging²³, T.B. Huffman¹²¹, E.W. Hughes³⁷, G. Hughes⁷⁴, M. Huhtinen³², T.A. Hülsing⁸⁵, P. Huo¹⁴⁹, N. Huseynov^{67,b}, J. Huston⁹², J. Huth⁵⁹, G. Iacobucci⁵¹, G. Iakovidis²⁷, I. Ibragimov¹⁴², L. Iconomidou-Fayard¹¹⁸, E. Ideal¹⁷⁶, Z. Idrissi^{136e}, P. Iengo³², O. Igonkina^{108,u}, T. Iizawa¹⁷¹, Y. Ikegami⁶⁸, M. Ikeno⁶⁸, Y. Ilchenko^{11,v}, D. Iliadis¹⁵⁵, N. Ilic¹⁴⁴, T. Ince¹⁰², G. Introzzi^{122a,122b}, P. Ioannou^{9,*}, M. Iodice^{135a}, K. Iordanidou³⁷, V. Ippolito⁵⁹, M. Ishino⁷⁰, M. Ishitsuka¹⁵⁸, R. Ishmukhametov¹¹², C. Issever¹²¹, S. Istin^{20a}, F. Ito¹⁶¹, J.M. Iturbe Ponce⁸⁶, R. Iuppa^{134a,134b}, W. Iwanski⁴¹, H. Iwasaki⁶⁸, J.M. Izen⁴³, V. Izzo^{105a}, S. Jabbar³, B. Jackson¹²³, M. Jackson⁷⁶, P. Jackson¹, V. Jain², K.B. Jakobi⁸⁵, K. Jakobs⁵⁰, S. Jakobsen³², T. Jakoubek¹²⁸, D.O. Jamin¹¹⁵, D.K. Jana⁸¹, E. Jansen⁸⁰, R. Jansky⁶⁴, J. Janssen²³, M. Janus⁵⁶, G. Jarlskog⁸³, N. Javadov^{67,b}, T. Javůrek⁵⁰, F. Jeanneau¹³⁷, L. Jeanty¹⁶, J. Jejelava^{53a,w}, G.-Y. Jeng¹⁵¹, D. Jennens⁹⁰, P. Jenni^{50,x}, J. Jentsch⁴⁵, C. Jeske¹⁷⁰, S. Jézéquel⁵, H. Ji¹⁷³, J. Jia¹⁴⁹, H. Jiang⁶⁶, Y. Jiang^{35b}, S. Jiggins⁸⁰, J. Jimenez Pena¹⁶⁷, S. Jin^{35a}, A. Jinaru^{28b}, O. Jinnouchi¹⁵⁸, P. Johansson¹⁴⁰, K.A. Johns⁷, W.J. Johnson¹³⁹, K. Jon-And^{147a,147b}, G. Jones¹⁷⁰, R.W.L. Jones⁷⁴, S. Jones⁷, T.J. Jones⁷⁶, J. Jongmanns^{60a}, P.M. Jorge^{127a,127b}, J. Jovicevic^{160a}, X. Ju¹⁷³, A. Juste Rozas^{13,r}, M.K. Köhler¹⁷², A. Kaczmarska⁴¹,

M. Kado¹¹⁸, H. Kagan¹¹², M. Kagan¹⁴⁴, S.J. Kahn⁸⁷, E. Kajomovitz⁴⁷, C.W. Kalderon¹²¹, A. Kaluza⁸⁵, S. Kama⁴², A. Kamenshchikov¹³¹, N. Kanaya¹⁵⁶, S. Kaneti³⁰, L. Kanjir⁷⁷, V.A. Kantserov⁹⁹, J. Kanzaki⁶⁸, B. Kaplan¹¹¹, L.S. Kaplan¹⁷³, A. Kapliy³³, D. Kar^{146c}, K. Karakostas¹⁰, A. Karamaoun³, N. Karastathis¹⁰, M.J. Kareem⁵⁶, E. Karentzos¹⁰, M. Karnevskiy⁸⁵, S.N. Karpov⁶⁷, Z.M. Karpova⁶⁷, K. Karthik¹¹¹, V. Kartvelishvili⁷⁴, A.N. Karyukhin¹³¹, K. Kasahara¹⁶¹, L. Kashif¹⁷³, R.D. Kass¹¹², A. Kastanas¹⁵, Y. Kataoka¹⁵⁶, C. Kato¹⁵⁶, A. Katre⁵¹, J. Katzy⁴⁴, K. Kawagoe⁷², T. Kawamoto¹⁵⁶, G. Kawamura⁵⁶, S. Kazama¹⁵⁶, V.F. Kazanin^{110,c}, R. Keeler¹⁶⁹, R. Kehoe⁴², J.S. Keller⁴⁴, J.J. Kempster⁷⁹, K. Kentaro¹⁰⁴, H. Keoshkerian¹⁵⁹, O. Kepka¹²⁸, B.P. Kerševan⁷⁷, S. Kersten¹⁷⁵, R.A. Keyes⁸⁹, F. Khalil-zada¹², A. Khanov¹¹⁵, A.G. Kharlamov^{110,c}, T.J. Khoo⁵¹, V. Khovanskiy⁹⁸, E. Khramov⁶⁷, J. Khubua^{53b,y}, S. Kido⁶⁹, H.Y. Kim⁸, S.H. Kim¹⁶¹, Y.K. Kim³³, N. Kimura¹⁵⁵, O.M. Kind¹⁷, B.T. King⁷⁶, M. King¹⁶⁷, S.B. King¹⁶⁸, J. Kirk¹³², A.E. Kiryunin¹⁰², T. Kishimoto⁶⁹, D. Kisiielewska^{40a}, F. Kiss⁵⁰, K. Kiuchi¹⁶¹, O. Kivernyk¹³⁷, E. Kladiva^{145b}, M.H. Klein³⁷, M. Klein⁷⁶, U. Klein⁷⁶, K. Kleinknecht⁸⁵, P. Klimek^{147a,147b}, A. Klimentov²⁷, R. Klingenberg⁴⁵, J.A. Klinger¹⁴⁰, T. Klioutchnikova³², E.-E. Kluge^{60a}, P. Kluit¹⁰⁸, S. Kluth¹⁰², J. Knapik⁴¹, E. Kneringer⁶⁴, E.B.F.G. Knoop⁸⁷, A. Knue⁵⁵, A. Kobayashi¹⁵⁶, D. Kobayashi¹⁵⁸, T. Kobayashi¹⁵⁶, M. Kobel⁴⁶, M. Kocian¹⁴⁴, P. Kodys¹³⁰, T. Koffas³¹, E. Koffeman¹⁰⁸, T. Koi¹⁴⁴, H. Kolanoski¹⁷, M. Kolb^{60b}, I. Koletsou⁵, A.A. Komar^{97,*}, Y. Komori¹⁵⁶, T. Kondo⁶⁸, N. Kondrashova⁴⁴, K. Köneke⁵⁰, A.C. König¹⁰⁷, T. Kono^{68,z}, R. Konoplich^{111,aa}, N. Konstantinidis⁸⁰, R. Kopeliansky⁶³, S. Koperly^{40a}, L. Köpke⁸⁵, A.K. Kopp⁵⁰, K. Korcyl⁴¹, K. Kordas¹⁵⁵, A. Korn⁸⁰, A.A. Korol^{110,c}, I. Korolkov¹³, E.V. Korolkova¹⁴⁰, O. Kortner¹⁰², S. Kortner¹⁰², T. Kosek¹³⁰, V.V. Kostyukhin²³, A. Kotwal⁴⁷, A. Kourkouveli-Charalampidi¹⁵⁵, C. Kourkouvelis⁹, V. Kouskoura²⁷, A.B. Kowalewska⁴¹, R. Kowalewski¹⁶⁹, T.Z. Kowalski^{40a}, C. Kozakai¹⁵⁶, W. Kozanecki¹³⁷, A.S. Kozhin¹³¹, V.A. Kramarenko¹⁰⁰, G. Kramberger⁷⁷, D. Krasnopevtsev⁹⁹, M.W. Krasny⁸², A. Krasznahorkay³², J.K. Kraus²³, A. Kravchenko²⁷, M. Kretz^{60c}, J. Kretzschmar⁷⁶, K. Kreutzfeldt⁵⁴, P. Krieger¹⁵⁹, K. Krizka³³, K. Kroeninger⁴⁵, H. Kroha¹⁰², J. Kroll¹²³, J. Kroseberg²³, J. Krstic¹⁴, U. Kruchonak⁶⁷, H. Krüger²³, N. Krumnack⁶⁶, A. Kruse¹⁷³, M.C. Kruse⁴⁷, M. Kruskal²⁴, T. Kubota⁹⁰, H. Kucuk⁸⁰, S. Kudah^{4b}, J.T. Kuechler¹⁷⁵, S. Kuehn⁵⁰, A. Kugel^{60c}, F. Kuger¹⁷⁴, A. Kuhl¹³⁸, T. Kuhl⁴⁴, V. Kukhtin⁶⁷, R. Kukla¹³⁷, Y. Kulchitsky⁹⁴, S. Kuleshov^{34b}, M. Kuna^{133a,133b}, T. Kunigo⁷⁰, A. Kupco¹²⁸, H. Kurashige⁶⁹, Y.A. Kurochkin⁹⁴, V. Kus¹²⁸, E.S. Kuwertz¹⁶⁹, M. Kuze¹⁵⁸, J. Kvita¹¹⁶, T. Kwan¹⁶⁹, D. Kyriazopoulos¹⁴⁰, A. La Rosa¹⁰², J.L. La Rosa Navarro^{26d}, L. La Rotonda^{39a,39b}, C. Lacasta¹⁶⁷, F. Lacava^{133a,133b}, J. Lacey³¹, H. Lacker¹⁷, D. Lacour⁸², V.R. Lacuesta¹⁶⁷, E. Ladygin⁶⁷, R. Lafaye⁵, B. Laforge⁸², T. Lagouri¹⁷⁶, S. Lai⁵⁶, S. Lammers⁶³, W. Lampl⁷, E. Lançon¹³⁷, U. Landgraf⁵⁰, M.P.J. Landon⁷⁸, V.S. Lang^{60a}, J.C. Lange¹³, A.J. Lankford¹⁶³, F. Lanni²⁷, K. Lantzsch²³, A. Lanza^{122a}, S. Laplace⁸², C. Lapoire³², J.F. Laporte¹³⁷, T. Lari^{93a}, F. Lasagni Manghi^{22a,22b}, M. Lassnig³², P. Laurelli⁴⁹, W. Lavrijsen¹⁶, A.T. Law¹³⁸, P. Laycock⁷⁶, T. Lazovich⁵⁹, M. Lazzaroni^{93a,93b}, B. Le⁹⁰, O. Le Dortz⁸², E. Le Guirriec⁸⁷, E.P. Le Quilleuc¹³⁷, M. LeBlanc¹⁶⁹, T. LeCompte⁶, F. Ledroit-Guillon⁵⁷, C.A. Lee²⁷, S.C. Lee¹⁵², L. Lee¹, G. Lefebvre⁸², M. Lefebvre¹⁶⁹, F. Legger¹⁰¹, C. Leggett¹⁶, A. Lehan⁷⁶, G. Lehmann Miotto³², X. Lei⁷, W.A. Leight³¹, A. Leisos^{155,ab}, A.G. Leister¹⁷⁶, M.A.L. Leite^{26d}, R. Leitner¹³⁰, D. Lellouch¹⁷², B. Lemmer⁵⁶, K.J.C. Leney⁸⁰, T. Lenz²³, B. Lenzi³², R. Leone⁷, S. Leone^{125a,125b}, C. Leonidopoulos⁴⁸, S. Leontsinis¹⁰, G. Lerner¹⁵⁰, C. Leroy⁹⁶, A.A.J. Lesage¹³⁷, C.G. Lester³⁰, M. Levchenko¹²⁴, J. Levêque⁵, D. Levin⁹¹, L.J. Levinson¹⁷², M. Levy¹⁹, D. Lewis⁷⁸, A.M. Leyko²³, M. Leyton⁴³, B. Li^{35b,o}, H. Li¹⁴⁹, H.L. Li³³, L. Li⁴⁷, L. Li^{35e}, Q. Li^{35a}, S. Li⁴⁷, X. Li⁸⁶, Y. Li¹⁴², Z. Liang^{35a}, B. Liberti^{134a}, A. Liblong¹⁵⁹, P. Lichard³², K. Lie¹⁶⁶, J. Liebal²³, W. Liebig¹⁵, A. Limosani¹⁵¹, S.C. Lin^{152,ac}, T.H. Lin⁸⁵, B.E. Lindquist¹⁴⁹, A.E. Lioni⁵¹, E. Lipeles¹²³, A. Lipniacka¹⁵, M. Lisovyi^{60b}, T.M. Liss¹⁶⁶, A. Lister¹⁶⁸, A.M. Litke¹³⁸, B. Liu^{152,ad}, D. Liu¹⁵², H. Liu⁹¹, H. Liu²⁷, J. Liu⁸⁷, J.B. Liu^{35b}, K. Liu⁸⁷, L. Liu¹⁶⁶, M. Liu⁴⁷, M. Liu^{35b}, Y.L. Liu^{35b}, Y. Liu^{35b}, M. Livan^{122a,122b}, A. Lleres⁵⁷, J. Llorente Merino^{35a}, S.L. Lloyd⁷⁸, F. Lo Sterzo¹⁵², E. Lobodzinska⁴⁴, P. Loch⁷, W.S. Lockman¹³⁸, F.K. Loebinger⁸⁶, A.E. Loevschall-Jensen³⁸, K.M. Loew²⁵, A. Loginov¹⁷⁶, T. Lohse¹⁷, K. Lohwasser⁴⁴, M. Lokajicek¹²⁸, B.A. Long²⁴, J.D. Long¹⁶⁶, R.E. Long⁷⁴, L. Longo^{75a,75b}, K.A. Looper¹¹², L. Lopes^{127a}, D. Lopez Mateos⁵⁹, B. Lopez Paredes¹⁴⁰, I. Lopez Paz¹³, A. Lopez Solis⁸², J. Lorenz¹⁰¹, N. Lorenzo Martinez⁶³, M. Losada²¹, P.J. Lösel¹⁰¹, X. Lou^{35a}, A. Lounis¹¹⁸, J. Love⁶, P.A. Love⁷⁴, H. Lu^{62a}, N. Lu⁹¹, H.J. Lubatti¹³⁹, C. Luci^{133a,133b}, A. Lucotte⁵⁷, C. Luedtke⁵⁰, F. Luehring⁶³, W. Lukas⁶⁴, L. Luminari^{133a}, O. Lundberg^{147a,147b}, B. Lund-Jensen¹⁴⁸, D. Lynn²⁷, R. Lysak¹²⁸, E. Lytken⁸³, V. Lyubushkin⁶⁷, H. Ma²⁷, L.L. Ma^{35d}, Y. Ma^{35d}, G. Maccarrone⁴⁹,

A. Macchiolo¹⁰², C.M. Macdonald¹⁴⁰, B. Maček⁷⁷, J. Machado Miguens^{123,127b}, D. Madaffari⁸⁷, R. Madar³⁶, H.J. Maddocks¹⁶⁵, W.F. Mader⁴⁶, A. Madsen⁴⁴, J. Maeda⁶⁹, S. Maeland¹⁵, T. Maeno²⁷, A. Maevskiy¹⁰⁰, E. Magradze⁵⁶, J. Mahlstedt¹⁰⁸, C. Maiani¹¹⁸, C. Maidantchik^{26a}, A.A. Maier¹⁰², T. Maier¹⁰¹, A. Maio^{127a,127b,127d}, S. Majewski¹¹⁷, Y. Makida⁶⁸, N. Makovec¹¹⁸, B. Malaescu⁸², Pa. Malecki⁴¹, V.P. Maleev¹²⁴, F. Malek⁵⁷, U. Mallik⁶⁵, D. Malon⁶, C. Malone¹⁴⁴, S. Maltezos¹⁰, S. Malyukov³², J. Mamuzic¹⁶⁷, G. Mancini⁴⁹, B. Mandelli³², L. Mandelli^{93a}, I. Mandić⁷⁷, J. Maneira^{127a,127b}, L. Manhaes de Andrade Filho^{26b}, J. Manjarres Ramos^{160b}, A. Mann¹⁰¹, A. Manousos³², B. Mansoulie¹³⁷, J.D. Mansour^{35a}, R. Mantifel⁸⁹, M. Mantoani⁵⁶, S. Manzoni^{93a,93b}, L. Mapelli³², G. Marceca²⁹, L. March⁵¹, G. Marchiori⁸², M. Marcisovsky¹²⁸, M. Marjanovic¹⁴, D.E. Marley⁹¹, F. Marroquim^{26a}, S.P. Marsden⁸⁶, Z. Marshall¹⁶, S. Marti-Garcia¹⁶⁷, B. Martin⁹², T.A. Martin¹⁷⁰, V.J. Martin⁴⁸, B. Martin dit Latour¹⁵, M. Martinez^{13,r}, S. Martin-Haugh¹³², V.S. Martoiu^{28b}, A.C. Martyniuk⁸⁰, M. Marx¹³⁹, A. Marzin³², L. Masetti⁸⁵, T. Mashimo¹⁵⁶, R. Mashinistov⁹⁷, J. Masik⁸⁶, A.L. Maslennikov^{110,c}, I. Massa^{22a,22b}, L. Massa^{22a,22b}, P. Mastrandrea⁵, A. Mastroberardino^{39a,39b}, T. Masubuchi¹⁵⁶, P. Mättig¹⁷⁵, J. Mattmann⁸⁵, J. Maurer^{28b}, S.J. Maxfield⁷⁶, D.A. Maximov^{110,c}, R. Mazini¹⁵², S.M. Mazza^{93a,93b}, N.C. Mc Fadden¹⁰⁶, G. Mc Goldrick¹⁵⁹, S.P. Mc Kee⁹¹, A. McCarn⁹¹, R.L. McCarthy¹⁴⁹, T.G. McCarthy³¹, L.I. McClymont⁸⁰, E.F. McDonald⁹⁰, K.W. McFarlane^{58,*}, J.A. Mcfayden⁸⁰, G. Mchedlidze⁵⁶, S.J. McMahon¹³², R.A. McPherson^{169,l}, M. Medinnis⁴⁴, S. Meehan¹³⁹, S. Mehlhase¹⁰¹, A. Mehta⁷⁶, K. Meier^{60a}, C. Meineck¹⁰¹, B. Meirose⁴³, D. Melini¹⁶⁷, B.R. Mellado Garcia^{146c}, M. Melo^{145a}, F. Meloni¹⁸, A. Mengarelli^{22a,22b}, S. Menke¹⁰², E. Meoni¹⁶², S. Mergelmeyer¹⁷, P. Mermod⁵¹, L. Merola^{105a,105b}, C. Meroni^{93a}, F.S. Merritt³³, A. Messina^{133a,133b}, J. Metcalfe⁶, A.S. Mete¹⁶³, C. Meyer⁸⁵, C. Meyer¹²³, J-P. Meyer¹³⁷, J. Meyer¹⁰⁸, H. Meyer Zu Theenhausen^{60a}, F. Miano¹⁵⁰, R.P. Middleton¹³², S. Miglioranza^{52a,52b}, L. Mijović²³, G. Mikenberg¹⁷², M. Mikesstikova¹²⁸, M. Mikuž⁷⁷, M. Milesi⁹⁰, A. Milic⁶⁴, D.W. Miller³³, C. Mills⁴⁸, A. Milov¹⁷², D.A. Milstead^{147a,147b}, A.A. Minaenko¹³¹, Y. Minami¹⁵⁶, I.A. Minashvili⁶⁷, A.I. Mincer¹¹¹, B. Mindur^{40a}, M. Mineev⁶⁷, Y. Ming¹⁷³, L.M. Mir¹³, K.P. Mistry¹²³, T. Mitani¹⁷¹, J. Mitrevski¹⁰¹, V.A. Mitsou¹⁶⁷, A. Miucci⁵¹, P.S. Miyagawa¹⁴⁰, J.U. Mjörnmark⁸³, T. Moa^{147a,147b}, K. Mochizuki⁹⁶, S. Mohapatra³⁷, S. Molander^{147a,147b}, R. Moles-Valls²³, R. Monden⁷⁰, M.C. Mondragon⁹², K. Mönig⁴⁴, J. Monk³⁸, E. Monnier⁸⁷, A. Montalbano¹⁴⁹, J. Montejo Berlingen³², F. Monticelli⁷³, S. Monzani^{93a,93b}, R.W. Moore³, N. Morange¹¹⁸, D. Moreno²¹, M. Moreno Llacer⁵⁶, P. Morettini^{52a}, D. Mori¹⁴³, T. Mori¹⁵⁶, M. Morii⁵⁹, M. Morinaga¹⁵⁶, V. Morisbak¹²⁰, S. Moritz⁸⁵, A.K. Morley¹⁵¹, G. Mornacchi³², J.D. Morris⁷⁸, S.S. Mortensen³⁸, L. Morvaj¹⁴⁹, M. Mosidze^{53b}, J. Moss¹⁴⁴, K. Motohashi¹⁵⁸, R. Mount¹⁴⁴, E. Mountricha²⁷, S.V. Mouraviev^{97,*}, E.J.W. Moyse⁸⁸, S. Muanza⁸⁷, R.D. Mudd¹⁹, F. Mueller¹⁰², J. Mueller¹²⁶, R.S.P. Mueller¹⁰¹, T. Mueller³⁰, D. Muenstermann⁷⁴, P. Mullen⁵⁵, G.A. Mullier¹⁸, F.J. Munoz Sanchez⁸⁶, J.A. Murillo Quijada¹⁹, W.J. Murray^{170,132}, H. Musheghyan⁵⁶, M. Muškinja⁷⁷, A.G. Myagkov^{131,ae}, M. Myska¹²⁹, B.P. Nachman¹⁴⁴, O. Nackenhorst⁵¹, K. Nagai¹²¹, R. Nagai^{68,z}, K. Nagano⁶⁸, Y. Nagasaka⁶¹, K. Nagata¹⁶¹, M. Nagel⁵⁰, E. Nagy⁸⁷, A.M. Nairz³², Y. Nakahama³², K. Nakamura⁶⁸, T. Nakamura¹⁵⁶, I. Nakano¹¹³, H. Namasivayam⁴³, R.F. Naranjo Garcia⁴⁴, R. Narayan¹¹, D.I. Narrias Villar^{60a}, I. Naryshkin¹²⁴, T. Naumann⁴⁴, G. Navarro²¹, R. Nayyar⁷, H.A. Neal⁹¹, P.Yu. Nechaeva⁹⁷, T.J. Neep⁸⁶, P.D. Nef¹⁴⁴, A. Negri^{122a,122b}, M. Negrini^{22a}, S. Nektarijevic¹⁰⁷, C. Nellist¹¹⁸, A. Nelson¹⁶³, S. Nemecek¹²⁸, P. Nemethy¹¹¹, A.A. Nepomuceno^{26a}, M. Nessi^{32,qf}, M.S. Neubauer¹⁶⁶, M. Neumann¹⁷⁵, R.M. Neves¹¹¹, P. Nevski²⁷, P.R. Newman¹⁹, D.H. Nguyen⁶, T. Nguyen Manh⁹⁶, R.B. Nickerson¹²¹, R. Nicolaidou¹³⁷, J. Nielsen¹³⁸, A. Nikiforov¹⁷, V. Nikolaenko^{131,ae}, I. Nikolic-Audit⁸², K. Nikolopoulos¹⁹, J.K. Nilsen¹²⁰, P. Nilsson²⁷, Y. Ninomiya¹⁵⁶, A. Nisati^{133a}, R. Nisius¹⁰², T. Nobe¹⁵⁶, L. Nodulman⁶, M. Nomachi¹¹⁹, I. Nomidis³¹, T. Nooney⁷⁸, S. Norberg¹¹⁴, M. Nordberg³², N. Norjoharuddeen¹²¹, O. Novgorodova⁴⁶, S. Nowak¹⁰², M. Nozaki⁶⁸, L. Nozka¹¹⁶, K. Ntekas¹⁰, E. Nurse⁸⁰, F. Nuti⁹⁰, F. O'grady⁷, D.C. O'Neil¹⁴³, A.A. O'Rourke⁴⁴, V. O'Shea⁵⁵, F.G. Oakham^{31,d}, H. Oberlack¹⁰², T. Obermann²³, J. Ocariz⁸², A. Ochi⁶⁹, I. Ochoa³⁷, J.P. Ochoa-Ricoux^{34a}, S. Oda⁷², S. Odaka⁶⁸, H. Ogren⁶³, A. Oh⁸⁶, S.H. Oh⁴⁷, C.C. Ohm¹⁶, H. Ohman¹⁶⁵, H. Oide³², H. Okawa¹⁶¹, Y. Okumura³³, T. Okuyama⁶⁸, A. Olariu^{28b}, L.F. Oleiro Seabra^{127a}, S.A. Olivares Pino⁴⁸, D. Oliveira Damazio²⁷, A. Olszewski⁴¹, J. Olszowska⁴¹, A. Onofre^{127a,127e}, K. Onogi¹⁰⁴, P.U.E. Onyisi^{11,v}, M.J. Oreglia³³, Y. Oren¹⁵⁴, D. Orestano^{135a,135b}, N. Orlando^{62b}, R.S. Orr¹⁵⁹, B. Osculati^{52a,52b}, R. Ospanov⁸⁶, G. Otero y Garzon²⁹, H. Otono⁷², M. Ouchrif^{136d}, F. Ould-Saada¹²⁰, A. Ouraou¹³⁷,

K.P. Oussoren¹⁰⁸, Q. Ouyang^{35a}, M. Owen⁵⁵, R.E. Owen¹⁹, V.E. Ozcan^{20a}, N. Ozturk⁸, K. Pachal¹⁴³, A. Pacheco Pages¹³, C. Padilla Aranda¹³, M. Pagáčová⁵⁰, S. Pagan Griso¹⁶, F. Paige²⁷, P. Pais⁸⁸, K. Pajchel¹²⁰, G. Palacino^{160b}, S. Palestini³², M. Palka^{40b}, D. Pallin³⁶, A. Palma^{127a,127b}, E. St. Panagiotopoulou¹⁰, C.E. Pandini⁸², J.G. Panduro Vazquez⁷⁹, P. Pani^{147a,147b}, S. Panitkin²⁷, D. Pantea^{28b}, L. Paolozzi⁵¹, Th.D. Papadopoulou¹⁰, K. Papageorgiou¹⁵⁵, A. Paramonov⁶, D. Paredes Hernandez¹⁷⁶, A.J. Parker⁷⁴, M.A. Parker³⁰, K.A. Parker¹⁴⁰, F. Parodi^{52a,52b}, J.A. Parsons³⁷, U. Parzefall⁵⁰, V.R. Pascuzzi¹⁵⁹, E. Pasqualucci^{133a}, S. Passaggio^{52a}, Fr. Pastore⁷⁹, G. Pásztor^{31,ag}, S. Patariaia¹⁷⁵, J.R. Pater⁸⁶, T. Pauly³², J. Pearce¹⁶⁹, B. Pearson¹¹⁴, L.E. Pedersen³⁸, M. Pedersen¹²⁰, S. Pedraza Lopez¹⁶⁷, R. Pedro^{127a,127b}, S.V. Peleganchuk^{110,c}, D. Pelikan¹⁶⁵, O. Penc¹²⁸, C. Peng^{35a}, H. Peng^{35b}, J. Penwell⁶³, B.S. Peralva^{26b}, M.M. Perego¹³⁷, D.V. Perepelitsa²⁷, E. Perez Codina^{160a}, L. Perini^{93a,93b}, H. Pernegger³², S. Perrella^{105a,105b}, R. Peschke⁴⁴, V.D. Peshekhonov⁶⁷, K. Peters⁴⁴, R.F.Y. Peters⁸⁶, B.A. Petersen³², T.C. Petersen³⁸, E. Petit⁵⁷, A. Petridis¹, C. Petridou¹⁵⁵, P. Petroff¹¹⁸, E. Petrolo^{133a}, M. Petrov¹²¹, F. Petrucci^{135a,135b}, N.E. Pettersson⁸⁸, A. Peyaud¹³⁷, R. Pezoa^{34b}, P.W. Phillips¹³², G. Piacquadio¹⁴⁴, E. Pianori¹⁷⁰, A. Picazio⁸⁸, E. Piccaro⁷⁸, M. Piccinini^{22a,22b}, M.A. Pickering¹²¹, R. Piegaia²⁹, J.E. Pilcher³³, A.D. Pilkington⁸⁶, A.W.J. Pin⁸⁶, M. Pinamonti^{164a,164c,ah}, J.L. Pinfold³, A. Pingel³⁸, S. Pires⁸², H. Pirumov⁴⁴, M. Pitt¹⁷², L. Plazak^{145a}, M.-A. Pleier²⁷, V. Pleskot⁸⁵, E. Plotnikova⁶⁷, P. Plucinski⁹², D. Pluth⁶⁶, R. Poettgen^{147a,147b}, L. Poggioli¹¹⁸, D. Pohl²³, G. Polesello^{122a}, A. Poley⁴⁴, A. Policicchio^{39a,39b}, R. Polifka¹⁵⁹, A. Polini^{22a}, C.S. Pollard⁵⁵, V. Polychronakos²⁷, K. Pommès³², L. Pontecorvo^{133a}, B.G. Pope⁹², G.A. Popeneciu^{28c}, D.S. Popovic¹⁴, A. Poppleton³², S. Pospisil¹²⁹, K. Potamianos¹⁶, I.N. Potrap⁶⁷, C.J. Potter³⁰, C.T. Potter¹¹⁷, G. Poulard³², J. Poveda³², V. Pozdnyakov⁶⁷, M.E. Pozo Astigarraga³², P. Pralavorio⁸⁷, A. Pranko¹⁶, S. Prell⁶⁶, D. Price⁸⁶, L.E. Price⁶, M. Primavera^{75a}, S. Prince⁸⁹, M. Proissl⁴⁸, K. Prokofiev^{62c}, F. Prokoshin^{34b}, S. Protopopescu²⁷, J. Proudfoot⁶, M. Przybycien^{40a}, D. Puddu^{135a,135b}, D. Poldon¹⁴⁹, M. Purohit^{27,ai}, P. Puzo¹¹⁸, J. Qian⁹¹, G. Qin⁵⁵, Y. Qin⁸⁶, A. Quadt⁵⁶, W.B. Quayle^{164a,164b}, M. Queitsch-Maitland⁸⁶, D. Quilty⁵⁵, S. Raddum¹²⁰, V. Radeka²⁷, V. Radescu^{60b}, S.K. Radhakrishnan¹⁴⁹, P. Radloff¹¹⁷, P. Rados⁹⁰, F. Ragusa^{93a,93b}, G. Rahal¹⁷⁸, J.A. Raine⁸⁶, S. Rajagopalan²⁷, M. Rammensee³², C. Rangel-Smith¹⁶⁵, M.G. Ratti^{93a,93b}, F. Rauscher¹⁰¹, S. Rave⁸⁵, T. Ravenscroft⁵⁵, I. Ravinovich¹⁷², M. Raymond³², A.L. Read¹²⁰, N.P. Readioff⁷⁶, M. Reale^{75a,75b}, D.M. Rebuzzi^{122a,122b}, A. Redelbach¹⁷⁴, G. Redlinger²⁷, R. Reece¹³⁸, K. Reeves⁴³, L. Rehnisch¹⁷, J. Reichert¹²³, H. Reisin²⁹, C. Rembser³², H. Ren^{35a}, M. Rescigno^{133a}, S. Resconi^{93a}, O.L. Rezanova^{110,c}, P. Reznicek¹³⁰, R. Rezvani⁹⁶, R. Richter¹⁰², S. Richter⁸⁰, E. Richter-Was^{40b}, O. Ricken²³, M. Ridel⁸², P. Rieck¹⁷, C.J. Riegel¹⁷⁵, J. Rieger⁵⁶, O. Rifki¹¹⁴, M. Rijssenbeek¹⁴⁹, A. Rimoldi^{122a,122b}, M. Rimoldi¹⁸, L. Rinaldi^{22a}, B. Ristić⁵¹, E. Ritsch³², I. Riu¹³, F. Rizatdinova¹¹⁵, E. Rizvi⁷⁸, C. Rizzi¹³, S.H. Robertson^{89,l}, A. Robichaud-Veronneau⁸⁹, D. Robinson³⁰, J.E.M. Robinson⁴⁴, A. Robson⁵⁵, C. Roda^{125a,125b}, Y. Rodina⁸⁷, A. Rodriguez Perez¹³, D. Rodriguez Rodriguez¹⁶⁷, S. Roe³², C.S. Rogan⁵⁹, O. Röhne¹²⁰, A. Romaniouk⁹⁹, M. Romano^{22a,22b}, S.M. Romano Saez³⁶, E. Romero Adam¹⁶⁷, N. Rompotis¹³⁹, M. Ronzani⁵⁰, L. Roos⁸², E. Ros¹⁶⁷, S. Rosati^{133a}, K. Rosbach⁵⁰, P. Rose¹³⁸, O. Rosenthal¹⁴², N.-A. Rosien⁵⁶, V. Rossetti^{147a,147b}, E. Rossi^{105a,105b}, L.P. Rossi^{52a}, J.H.N. Rosten³⁰, R. Rosten¹³⁹, M. Rotaru^{28b}, I. Roth¹⁷², J. Rothberg¹³⁹, D. Rousseau¹¹⁸, C.R. Royon¹³⁷, A. Rozanov⁸⁷, Y. Rozen¹⁵³, X. Ruan^{146c}, F. Rubbo¹⁴⁴, M.S. Rudolph¹⁵⁹, F. Rühr⁵⁰, A. Ruiz-Martinez³¹, Z. Rurikova⁵⁰, N.A. Rusakovich⁶⁷, A. Ruschke¹⁰¹, H.L. Russell¹³⁹, J.P. Rutherford⁷, N. Ruthmann³², Y.F. Ryabov¹²⁴, M. Rybar¹⁶⁶, G. Rybkin¹¹⁸, S. Ryu⁶, A. Ryzhov¹³¹, G.F. Rzehorz⁵⁶, A.F. Saavedra¹⁵¹, G. Sabato¹⁰⁸, S. Sacerdoti²⁹, H.F-W. Sadrozinski¹³⁸, R. Sadykov⁶⁷, F. Safai Tehrani^{133a}, P. Saha¹⁰⁹, M. Sahinsoy^{60a}, M. Saimpert¹³⁷, T. Saito¹⁵⁶, H. Sakamoto¹⁵⁶, Y. Sakurai¹⁷¹, G. Salamanna^{135a,135b}, A. Salamon^{134a,134b}, J.E. Salazar Loyola^{34b}, D. Salek¹⁰⁸, P.H. Sales De Bruin¹³⁹, D. Salihagic¹⁰², A. Salnikov¹⁴⁴, J. Salt¹⁶⁷, D. Salvatore^{39a,39b}, F. Salvatore¹⁵⁰, A. Salvucci^{62a}, A. Salzburger³², D. Sammel⁵⁰, D. Sampsonidis¹⁵⁵, A. Sanchez^{105a,105b}, J. Sánchez¹⁶⁷, V. Sanchez Martinez¹⁶⁷, H. Sandaker¹²⁰, R.L. Sandbach⁷⁸, H.G. Sander⁸⁵, M. Sandhoff¹⁷⁵, C. Sandoval²¹, R. Sandstroem¹⁰², D.P.C. Sankey¹³², M. Sannino^{52a,52b}, A. Sansoni⁴⁹, C. Santoni³⁶, R. Santonico^{134a,134b}, H. Santos^{127a}, I. Santoyo Castillo¹⁵⁰, K. Sapp¹²⁶, A. Saponov⁶⁷, J.G. Saraiva^{127a,127d}, B. Sarrazin²³, O. Sasaki⁶⁸, Y. Sasaki¹⁵⁶, K. Sato¹⁶¹, G. Sauvage^{5,*}, E. Sauvan⁵, G. Savage⁷⁹, P. Savard^{159,d}, C. Sawyer¹³², L. Sawyer^{81,q}, J. Saxon³³, C. Sbarra^{22a}, A. Sbrizzi^{22a,22b}, T. Scanlon⁸⁰, D.A. Scannicchio¹⁶³, M. Scarcella¹⁵¹, V. Scarfone^{39a,39b}, J. Schaarschmidt¹⁷², P. Schacht¹⁰², B.M. Schachtner¹⁰¹, D. Schaefer³²,

R. Schaefer⁴⁴, J. Schaeffer⁸⁵, S. Schaepe²³, S. Schaetzel^{60b}, U. Schäfer⁸⁵, A.C. Schaffer¹¹⁸, D. Schaile¹⁰¹, R.D. Schamberger¹⁴⁹, V. Scharf^{60a}, V.A. Schegelsky¹²⁴, D. Scheirich¹³⁰, M. Schernau¹⁶³, C. Schiavi^{52a,52b}, S. Schier¹³⁸, C. Schillo⁵⁰, M. Schioppa^{39a,39b}, S. Schlenker³², K.R. Schmidt-Sommerfeld¹⁰², K. Schmieden³², C. Schmitt⁸⁵, S. Schmitt⁴⁴, S. Schmitz⁸⁵, B. Schneider^{160a}, U. Schnoor⁵⁰, L. Schoeffel¹³⁷, A. Schoening^{60b}, B.D. Schoenrock⁹², E. Schopf²³, M. Schott⁸⁵, J. Schovancova⁸, S. Schramm⁵¹, M. Schreyer¹⁷⁴, N. Schuh⁸⁵, M.J. Schultens²³, H.-C. Schultz-Coulon^{60a}, H. Schulz¹⁷, M. Schumacher⁵⁰, B.A. Schumm¹³⁸, Ph. Schune¹³⁷, A. Schwartzman¹⁴⁴, T.A. Schwarz⁹¹, Ph. Schwegler¹⁰², H. Schweiger⁸⁶, Ph. Schwemling¹³⁷, R. Schwienhorst⁹², J. Schwindling¹³⁷, T. Schwindt²³, G. Sciolla²⁵, F. Scuri^{125a,125b}, F. Scutti⁹⁰, J. Searcy⁹¹, P. Seema²³, S.C. Seidel¹⁰⁶, A. Seiden¹³⁸, F. Seifert¹²⁹, J.M. Seixas^{26a}, G. Sekhniaidze^{105a}, K. Sekhon⁹¹, S.J. Sekula⁴², D.M. Seliverstov^{124,*}, N. Semprini-Cesari^{22a,22b}, C. Serfon¹²⁰, L. Serin¹¹⁸, L. Serkin^{164a,164b}, M. Sessa^{135a,135b}, R. Seuster¹⁶⁹, H. Severini¹¹⁴, T. Sfiligoi⁷⁷, F. Sforza³², A. Sfyrila⁵¹, E. Shabalina⁵⁶, N.W. Shaikh^{147a,147b}, L.Y. Shan^{35a}, R. Shang¹⁶⁶, J.T. Shank²⁴, M. Shapiro¹⁶, P.B. Shatalov⁹⁸, K. Shaw^{164a,164b}, S.M. Shaw⁸⁶, A. Shcherbakova^{147a,147b}, C.Y. Shehu¹⁵⁰, P. Sherwood⁸⁰, L. Shi^{152,qj}, S. Shimizu⁶⁹, C.O. Shimmin¹⁶³, M. Shimojima¹⁰³, M. Shiyakova^{67,ak}, A. Shmeleva⁹⁷, D. Shoaleh Saadi⁹⁶, M.J. Shochet³³, S. Shojaii^{93a,93b}, S. Shrestha¹¹², E. Shulga⁹⁹, M.A. Shupe⁷, P. Sicho¹²⁸, A.M. Sickles¹⁶⁶, P.E. Sidebo¹⁴⁸, O. Sidiropoulou¹⁷⁴, D. Sidorov¹¹⁵, A. Sidoti^{22a,22b}, F. Siegert⁴⁶, Dj. Sijacki¹⁴, J. Silva^{127a,127d}, S.B. Silverstein^{147a}, V. Simak¹²⁹, O. Simard⁵, Lj. Simic¹⁴, S. Simion¹¹⁸, E. Simioni⁸⁵, B. Simmons⁸⁰, D. Simon³⁶, M. Simon⁸⁵, P. Sinervo¹⁵⁹, N.B. Sinev¹¹⁷, M. Sioli^{22a,22b}, G. Siragusa¹⁷⁴, S.Yu. Sivoklov¹⁰⁰, J. Sjölin^{147a,147b}, T.B. Sjursen¹⁵, M.B. Skinner⁷⁴, H.P. Skottowe⁵⁹, P. Skubic¹¹⁴, M. Slater¹⁹, T. Slavicek¹²⁹, M. Slawinska¹⁰⁸, K. Sliwa¹⁶², R. Slovak¹³⁰, V. Smakhtin¹⁷², B.H. Smart⁵, L. Smestad¹⁵, J. Smiesko^{145a}, S.Yu. Smirnov⁹⁹, Y. Smirnov⁹⁹, L.N. Smirnova^{100,al}, O. Smirnova⁸³, M.N.K. Smith³⁷, R.W. Smith³⁷, M. Smizanska⁷⁴, K. Smolek¹²⁹, A.A. Snesarev⁹⁷, S. Snyder²⁷, R. Sobie^{169,l}, F. Socher⁴⁶, A. Soffer¹⁵⁴, D.A. Soh¹⁵², G. Sokhrannyi⁷⁷, C.A. Solans Sanchez³², M. Solar¹²⁹, E.Yu. Soldatov⁹⁹, U. Soldevila¹⁶⁷, A.A. Solodkov¹³¹, A. Soloshenko⁶⁷, O.V. Solovyanov¹³¹, V. Solovyev¹²⁴, P. Sommer⁵⁰, H. Son¹⁶², H.Y. Song^{35b,am}, A. Sood¹⁶, A. Sopczak¹²⁹, V. Sopko¹²⁹, V. Sorin¹³, D. Sosa^{60b}, C.L. Sotiropoulou^{125a,125b}, R. Soualah^{164a,164c}, A.M. Soukharev^{110,c}, D. South⁴⁴, B.C. Sowden⁷⁹, S. Spagnolo^{75a,75b}, M. Spalla^{125a,125b}, M. Spangenberg¹⁷⁰, F. Spanò⁷⁹, D. Sperlich¹⁷, F. Spettel¹⁰², R. Spighi^{22a}, G. Spigo³², L.A. Spiller⁹⁰, M. Spousta¹³⁰, R.D. St. Denis^{55,*}, A. Stabile^{93a}, R. Stamen^{60a}, S. Stamm¹⁷, E. Stanecka⁴¹, R.W. Stanek⁶, C. Stancu^{135a}, M. Stancu-Bellu⁴⁴, M.M. Stanitzki⁴⁴, S. Stapnes¹²⁰, E.A. Starchenko¹³¹, G.H. Stark³³, J. Stark⁵⁷, P. Staroba¹²⁸, P. Starovoitov^{60a}, S. Stärz³², R. Staszewski⁴¹, P. Steinberg²⁷, B. Stelzer¹⁴³, H.J. Stelzer³², O. Stelzer-Chilton^{160a}, H. Stenzel⁵⁴, G.A. Stewart⁵⁵, J.A. Stillings²³, M.C. Stockton⁸⁹, M. Stoebe⁸⁹, G. Stoicea^{28b}, P. Stolte⁵⁶, S. Stonjek¹⁰², A.R. Stradling⁸, A. Straessner⁴⁶, M.E. Stramaglia¹⁸, J. Strandberg¹⁴⁸, S. Strandberg^{147a,147b}, A. Strandlie¹²⁰, M. Strauss¹¹⁴, P. Strizenec^{145b}, R. Ströhmer¹⁷⁴, D.M. Strom¹¹⁷, R. Stroynowski⁴², A. Strubig¹⁰⁷, S.A. Stucci¹⁸, B. Stugu¹⁵, N.A. Styles⁴⁴, D. Su¹⁴⁴, J. Su¹²⁶, R. Subramaniam⁸¹, S. Suchek^{60a}, Y. Sugaya¹¹⁹, M. Suk¹²⁹, V.V. Sulin⁹⁷, S. Sultansoy^{4c}, T. Sumida⁷⁰, S. Sun⁵⁹, X. Sun^{35a}, J.E. Sundermann⁵⁰, K. Suruliz¹⁵⁰, G. Susinno^{39a,39b}, M.R. Sutton¹⁵⁰, S. Suzuki⁶⁸, M. Svatos¹²⁸, M. Swiatlowski³³, I. Sykora^{145a}, T. Sykora¹³⁰, D. Ta⁵⁰, C. Taccini^{135a,135b}, K. Tackmann⁴⁴, J. Taenzer¹⁵⁹, A. Taffard¹⁶³, R. Tafirot^{160a}, N. Taiblum¹⁵⁴, H. Takai²⁷, R. Takashima⁷¹, T. Takeshita¹⁴¹, Y. Takubo⁶⁸, M. Talby⁸⁷, A.A. Talyshev^{110,c}, K.G. Tan⁹⁰, J. Tanaka¹⁵⁶, R. Tanaka¹¹⁸, S. Tanaka⁶⁸, B.B. Tannenwald¹¹², S. Tapia Araya^{34b}, S. Tapprogge⁸⁵, S. Tarem¹⁵³, G.F. Tartarelli^{93a}, P. Tas¹³⁰, M. Tasevsky¹²⁸, T. Tashiro⁷⁰, E. Tassi^{39a,39b}, A. Tavares Delgado^{127a,127b}, Y. Tayalati^{136d}, A.C. Taylor¹⁰⁶, G.N. Taylor⁹⁰, P.T.E. Taylor⁹⁰, W. Taylor^{160b}, F.A. Teischinger³², P. Teixeira-Dias⁷⁹, K.K. Temming⁵⁰, D. Temple¹⁴³, H. Ten Kate³², P.K. Teng¹⁵², J.J. Teoh¹¹⁹, F. Tepel¹⁷⁵, S. Terada⁶⁸, K. Terashi¹⁵⁶, J. Terron⁸⁴, S. Terzo¹⁰², M. Testa⁴⁹, R.J. Teuscher^{159,l}, T. Theveneaux-Pelzer⁸⁷, J.P. Thomas¹⁹, J. Thomas-Wilsker⁷⁹, E.N. Thompson³⁷, P.D. Thompson¹⁹, A.S. Thompson⁵⁵, L.A. Thomsen¹⁷⁶, E. Thomson¹²³, M. Thomson³⁰, M.J. Tibbetts¹⁶, R.E. Ticse Torres⁸⁷, V.O. Tikhomirov^{97,an}, Yu.A. Tikhonov^{110,c}, S. Timoshenko⁹⁹, P. Tipton¹⁷⁶, S. Tisserant⁸⁷, K. Todome¹⁵⁸, T. Todorov^{5,*}, S. Todorova-Nova¹³⁰, J. Tojo⁷², S. Tokár^{145a}, K. Tokushuku⁶⁸, E. Tolley⁵⁹, L. Tomlinson⁸⁶, M. Tomoto¹⁰⁴, L. Tompkins^{144,ao}, K. Toms¹⁰⁶, B. Tong⁵⁹, E. Torrence¹¹⁷, H. Torres¹⁴³, E. Torró Pastor¹³⁹, J. Toth^{87,ap}, F. Touchard⁸⁷, D.R. Tovey¹⁴⁰, T. Trefzger¹⁷⁴, A. Tricoli²⁷, I.M. Trigger^{160a}, S. Trincaz-Duvoid⁸², M.F. Tripania¹³, W. Trischuk¹⁵⁹, B. Trocme⁵⁷,

A. Trofymov⁴⁴, C. Troncon^{93a}, M. Trottier-McDonald¹⁶, M. Trovatelli¹⁶⁹, L. Truong^{164a,164c},
M. Trzebinski⁴¹, A. Trzupek⁴¹, J.C.-L. Tseng¹²¹, P.V. Tsiareshka⁹⁴, G. Tsipolitis¹⁰, N. Tsirintanis⁹,
S. Tsiskaridze¹³, V. Tsiskaridze⁵⁰, E.G. Tskhadadze^{53a}, K.M. Tsui^{62a}, I.I. Tsukerman⁹⁸, V. Tsulaia¹⁶,
S. Tsuno⁶⁸, D. Tsybychev¹⁴⁹, A. Tudorache^{28b}, V. Tudorache^{28b}, A.N. Tuna⁵⁹, S.A. Tupputi^{22a,22b},
S. Turchikhin^{100,al}, D. Turecek¹²⁹, D. Turgeman¹⁷², R. Turra^{93a,93b}, A.J. Turvey⁴², P.M. Tuts³⁷,
M. Tyndel¹³², G. Uccielli^{22a,22b}, I. Ueda¹⁵⁶, R. Ueno³¹, M. Ughetto^{147a,147b}, F. Ukegawa¹⁶¹, G. Unal³²,
A. Undrus²⁷, G. Unel¹⁶³, F.C. Ungaro⁹⁰, Y. Unno⁶⁸, C. Unverdorben¹⁰¹, J. Urban^{145b}, P. Urquijo⁹⁰,
P. Urrejola⁸⁵, G. Usai⁸, A. Usanova⁶⁴, L. Vacavant⁸⁷, V. Vacek¹²⁹, B. Vachon⁸⁹, C. Valderanis¹⁰¹,
E. Valdes Santurio^{147a,147b}, N. Valencic¹⁰⁸, S. Valentini^{22a,22b}, A. Valero¹⁶⁷, L. Valery¹³, S. Valkar¹³⁰,
S. Vallecorsa⁵¹, J.A. Valls Ferrer¹⁶⁷, W. Van Den Wollenberg¹⁰⁸, P.C. Van Der Deijl¹⁰⁸,
R. van der Geer¹⁰⁸, H. van der Graaf¹⁰⁸, N. van Eldik¹⁵³, P. van Gemmeren⁶, J. Van Nieuwkoop¹⁴³,
I. van Vulpen¹⁰⁸, M.C. van Woerden³², M. Vanadia^{133a,133b}, W. Vandelli³², R. Vanguri¹²³,
A. Vaniachine⁶, P. Vankov¹⁰⁸, G. Vardanyan¹⁷⁷, R. Vari^{133a}, E.W. Varnes⁷, T. Varol⁴², D. Varouchas⁸²,
A. Vartapetian⁸, K.E. Varvell¹⁵¹, J.G. Vasquez¹⁷⁶, F. Vazeille³⁶, T. Vazquez Schroeder⁸⁹, J. Veatch⁵⁶,
L.M. Veloce¹⁵⁹, F. Veloso^{127a,127c}, S. Veneziano^{133a}, A. Ventura^{75a,75b}, M. Venturi¹⁶⁹, N. Venturi¹⁵⁹,
A. Venturini²⁵, V. Vercesi^{122a}, M. Verducci^{133a,133b}, W. Verkerke¹⁰⁸, J.C. Vermeulen¹⁰⁸, A. Vest^{46,aq},
M.C. Vetterli^{143,d}, O. Viazlo⁸³, I. Vichou¹⁶⁶, T. Vickey¹⁴⁰, O.E. Vicky Boeriu¹⁴⁰, G.H.A. Viehhauser¹²¹,
S. Viel¹⁶, L. Vigani¹²¹, R. Vigne⁶⁴, M. Villa^{22a,22b}, M. Villaplana Perez^{93a,93b}, E. Vilucchi⁴⁹,
M.G. Vincker³¹, V.B. Vinogradov⁶⁷, C. Vittori^{22a,22b}, I. Vivarelli¹⁵⁰, S. Vlachos¹⁰, M. Vlasak¹²⁹,
M. Vogel¹⁷⁵, P. Vokac¹²⁹, G. Volpi^{125a,125b}, M. Volpi⁹⁰, H. von der Schmitt¹⁰², E. von Toerne²³,
V. Vorobel¹³⁰, K. Vorobev⁹⁹, M. Vos¹⁶⁷, R. Voss³², J.H. Vosseveld⁷⁶, N. Vranjes¹⁴,
M. Vranjes Milosavljevic¹⁴, V. Vrba¹²⁸, M. Vreeswijk¹⁰⁸, R. Vuillermet³², I. Vukotic³³, Z. Vykydal¹²⁹,
P. Wagner²³, W. Wagner¹⁷⁵, H. Wahlberg⁷³, S. Wahrmund⁴⁶, J. Wakabayashi¹⁰⁴, J. Walder⁷⁴,
R. Walker¹⁰¹, W. Walkowiak¹⁴², V. Wallangen^{147a,147b}, C. Wang^{35c}, C. Wang^{35d,87}, F. Wang¹⁷³,
H. Wang¹⁶, H. Wang⁴², J. Wang⁴⁴, J. Wang¹⁵¹, K. Wang⁸⁹, R. Wang⁶, S.M. Wang¹⁵², T. Wang²³,
T. Wang³⁷, W. Wang^{35b}, X. Wang¹⁷⁶, C. Wanotayaroj¹¹⁷, A. Warburton⁸⁹, C.P. Ward³⁰, D.R. Wardrope⁸⁰,
A. Washbrook⁴⁸, P.M. Watkins¹⁹, A.T. Watson¹⁹, M.F. Watson¹⁹, G. Watts¹³⁹, S. Watts⁸⁶, B.M. Waugh⁸⁰,
S. Webb⁸⁵, M.S. Weber¹⁸, S.W. Weber¹⁷⁴, J.S. Webster⁶, A.R. Weidberg¹²¹, B. Weinert⁶³,
J. Weingarten⁵⁶, C. Weiser⁵⁰, H. Weits¹⁰⁸, P.S. Wells³², T. Wenaus²⁷, T. Wengler³², S. Wenig³²,
N. Wermes²³, M. Werner⁵⁰, P. Werner³², M. Wessels^{60a}, J. Wetter¹⁶², K. Whalen¹¹⁷, N.L. Whallon¹³⁹,
A.M. Wharton⁷⁴, A. White⁸, M.J. White¹, R. White^{34b}, D. Whiteson¹⁶³, F.J. Wickens¹³²,
W. Wiedenmann¹⁷³, M. Wielers¹³², P. Wienemann²³, C. Wigglesworth³⁸, L.A.M. Wiik-Fuchs²³,
A. Wildauer¹⁰², F. Wilk⁸⁶, H.G. Wilkens³², H.H. Williams¹²³, S. Williams¹⁰⁸, C. Willis⁹², S. Willocq⁸⁸,
J.A. Wilson¹⁹, I. Wingerter-Seez⁵, F. Winklmeier¹¹⁷, O.J. Winston¹⁵⁰, B.T. Winter²³, M. Wittgen¹⁴⁴,
J. Wittkowski¹⁰¹, S.J. Wollstadt⁸⁵, M.W. Wolter⁴¹, H. Wolters^{127a,127c}, B.K. Wosiek⁴¹, J. Wotschack³²,
M.J. Woudstra⁸⁶, K.W. Wozniak⁴¹, M. Wu⁵⁷, M. Wu³³, S.L. Wu¹⁷³, X. Wu⁵¹, Y. Wu⁹¹, T.R. Wyatt⁸⁶,
B.M. Wynne⁴⁸, S. Xella³⁸, D. Xu^{35a}, L. Xu²⁷, B. Yabsley¹⁵¹, S. Yacoub^{146a}, R. Yakabe⁶⁹, D. Yamaguchi¹⁵⁸,
Y. Yamaguchi¹¹⁹, A. Yamamoto⁶⁸, S. Yamamoto¹⁵⁶, T. Yamanaka¹⁵⁶, K. Yamauchi¹⁰⁴, Y. Yamazaki⁶⁹,
Z. Yan²⁴, H. Yang^{35e}, H. Yang¹⁷³, Y. Yang¹⁵², Z. Yang¹⁵, W.-M. Yao¹⁶, Y.C. Yap⁸², Y. Yasu⁶⁸, E. Yatsenko⁵,
K.H. Yau Wong²³, J. Ye⁴², S. Ye²⁷, I. Yeletsikh⁶⁷, A.L. Yen⁵⁹, E. Yildirim⁸⁵, K. Yorita¹⁷¹, R. Yoshida⁶,
K. Yoshihara¹²³, C. Young¹⁴⁴, C.J.S. Young³², S. Youssef²⁴, D.R. Yu¹⁶, J. Yu⁸, J.M. Yu⁹¹, J. Yu⁶⁶, L. Yuan⁶⁹,
S.P.Y. Yuen²³, I. Yusuff^{30,ar}, B. Zabinski⁴¹, R. Zaidan^{35d}, A.M. Zaitsev^{131,ae}, N. Zakharchuk⁴⁴,
J. Zalieckas¹⁵, A. Zaman¹⁴⁹, S. Zambito⁵⁹, L. Zanello^{133a,133b}, D. Zanzi⁹⁰, C. Zeitnitz¹⁷⁵, M. Zeman¹²⁹,
A. Zemla^{40a}, J.C. Zeng¹⁶⁶, Q. Zeng¹⁴⁴, K. Zengel²⁵, O. Zenin¹³¹, T. Ženiš^{145a}, D. Zerwas¹¹⁸, D. Zhang⁹¹,
F. Zhang¹⁷³, G. Zhang^{35b,am}, H. Zhang^{35c}, J. Zhang⁶, L. Zhang⁵⁰, R. Zhang²³, R. Zhang^{35b,as},
X. Zhang^{35d}, Z. Zhang¹¹⁸, X. Zhao⁴², Y. Zhao^{35d}, Z. Zhao^{35b}, A. Zhemchugov⁶⁷, J. Zhong¹²¹, B. Zhou⁹¹,
C. Zhou⁴⁷, L. Zhou³⁷, L. Zhou⁴², M. Zhou¹⁴⁹, N. Zhou^{35f}, C.G. Zhu^{35d}, H. Zhu^{35a}, J. Zhu⁹¹, Y. Zhu^{35b},
X. Zhuang^{35a}, K. Zhukov⁹⁷, A. Zibell¹⁷⁴, D. Zieminska⁶³, N.I. Zimine⁶⁷, C. Zimmermann⁸⁵,
S. Zimmermann⁵⁰, Z. Zinonos⁵⁶, M. Zinser⁸⁵, M. Ziolkowski¹⁴², L. Živković¹⁴, G. Zobernig¹⁷³,
A. Zoccoli^{22a,22b}, M. zur Nedden¹⁷, G. Zurzolo^{105a,105b}, L. Zwalinski³²

¹ Department of Physics, University of Adelaide, Adelaide, Australia² Physics Department, SUNY Albany, Albany NY, United States³ Department of Physics, University of Alberta, Edmonton AB, Canada

- ⁴ (a) Department of Physics, Ankara University, Ankara; (b) Istanbul Aydin University, Istanbul; (c) Division of Physics, TOBB University of Economics and Technology, Ankara, Turkey
- ⁵ LAPP, CNRS/IN2P3 and Université Savoie Mont Blanc, Annecy-le-Vieux, France
- ⁶ High Energy Physics Division, Argonne National Laboratory, Argonne IL, United States
- ⁷ Department of Physics, University of Arizona, Tucson AZ, United States
- ⁸ Department of Physics, The University of Texas at Arlington, Arlington TX, United States
- ⁹ Physics Department, University of Athens, Athens, Greece
- ¹⁰ Physics Department, National Technical University of Athens, Zografou, Greece
- ¹¹ Department of Physics, The University of Texas at Austin, Austin TX, United States
- ¹² Institute of Physics, Azerbaijan Academy of Sciences, Baku, Azerbaijan
- ¹³ Institut de Física d'Altes Energies (IFAE), The Barcelona Institute of Science and Technology, Barcelona, Spain, Spain
- ¹⁴ Institute of Physics, University of Belgrade, Belgrade, Serbia
- ¹⁵ Department for Physics and Technology, University of Bergen, Bergen, Norway
- ¹⁶ Physics Division, Lawrence Berkeley National Laboratory and University of California, Berkeley CA, United States
- ¹⁷ Department of Physics, Humboldt University, Berlin, Germany
- ¹⁸ Albert Einstein Center for Fundamental Physics and Laboratory for High Energy Physics, University of Bern, Bern, Switzerland
- ¹⁹ School of Physics and Astronomy, University of Birmingham, Birmingham, United Kingdom
- ²⁰ (a) Department of Physics, Bogazici University, Istanbul; (b) Department of Physics Engineering, Gaziantep University, Gaziantep; (d) Istanbul Bilgi University, Faculty of Engineering and Natural Sciences, Istanbul; (e) Bahcesehir University, Faculty of Engineering and Natural Sciences, Istanbul, Turkey
- ²¹ Centro de Investigaciones, Universidad Antonio Narino, Bogota, Colombia
- ²² (a) INFN Sezione di Bologna; (b) Dipartimento di Fisica e Astronomia, Università di Bologna, Bologna, Italy
- ²³ Physikalisches Institut, University of Bonn, Bonn, Germany
- ²⁴ Department of Physics, Boston University, Boston MA, United States
- ²⁵ Department of Physics, Brandeis University, Waltham MA, United States
- ²⁶ (a) Universidade Federal do Rio De Janeiro COPPE/EE/IF, Rio de Janeiro; (b) Electrical Circuits Department, Federal University of Juiz de Fora (UFJF), Juiz de Fora; (c) Federal University of Sao Joao del Rei (UFSJ), Sao Joao del Rei; (d) Instituto de Física, Universidade de Sao Paulo, Sao Paulo, Brazil
- ²⁷ Physics Department, Brookhaven National Laboratory, Upton NY, United States
- ²⁸ (a) Transilvania University of Brasov, Brasov; (b) National Institute of Physics and Nuclear Engineering, Bucharest; (c) National Institute for Research and Development of Isotopic and Molecular Technologies, Physics Department, Cluj Napoca; (d) University Politehnica Bucharest, Bucharest; (e) West University in Timisoara, Timisoara, Romania
- ²⁹ Departamento de Física, Universidad de Buenos Aires, Buenos Aires, Argentina
- ³⁰ Cavendish Laboratory, University of Cambridge, Cambridge, United Kingdom
- ³¹ Department of Physics, Carleton University, Ottawa ON, Canada
- ³² CERN, Geneva, Switzerland
- ³³ Enrico Fermi Institute, University of Chicago, Chicago IL, United States
- ³⁴ (a) Departamento de Física, Pontificia Universidad Católica de Chile, Santiago; (b) Departamento de Física, Universidad Técnica Federico Santa María, Valparaíso, Chile
- ³⁵ (a) Institute of High Energy Physics, Chinese Academy of Sciences, Beijing; (b) Department of Modern Physics, University of Science and Technology of China, Anhui; (c) Department of Physics, Nanjing University, Jiangsu; (d) School of Physics, Shandong University, Shandong; (e) Department of Physics and Astronomy, Shanghai Key Laboratory for Particle Physics and Cosmology, Shanghai Jiao Tong University, Shanghai⁴¹; (f) Physics Department, Tsinghua University, Beijing 100084, China
- ³⁶ Laboratoire de Physique Corpusculaire, Clermont Université and Université Blaise Pascal and CNRS/IN2P3, Clermont-Ferrand, France
- ³⁷ Nevis Laboratory, Columbia University, Irvington NY, United States
- ³⁸ Niels Bohr Institute, University of Copenhagen, Copenhagen, Denmark
- ³⁹ (a) INFN Gruppo Collegato di Cosenza, Laboratori Nazionali di Frascati; (b) Dipartimento di Fisica, Università della Calabria, Rende, Italy
- ⁴⁰ (a) AGH University of Science and Technology, Faculty of Physics and Applied Computer Science, Krakow; (b) Marian Smoluchowski Institute of Physics, Jagiellonian University, Krakow, Poland
- ⁴¹ Institute of Nuclear Physics Polish Academy of Sciences, Krakow, Poland
- ⁴² Physics Department, Southern Methodist University, Dallas TX, United States
- ⁴³ Physics Department, University of Texas at Dallas, Richardson TX, United States
- ⁴⁴ DESY, Hamburg and Zeuthen, Germany
- ⁴⁵ Institut für Experimentelle Physik IV, Technische Universität Dortmund, Dortmund, Germany
- ⁴⁶ Institut für Kern- und Teilchenphysik, Technische Universität Dresden, Dresden, Germany
- ⁴⁷ Department of Physics, Duke University, Durham NC, United States
- ⁴⁸ SUPA – School of Physics and Astronomy, University of Edinburgh, Edinburgh, United Kingdom
- ⁴⁹ INFN Laboratori Nazionali di Frascati, Frascati, Italy
- ⁵⁰ Fakultät für Mathematik und Physik, Albert-Ludwigs-Universität, Freiburg, Germany
- ⁵¹ Section de Physique, Université de Genève, Geneva, Switzerland
- ⁵² (a) INFN Sezione di Genova; (b) Dipartimento di Fisica, Università di Genova, Genova, Italy
- ⁵³ (a) E. Andronikashvili Institute of Physics, Iv. Javakishvili Tbilisi State University, Tbilisi; (b) High Energy Physics Institute, Tbilisi State University, Tbilisi, Georgia
- ⁵⁴ II Physikalisches Institut, Justus-Liebig-Universität Giessen, Giessen, Germany
- ⁵⁵ SUPA – School of Physics and Astronomy, University of Glasgow, Glasgow, United Kingdom
- ⁵⁶ II Physikalisches Institut, Georg-August-Universität, Göttingen, Germany
- ⁵⁷ Laboratoire de Physique Subatomique et de Cosmologie, Université Grenoble-Alpes, CNRS/IN2P3, Grenoble, France
- ⁵⁸ Department of Physics, Hampton University, Hampton VA, United States
- ⁵⁹ Laboratory for Particle Physics and Cosmology, Harvard University, Cambridge MA, United States
- ⁶⁰ (a) Kirchhoff-Institut für Physik, Ruprecht-Karls-Universität Heidelberg, Heidelberg; (b) Physikalisches Institut, Ruprecht-Karls-Universität Heidelberg, Heidelberg; (c) ZITI Institut für technische Informatik, Ruprecht-Karls-Universität Heidelberg, Mannheim, Germany
- ⁶¹ Faculty of Applied Information Science, Hiroshima Institute of Technology, Hiroshima, Japan
- ⁶² (a) Department of Physics, The Chinese University of Hong Kong, Shatin, N.T., Hong Kong; (b) Department of Physics, The University of Hong Kong, Hong Kong; (c) Department of Physics, The Hong Kong University of Science and Technology, Clear Water Bay, Kowloon, Hong Kong, China
- ⁶³ Department of Physics, Indiana University, Bloomington IN, United States
- ⁶⁴ Institut für Astro- und Teilchenphysik, Leopold-Franzens-Universität, Innsbruck, Austria
- ⁶⁵ University of Iowa, Iowa City IA, United States
- ⁶⁶ Department of Physics and Astronomy, Iowa State University, Ames IA, United States
- ⁶⁷ Joint Institute for Nuclear Research, JINR Dubna, Dubna, Russia
- ⁶⁸ KEK, High Energy Accelerator Research Organization, Tsukuba, Japan
- ⁶⁹ Graduate School of Science, Kobe University, Kobe, Japan
- ⁷⁰ Faculty of Science, Kyoto University, Kyoto, Japan
- ⁷¹ Kyoto University of Education, Kyoto, Japan
- ⁷² Department of Physics, Kyushu University, Fukuoka, Japan
- ⁷³ Instituto de Física La Plata, Universidad Nacional de La Plata and CONICET, La Plata, Argentina
- ⁷⁴ Physics Department, Lancaster University, Lancaster, United Kingdom

- ⁷⁵ ^(a) INFN Sezione di Lecce; ^(b) Dipartimento di Matematica e Fisica, Università del Salento, Lecce, Italy
- ⁷⁶ Oliver Lodge Laboratory, University of Liverpool, Liverpool, United Kingdom
- ⁷⁷ Department of Physics, Jožef Stefan Institute and University of Ljubljana, Ljubljana, Slovenia
- ⁷⁸ School of Physics and Astronomy, Queen Mary University of London, London, United Kingdom
- ⁷⁹ Department of Physics, Royal Holloway University of London, Surrey, United Kingdom
- ⁸⁰ Department of Physics and Astronomy, University College London, London, United Kingdom
- ⁸¹ Louisiana Tech University, Ruston LA, United States
- ⁸² Laboratoire de Physique Nucléaire et de Hautes Energies, UPMC and Université Paris-Diderot and CNRS/IN2P3, Paris, France
- ⁸³ Fysiska institutionen, Lunds universitet, Lund, Sweden
- ⁸⁴ Departamento de Física Teórica C-15, Universidad Autónoma de Madrid, Madrid, Spain
- ⁸⁵ Institut für Physik, Universität Mainz, Mainz, Germany
- ⁸⁶ School of Physics and Astronomy, University of Manchester, Manchester, United Kingdom
- ⁸⁷ CPPM, Aix-Marseille Université and CNRS/IN2P3, Marseille, France
- ⁸⁸ Department of Physics, University of Massachusetts, Amherst MA, United States
- ⁸⁹ Department of Physics, McGill University, Montreal QC, Canada
- ⁹⁰ School of Physics, University of Melbourne, Victoria, Australia
- ⁹¹ Department of Physics, The University of Michigan, Ann Arbor MI, United States
- ⁹² Department of Physics and Astronomy, Michigan State University, East Lansing MI, United States
- ⁹³ ^(a) INFN Sezione di Milano; ^(b) Dipartimento di Fisica, Università di Milano, Milano, Italy
- ⁹⁴ B.I. Stepanov Institute of Physics, National Academy of Sciences of Belarus, Minsk, Belarus
- ⁹⁵ National Scientific and Educational Centre for Particle and High Energy Physics, Minsk, Belarus
- ⁹⁶ Group of Particle Physics, University of Montreal, Montreal QC, Canada
- ⁹⁷ P.N. Lebedev Physical Institute of the Russian Academy of Sciences, Moscow, Russia
- ⁹⁸ Institute for Theoretical and Experimental Physics (ITEP), Moscow, Russia
- ⁹⁹ National Research Nuclear University MEPhI, Moscow, Russia
- ¹⁰⁰ D.V. Skobeltsyn Institute of Nuclear Physics, M.V. Lomonosov Moscow State University, Moscow, Russia
- ¹⁰¹ Fakultät für Physik, Ludwig-Maximilians-Universität München, München, Germany
- ¹⁰² Max-Planck-Institut für Physik (Werner-Heisenberg-Institut), München, Germany
- ¹⁰³ Nagasaki Institute of Applied Science, Nagasaki, Japan
- ¹⁰⁴ Graduate School of Science and Kobayashi-Maskawa Institute, Nagoya University, Nagoya, Japan
- ¹⁰⁵ ^(a) INFN Sezione di Napoli; ^(b) Dipartimento di Fisica, Università di Napoli, Napoli, Italy
- ¹⁰⁶ Department of Physics and Astronomy, University of New Mexico, Albuquerque NM, United States
- ¹⁰⁷ Institute for Mathematics, Astrophysics and Particle Physics, Radboud University Nijmegen/Nikhef, Nijmegen, Netherlands
- ¹⁰⁸ Nikhef National Institute for Subatomic Physics and University of Amsterdam, Amsterdam, Netherlands
- ¹⁰⁹ Department of Physics, Northern Illinois University, DeKalb IL, United States
- ¹¹⁰ Budker Institute of Nuclear Physics, SB RAS, Novosibirsk, Russia
- ¹¹¹ Department of Physics, New York University, New York NY, United States
- ¹¹² Ohio State University, Columbus OH, United States
- ¹¹³ Faculty of Science, Okayama University, Okayama, Japan
- ¹¹⁴ Homer L. Dodge Department of Physics and Astronomy, University of Oklahoma, Norman OK, United States
- ¹¹⁵ Department of Physics, Oklahoma State University, Stillwater OK, United States
- ¹¹⁶ Palacký University, RCPM, Olomouc, Czechia
- ¹¹⁷ Center for High Energy Physics, University of Oregon, Eugene OR, United States
- ¹¹⁸ LAL, Univ. Paris-Sud, CNRS/IN2P3, Université Paris-Saclay, Orsay, France
- ¹¹⁹ Graduate School of Science, Osaka University, Osaka, Japan
- ¹²⁰ Department of Physics, University of Oslo, Oslo, Norway
- ¹²¹ Department of Physics, Oxford University, Oxford, United Kingdom
- ¹²² ^(a) INFN Sezione di Pavia; ^(b) Dipartimento di Fisica, Università di Pavia, Pavia, Italy
- ¹²³ Department of Physics, University of Pennsylvania, Philadelphia PA, United States
- ¹²⁴ National Research Centre “Kurchatov Institute” B.P. Konstantinov Petersburg Nuclear Physics Institute, St. Petersburg, Russia
- ¹²⁵ ^(a) INFN Sezione di Pisa; ^(b) Dipartimento di Fisica E. Fermi, Università di Pisa, Pisa, Italy
- ¹²⁶ Department of Physics and Astronomy, University of Pittsburgh, Pittsburgh PA, United States
- ¹²⁷ ^(a) Laboratório de Instrumentação e Física Experimental de Partículas – LIP, Lisboa; ^(b) Faculdade de Ciências, Universidade de Lisboa, Lisboa; ^(c) Department of Physics, University of Coimbra, Coimbra; ^(d) Centro de Física Nuclear da Universidade de Lisboa, Lisboa; ^(e) Departamento de Física, Universidade do Minho, Braga; ^(f) Departamento de Física Teórica y del Cosmos and CAFPE, Universidad de Granada, Granada (Spain); ^(g) Dep Física and CEFITEC de Faculdade de Ciências e Tecnologia, Universidade Nova de Lisboa, Caparica, Portugal
- ¹²⁸ Institute of Physics, Academy of Sciences of the Czech Republic, Praha, Czechia
- ¹²⁹ Czech Technical University in Prague, Praha, Czechia
- ¹³⁰ Faculty of Mathematics and Physics, Charles University in Prague, Praha, Czechia
- ¹³¹ State Research Center Institute for High Energy Physics (Protvino), NRC KI, Russia
- ¹³² Particle Physics Department, Rutherford Appleton Laboratory, Didcot, United Kingdom
- ¹³³ ^(a) INFN Sezione di Roma; ^(b) Dipartimento di Fisica, Sapienza Università di Roma, Roma, Italy
- ¹³⁴ ^(a) INFN Sezione di Roma Tor Vergata; ^(b) Dipartimento di Fisica, Università di Roma Tor Vergata, Roma, Italy
- ¹³⁵ ^(a) INFN Sezione di Roma Tre; ^(b) Dipartimento di Matematica e Fisica, Università Roma Tre, Roma, Italy
- ¹³⁶ ^(a) Faculté des Sciences Ain Chock, Réseau Universitaire de Physique des Hautes Energies – Université Hassan II, Casablanca; ^(b) Centre National de l’Energie des Sciences Techniques Nucleaires, Rabat; ^(c) Faculté des Sciences Semlalia, Université Cadi Ayyad, LPHEA-Marrakech; ^(d) Faculté des Sciences, Université Mohamed Premier and LPTPM, Oujda; ^(e) Faculté des sciences, Université Mohammed V, Rabat, Morocco
- ¹³⁷ DSM/IRFU (Institut de Recherches sur les Lois Fondamentales de l’Univers), CEA Saclay (Commissariat à l’Energie Atomique et aux Energies Alternatives), Gif-sur-Yvette, France
- ¹³⁸ Santa Cruz Institute for Particle Physics, University of California Santa Cruz, Santa Cruz CA, United States
- ¹³⁹ Department of Physics, University of Washington, Seattle WA, United States
- ¹⁴⁰ Department of Physics and Astronomy, University of Sheffield, Sheffield, United Kingdom
- ¹⁴¹ Department of Physics, Shinshu University, Nagano, Japan
- ¹⁴² Fachbereich Physik, Universität Siegen, Siegen, Germany
- ¹⁴³ Department of Physics, Simon Fraser University, Burnaby BC, Canada
- ¹⁴⁴ SLAC National Accelerator Laboratory, Stanford CA, United States
- ¹⁴⁵ ^(a) Faculty of Mathematics, Physics & Informatics, Comenius University, Bratislava; ^(b) Department of Subnuclear Physics, Institute of Experimental Physics of the Slovak Academy of Sciences, Kosice, Slovak Republic
- ¹⁴⁶ ^(a) Department of Physics, University of Cape Town, Cape Town; ^(b) Department of Physics, University of Johannesburg, Johannesburg; ^(c) School of Physics, University of the Witwatersrand, Johannesburg, South Africa
- ¹⁴⁷ ^(a) Department of Physics, Stockholm University; ^(b) The Oskar Klein Centre, Stockholm, Sweden

- ¹⁴⁸ Physics Department, Royal Institute of Technology, Stockholm, Sweden
¹⁴⁹ Departments of Physics & Astronomy and Chemistry, Stony Brook University, Stony Brook NY, United States
¹⁵⁰ Department of Physics and Astronomy, University of Sussex, Brighton, United Kingdom
¹⁵¹ School of Physics, University of Sydney, Sydney, Australia
¹⁵² Institute of Physics, Academia Sinica, Taipei, Taiwan
¹⁵³ Department of Physics, Technion: Israel Institute of Technology, Haifa, Israel
¹⁵⁴ Raymond and Beverly Sackler School of Physics and Astronomy, Tel Aviv University, Tel Aviv, Israel
¹⁵⁵ Department of Physics, Aristotle University of Thessaloniki, Thessaloniki, Greece
¹⁵⁶ International Center for Elementary Particle Physics and Department of Physics, The University of Tokyo, Tokyo, Japan
¹⁵⁷ Graduate School of Science and Technology, Tokyo Metropolitan University, Tokyo, Japan
¹⁵⁸ Department of Physics, Tokyo Institute of Technology, Tokyo, Japan
¹⁵⁹ Department of Physics, University of Toronto, Toronto ON, Canada
¹⁶⁰ ^(a) TRIUMF, Vancouver BC; ^(b) Department of Physics and Astronomy, York University, Toronto ON, Canada
¹⁶¹ Faculty of Pure and Applied Sciences, and Center for Integrated Research in Fundamental Science and Engineering, University of Tsukuba, Tsukuba, Japan
¹⁶² Department of Physics and Astronomy, Tufts University, Medford MA, United States
¹⁶³ Department of Physics and Astronomy, University of California Irvine, Irvine CA, United States
¹⁶⁴ ^(a) INFN Gruppo Collegato di Udine, Sezione di Trieste, Udine; ^(b) ICTP, Trieste; ^(c) Dipartimento di Chimica, Fisica e Ambiente, Università di Udine, Udine, Italy
¹⁶⁵ Department of Physics and Astronomy, University of Uppsala, Uppsala, Sweden
¹⁶⁶ Department of Physics, University of Illinois, Urbana IL, United States
¹⁶⁷ Instituto de Física Corpuscular (IFIC) and Departamento de Física Atomica, Molecular y Nuclear and Departamento de Ingeniería Electrónica and Instituto de Microelectrónica de Barcelona (IMB-CNM), University of Valencia and CSIC, Valencia, Spain
¹⁶⁸ Department of Physics, University of British Columbia, Vancouver BC, Canada
¹⁶⁹ Department of Physics and Astronomy, University of Victoria, Victoria BC, Canada
¹⁷⁰ Department of Physics, University of Warwick, Coventry, United Kingdom
¹⁷¹ Waseda University, Tokyo, Japan
¹⁷² Department of Particle Physics, The Weizmann Institute of Science, Rehovot, Israel
¹⁷³ Department of Physics, University of Wisconsin, Madison WI, United States
¹⁷⁴ Fakultät für Physik und Astronomie, Julius-Maximilians-Universität, Würzburg, Germany
¹⁷⁵ Fakultät für Mathematik und Naturwissenschaften, Fachgruppe Physik, Bergische Universität Wuppertal, Wuppertal, Germany
¹⁷⁶ Department of Physics, Yale University, New Haven CT, United States
¹⁷⁷ Yerevan Physics Institute, Yerevan, Armenia
¹⁷⁸ Centre de Calcul de l'Institut National de Physique Nucléaire et de Physique des Particules (IN2P3), Villeurbanne, France

^a Also at Department of Physics, King's College London, London, United Kingdom.

^b Also at Institute of Physics, Azerbaijan Academy of Sciences, Baku, Azerbaijan.

^c Also at Novosibirsk State University, Novosibirsk, Russia.

^d Also at TRIUMF, Vancouver BC, Canada.

^e Also at Department of Physics & Astronomy, University of Louisville, Louisville, KY, United States of America.

^f Also at Department of Physics, California State University, Fresno CA, United States of America.

^g Also at Department of Physics, University of Fribourg, Fribourg, Switzerland.

^h Also at Departament de Física de la Universitat Autònoma de Barcelona, Barcelona, Spain.

ⁱ Also at Departamento de Física e Astronomia, Faculdade de Ciências, Universidade do Porto, Portugal.

^j Also at Toms State University, Toms, Russia.

^k Also at Università di Napoli Parthenope, Napoli, Italy.

^l Also at Institute of Particle Physics (IPP), Canada.

^m Also at National Institute of Physics and Nuclear Engineering, Bucharest, Romania.

ⁿ Also at Department of Physics, St. Petersburg State Polytechnical University, St. Petersburg, Russia.

^o Also at Department of Physics, The University of Michigan, Ann Arbor MI, United States of America.

^p Also at Centre for High Performance Computing, CSIR Campus, Rosebank, Cape Town, South Africa.

^q Also at Louisiana Tech University, Ruston LA, United States of America.

^r Also at Institutio Catalana de Recerca i Estudis Avançats, ICREA, Barcelona, Spain.

^s Also at Graduate School of Science, Osaka University, Osaka, Japan.

^t Also at Department of Physics, National Tsing Hua University, Taiwan.

^u Also at Institute for Mathematics, Astrophysics and Particle Physics, Radboud University Nijmegen/Nikhef, Nijmegen, Netherlands.

^v Also at Department of Physics, The University of Texas at Austin, Austin TX, United States of America.

^w Also at Institute of Theoretical Physics, Ilia State University, Tbilisi, Georgia.

^x Also at CERN, Geneva, Switzerland.

^y Also at Georgian Technical University (GTU), Tbilisi, Georgia.

^z Also at Ochanomizu Academic Production, Ochanomizu University, Tokyo, Japan.

^{aa} Also at Manhattan College, New York NY, United States of America.

^{ab} Also at Hellenic Open University, Patras, Greece.

^{ac} Also at Academia Sinica Grid Computing, Institute of Physics, Academia Sinica, Taipei, Taiwan.

^{ad} Also at School of Physics, Shandong University, Shandong, China.

^{ae} Also at Moscow Institute of Physics and Technology State University, Dolgoprudny, Russia.

^{af} Also at Section de Physique, Université de Genève, Geneva, Switzerland.

^{ag} Also at Eotvos Lorand University, Budapest, Hungary.

^{ah} Also at International School for Advanced Studies (SISSA), Trieste, Italy.

^{ai} Also at Department of Physics and Astronomy, University of South Carolina, Columbia SC, United States of America.

^{aj} Also at School of Physics and Engineering, Sun Yat-sen University, Guangzhou, China.

^{ak} Also at Institute for Nuclear Research and Nuclear Energy (INRNE) of the Bulgarian Academy of Sciences, Sofia, Bulgaria.

^{al} Also at Faculty of Physics, M.V. Lomonosov Moscow State University, Moscow, Russia.

^{am} Also at Institute of Physics, Academia Sinica, Taipei, Taiwan.

^{an} Also at National Research Nuclear University MEPhI, Moscow, Russia.

^{ao} Also at Department of Physics, Stanford University, Stanford CA, United States of America.

^{ap} Also at Institute for Particle and Nuclear Physics, Wigner Research Centre for Physics, Budapest, Hungary.

^{aq} Also at Flensburg University of Applied Sciences, Flensburg, Germany.

^{ar} Also at University of Malaya, Department of Physics, Kuala Lumpur, Malaysia.

^{as} Also at CPPM, Aix-Marseille Université and CNRS/IN2P3, Marseille, France.

^{at} Also affiliated with PKU-CHEP.

* Deceased.